Contractor report series 77-3

A PHYSICAL OCEANOGRAPHIC STUDY OF HARO STRAIT: A DATA SUMMARY AND PRELIMINARY ANALYSIS

Ian Webster, M.Sc.
Dobrocky SEATECH Ltd
Victoria, B.C.

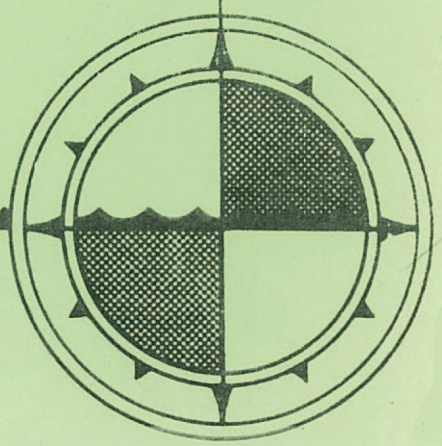

FOR

INSTITUTE OF OCEAN SCIENCES, PATRICIA BAY
Victoria, B.C.

Contractor Report Series 77-3

A PHYSICAL OCEANOGRAPHIC STUDY OF HARO STRAIT: A DATA SUMMARY AND PRELIMINARY ANALYSIS

by

Ian Webster, M.Sc.

Dobrocky SEATECH Ltd.

Victoria, B.C.

For

Institute of Ocean Sciences, Patricia Bay

Victoria, B.C.

July 1977

This report was prepared by Ian Webster of Dobrocky SEATECH Ltd., Victoria, B.C. under contract to the Institute of Ocean Sciences, Patricia Bay. The contents of this report are the responsibility of the Contractor.

A PHYSICAL OCEANOGRAPHIC STUDY OF HARO STRAIT: A DATA SUMMARY AND PRELIMINARY ANALYSIS

Ian Webster, M.Sc.

Dobrocky SEATECH Ltd.
130 Kingston Street
Victoria, B.C.

383-5323 - 383-2423

July 1977

TABLE OF CONTENTS

Table of Contents, cont'd. Page

LIST OF TABLES

LIST OF FIGURES

List of Figures, cont'd.

INTRODUCTION

Haro Strait is an irregular body of water approximately 35km long and varying from 4 to 11km wide connecting the Strait of Juan de Fuca with the Strait of Georgia of south western British Columbia (see Figure 1). The strait is important because it forms part of the route through which the bulk of the water within the Strait of Georgia ultimately exchanges with the sea.

During the period July 5 to September 10, 1976, a physical oceanographic study was carried out in Haro Strait to determine some of the major water characteristics and flow in that region for late summer. This study was carried out by Dobrocky SEATECH Ltd., under contract to the Institute of Ocean Sciences, Patricia Bay, Coastal Zone Oceanography, but much of the instrumentation and assistance in the data analysis were supplied by Tidal Surveys; also of the Institute.

The study included the installation of 21 Aanderaa current meters along a cross section of Haro Strait, the placement of two thermistor chains, the taking of several series of CTD profiles over 25 hours, and the collection of data on wind speeds and directions. The current meter and thermistor chain data were digitally filtered to examine low frequency variations and spectrally analysed to examine the contribution of the higher frequency variations including the tides. Coherences between pairs of current meters and between the two thermistor chains were computed. The series of CTD profiles were analysed to examine the changes in the vertical structure of the water column during several tidal cycles.

COLLECTION OF DATA

Current Meters

Twenty-one Aanderaa and 2 Geodyne current meters were moored in Haro Strait for the study. Following the recommendations outlined in "Data Survey and Recommendations for an Oceanographic Study of Haro Strait" by Chang (1976), these current meters were placed on 8 moorings in a line across the southern end of the strait. Figure 2 shows the placement of the moorings and Figure 3, a vertical section across the strait, shows the spatial configuration of the current meters. Table 1 includes a summary of the current meter mooring positions and the depths at which the meters were placed. Generally there were 3 current meters per mooring. The two moorings holding the Geodyne current meters employed Geodyne doughnut buoys for surface flotation while the other 6 moorings were supported by subsurface buoys. Figure 4 is a diagram of the two mooring systems. The Geodyne mooring systems were "tight lined" using cable which was sufficiently elastic to allow for vertical excursions of the buoy due to tidal water level changes. Each of the subsurface buoys used in the remaining 6 moorings had several hundred pounds of positive buoyancy, which proved to be insufficient for preventing the moorings from leaning over considerably during the periods of the strongest tidal currents in the strait.

The first current meters were positioned in Haro Strait on July 7, 1976 and the last removed from the strait on August 31, 1976. Several of the current meters were operational for the major part of this time interval but others provided useful data for only a portion of this period. Table 1 catalogues the period of successful operation of each meter; Figure 5 shows the coincidence of the periods of operation between the current meters and the other instrumentation employed in the study.

All the Aanderaa current meters used in the study were of the RCM4 type (see Aanderaa Instruments, Datasheet D147) which measures current speed, current direction, conductivity and temperature. Many of these meters were also equipped with pressure sensors. As deployed these meters recorded internally on magnetic tape at 10 minute intervals an instantaneous measurement of current direction, conductivity, temperature and pressure (if the meter was so equipped). Current speed was measured by counting the number of rotations of a rotor. At 10 minute intervals a measure of the rotor counts accumulated in the previous 10 minutes was recorded on the magnetic tape. Thus, recorded speeds are, in effect, 10 minute averages whereas the other parameters, including current direction, are observed instantaneously. The accuracies of the meters are given in Table 2. The Aanderaa current meter consists of a body, in which the speed sensor and electronics are located, which is attached to a large vane (see Figure 6). The whole system rotates on gimbals which enable the meter to align itself into the current. The gimbals are constructed in such fashion that the mooring line into which the meter is positioned can deviate approximately 23° from the vertical before the orientation of the meter is affected. At larger deviations of the line the meter itself will begin to tilt resulting in possible erroneous values from the rotor and interference in the operation of the compass which determines current direction. The maximum tilt of the

Table 1. Summary of C.M. mooring information.

Instrument #	Instrument type[1]	Station #	Station coordinates Lat.	Station coordinates Long.	Depth of meter (m)	Type of buoy[2]	Successful operation (PST) Start	Successful operation (PST) Stop	Sampling interval
338	A	181	48° 30.42' N	123° 09.28' W	100	A	July 8/76	Aug 17/76	10 min.
637	A	181	48° 30.42' N	123° 09.28' W	175	A	meter failed		10 min.
638	A	181	48° 30.42' N	123° 09.28' W	250	A	July 8/76	Aug 8/76	10 min.
731	A	182	48° 30.14' N	123° 10.00' W	40	A	July 8/76	Aug 16/76	10 min.
337	A	182	48° 30.14' N	123° 10.00' W	100	A	July 8/76	Aug 16/76	10 min.
639	A	182	48° 30.14' N	123° 10.00' W	175	A	July 8/76	Aug 16/76	10 min.
730	A	183	48° 29.81' N	123° 10.37' W	40	A	July 7/76	Aug 16/76	10 min.
739	A	183	48° 29.81' N	123° 10.37' W	100	A	July 7/76	Aug 16/76	10 min.
642	A	183	48° 29.81' N	123° 10.37' W	175	A	July 7/76	Aug 16/76*	10 min.
239	G	188	48° 29.9 ' N	123° 11.2 ' W	3	B			10 min.
1022	A	188	48° 29.9 ' N	123° 11.2 ' W	20	B	July 17/76	July 25/76	10 min.
1461	A	188	48° 29.9 ' N	123° 11.2 ' W	40	B	July 17/76	July 25/76	10 min.
738	A	184	48° 29.62' N	123° 11.10' W	40	A	July 7/76	Aug 27/76	10 min.
336	A	184	48° 29.62' N	123° 11.10' W	100	A	July 7/76	Aug 31/76	10 min.
335	A	184	48° 29.62' N	123° 11.10' W	175	A	July 7/76	Aug 13/76	10 min.
241	G	185	48° 29.5 ' N	123° 11.4 ' W	3	B			10 min.
643	A	185	48° 29.5 ' N	123° 11.4 ' W	20	B	July 17/76	Aug 19/76	10 min.
644	A	185	48° 29.5 ' N	123° 11.4 ' W	40	B	July 17/76	Aug 19/76	10 min.
1459	A	186	48° 29.1 ' N	123° 12.1 ' W	40	A	July 17/76	Aug 19/76	10 min.
1458	A	186	48° 29.1 ' N	123° 12.1 ' W	100	A	July 17/76	Aug 19/76	10 min.
1460	A	187	48° 28.6 ' N	123° 13.2 ' W	20	A	July 17/76	Aug 19/76	10 min.
1606	A	187	48° 28.6 ' N	123° 13.2 ' W	40	A	July 17/76	Aug 19/76	10 min.
333	A	187	48° 28.6 ' N	123° 13.2 ' W	100	A	July 17/76	Aug 20/76	10 min.

[1] A - Aanderaa current meter
G - Geodyne current meter

[2] A - sub-surface buoy
B - surface buoy

* includes 2 sections of bad data, one 3 and one 4 days long.

Table 2. Accuracies of Aanderaa Current Meters (Based on Aanderaa Instruments Datasheet D147 and configuration in which meters were used).

Temperature:

All meters except #335, 336, 337, 338, accuracy ± 0.15°C; resoluation 0.02°C.

Meters #335, 336, 337, 338, accuracy ± 0.15°C; resolution 0.03°C.

Pressure:

All meters except #730, 731, 1458, 1459, 1460, 1461, 1606, accuracy ± 7 dbar; resolution ± 0.1 dbar.

Meters #1458, 1459, 1460, 1461, 1606, accuracy ± 4 dbar; resolution ± 0.05 dbar.

Meters #730, 731, accuracy ± 1.5 dbar; resolution ± 0.02 dbar.

Current Speed:

All meters accuracy ± 1 cm/sec, or ± 2% of the actual speed whichever is greater.

Current Direction:

All meters accuracy ± 7.5° speed within 2.5 to 5 cm/sec, or 100 to 200 cm/sec; accuracy ± 5° speed within 5 to 100 cm/sec.

Conductivity:

The accuracies of individual meters have been shown to vary somewhat, but the accuracy of all the instruments should be better than ± 0.1 PPT (parts per thousand) equivalent salinity.

compass before its operation is affected, is estimated to be 12° (Aanderaa Instruments Datasheet D147).

The Geodyne current meter which employs a burst method of sampling is particularly appropriate for measuring currents near the surface. For such measurements the influence of mooring motion and wave currents can seriously affect the validity of measurements made using Aanderaa current meters. At the present time the data from the 2 Geodyne current meters used in Haro Strait has not been reduced and it will not be further discussed.

Thermistor Chains

Two thermistor chains were hung vertically from Geodyne surface buoys at positions designated TA1 and TA2, separated by approximately 9km along the longitudinal axis of Haro Strait. The southernmost chain at TA1 was positioned approximately in line with the current meter arrays (see Figure 2). The periods of operation of the two thermistor chains was such that they were collecting data simultaneously for 25 days (see Table 3 and Figure 5).

The thermistor chains were both of the Aanderaa type. Each consisted of a string of 11 thermistors positioned at 5m intervals with the top thermistor 5m below the surface and the bottom one 55m below the surface. At 10 minute intervals a temperature from each of the thermistors was determined and recorded on magnetic tape. The estimated accuracy of an individual temperature measurement is ±0.15 (Aanderaa Instruments Datasheet D131).

Near the end of the study period one of the thermistor chains (labelled T93) was installed for a second time in its original position at station TA1. This time it was set to sample temperatures at intervals of 1.25 minutes instead of 10 minutes in order that something could be determined of the nature of the higher frequency variations in water properties in the strait. The data sets derived from the first deployments of the thermistor chains will be termed T63/17 and T93/18 and the last data set derived using the shorter sampling interval will be referred to as T93/19.

CTD Measurements

CTD measurements were made on 4 separate occasions during the study. On each occasion it was intended to drop the CTD repeatedly over a period of 25 hours or approximately 1 lunar day hence these sets of CTD drops will be called Time Series #1, Time Series #2, etc. Time Series #1, #2 and #3 were all determined at the same position. Time Series #4 consisted of repeated drops at 6 stations distributed over 13km along the length of Haro Strait (see Figure 2 and Table 4).

Time Series #1 was carried out on July 26-27, 1976 coinciding with a time when the daily tidal ranges are large (spring tides) while Time Series #2 which was carried out 7 days later coincides with the occurrence of neap tides, or tides with relatively small daily tidal ranges. Unfortunately Time Series #3, 4 days later, had to be terminated prematurely because of breakdown of the survey vessel. Time Series #4 was undertaken at the end of the study after all the current meters had been removed. For this series which commenced 6 weeks after Time Series #1 the daily tidal ranges were relatively large.

Instrument number	Station number	Station coordinates	Successful operation (PST) Start	Stop	Depth of sensors (m)	Sampling Internal
T93/18	TA1	48° 29.3' N 123° 11.2' W	July 5/76	Aug 11/76	5, 10, 15, 20, 25, 30, 35, 40, 45, 50, 55	10 min.
D86/8	TA1	48° 29.3' N 123° 11.2' W	July 6/76	Aug 18/76	-3.3 (above water)	10 min.
T63/17	TA2	48° 34.1' N 123° 13.6' W	July 13/76	Aug 7/76	5, 10, 15, 20, 25, 30, 35, 40, 45, 50, 55	10 min.
D85/8	TA2	48° 34.1' N 123° 13.6' W	July 13/76	July 18/76	-3.3 (above water)	10 min.
T93/19	TA1	48° 29.3' N 123° 11.2' W	Sept 7/76	Sept 9/76	5, 10, 15, 20, 25, 30, 35, 40, 45, 50, 55	1.25 min.
D85/9	TA1	48° 29.3' N 123° 11.2' W	Sept 7/76	Sept 9/76	-3.3 (above water)	1.25 min.

Table 3. Summary of thermistor chain-anemometer moorings.

CTD Time Series #	Station	Latitude	Longitude	Start of time series (PST)	End of time series (PST)	Number of instruments cast
1		48° 29.5' N	123° 9.0' W	1145 July 26/76	1252 July 27/76	55
2		48° 29.5' N	123° 9.0' W	1009 Aug 3/76	1111 Aug 4/76	42
3		48° 29.5' N	123° 9.0' W	0828 Aug 9/76	1825 Aug 9/76	22
4	F1	48° 28.5' N	123° 8.5' W	0931 Sept 8/76	1036 Sept 9/76	38
	F2	48° 30.4' N	123° 9.3' W			
	F3	48° 31.4' N	123° 10.6' W			
	F4	48° 32.7' N	123° 11.5' W			
	F5	48° 33.8' N	123° 12.7' W			
	F6	48° 35.4' N	123° 13.0' W			

Table 4. Summary of CTD time series.

The CTD used in the present study was a Guildline Model 87011 analogue output unit ouned and operated by Coastal Zone Oceanography. The claimed accuracies of this machine as it was used in the present study are ±0.01 PPT equivalent salinity, and ±0.01 ^{o}C temperature (Guildline Instruments, Advance Bulletin 7460). The time constants of all the sensors are estimated to be less than 100ms and the sampling frequency of the recording electronics was 4 samples/sec. At the drop rate of 1m/sec (which was commonly used) the vertical resolution of the CTD was of order 25cm or better.

The data from the CTD probe was recorded on 9 track tape as the probe was both lowered and raised. However, in the following analyses only data obtained during the lowering of the probe will be discussed. Often bubbles which can cause spurious output still adhere to the sensors immediately after the probe is first lowered into the water. Hence data obtained by the CTD from the top 5m of the water column should be regarded with a certain amount of suspicion.

Wind Anemometers

Two wind anemometers were deployed in the study to collect background information on wind speeds and directions. The anemometers were mounted on top of the Geodyne buoys which supported the two thermistor chains; their estimated heights above the water level were 3.3m. The first of the anemometers started recording information on July 6, 1976 and the second on July 13, 1976. Both anemometers operated until August 18, 1976 (see Table 3 and Figure 5). The southernmost of the two anemometers was reinstalled for 3 days in September coincident with the operation of the single thermistor chain using the reduced sampling of interval 1.25 minutes.

The anemometers used in the study were Aanderaa models which utilize a cup speed sensor and a vane for a direction sensor. Ambient air temperature and the water temperature are also measured. As the anemometers were first installed, data from the sensors was recorded on magnetic tape at intervals of 10 minutes. However, when one of the anemometers was reinstalled in September the sampling interval was reduced to 1.25 minutes.

DATA ANALYSIS

The techniques used in the analysis of data from the Aanderaa current meters, from the thermistor chains, from the CTD, and from the anomometers are outlined in the sections following. Except where noted the analysis of the data from the Haro Strait project was carried out on the IBM 370 computer at the University of British Columbia.

Aanderaa Current Meter Data

Figure 7 is a schematic diagram of the steps followed in the analysis of the current meter data.

1. Translation and Calibration

The translation of the ¼" Aanderaa current meter data tapes to 9 track format was done on an HP2100 computer by Mr. A. Douglas of Tidal Surveys. In the conversion process each physical record was checked to see if it had the correct number of bits. If the record did not it was flagged as a negative number during the translation.

Frequently, current meter data contains spikes due to problems in the data encoder or other parts of the recording system. Plots of the raw current meter data from the Haro Strait study revealed that the majority of the records had at least some clearly recognizable spikes. A criterion was developed for identifying spikes by first computing a histogram of the first differences between the successive data points. Simple spikes appear in such a histogram as producing a pair of large first differences of opposite sign. From an examination of the histograms from a number of current meters, values for the maximum allowable first differences were established for current speed, temperature and conductivity. The positions of the occurrences of larger first differences were recorded as being the positions of possible spikes. If these were judged to be spikes after their individual examination the spike was replaced by a linear interpolation of 'good' data. The occurrences of negative data values were replaced in the same fashion. Next the current speeds and directions were resolved into their north-south and east-west vector components. These two time series were examined for spikes which, if found, were corrected using the interpolation technique employed previously. The current velocity, conductivity and temperature data records were corrected for spikes but the pressure record was not.

At this stage all the data records were calibrated for 2 components of velocity in cm/sec, temperature in degrees centigrade, conductivity in mmhos/cm^2 and pressure in decibars. The calibration was carried out using a program developed by Coastal Zone Oceanography. As part of the calibration procedure the number of translated data records was counted and checked against the number of records which should have been there given the starting time, the ending time, and the sampling rate. Table 5 provides the results of the comparison. If the actual number of data records matched the expected number the meter was "on time"; if the ending time of the current meter data was not recorded the accuracy of the meter time is regarded as being unknown. Meter #639 was the only meter definitely not on time as there were 12 fewer records than there should have been. However, from the appearance of the

Table 5. Summary of data analysis for current meters, thermistor chains, anemometers.

Instrument #	Instrument type[1]	Sensors operational[2]	Timing status[3]	Time series plotted	Low passed time series plotted	2-25 hr data sections plotted	Tidal analysis carried out	Start tidal analysis	Power spectral analysis done	Number of blocks in power spectral analysis	Start power spectral analysis
338	CM	T, C, P, S, D	OT	✓	✓	✓	✓	July 12/76	✓	4	
638	CM	T, C, P, S, D	OT	✓	✓	✓			✓	3	July 15/76
731	CM	T, C, P, S, D	OT	✓	✓	✓	✓	July 12/76	✓	4	
337	CM	T, C, P, S, D	OT	✓	✓	✓	✓	July 12/76	✓	4	July 15/76
639	CM	T, C, P, S, D	12 short	✓	✓	✓	✓	July 12/76	✓	4	July 15/76
730	CM	T, C, P, S, D	OT	✓	✓	✓	✓	July 12/76	✓	3	July 15/76
739	CM	T, C, P, S, D	OT	✓	✓	✓	✓	July 12/76	✓	4	July 15/76
642	CM	T, C, S, D	OT	✓	✓	✓	✓	July 12/76			
1022	CM	T, C, P, S, D	U	✓	✓						
1461	CM	T, C, P, S, D	U	✓	✓						
738	CM	T, C, P, S, D	U	✓	✓	✓	✓	July 12/76	✓	5	July 15/76
336	CM	T, C, P, S, D	U	✓	✓	✓	✓	July 12/76	✓	6	July 15/76
335	CM	T, S, D	U	✓	✓	✓	✓	July 12/76	✓	4	July 15/76
643	CM	T, C, S, D	OT	✓	✓	✓	✓	July 17/76	✓	3	July 22/76
644	CM	T, C, S, D	OT	✓	✓	✓	✓	July 17/76	✓	3	July 22/76
1459	CM	T, C, P, S, D	OT	✓	✓	✓	✓	July 17/76	✓	3	July 22/76
1458	CM	T, C, P, S, D	OT	✓	✓	✓	✓	July 17/76	✓	3	July 22/76
1460	CM	T, C, P, S, D	OT	✓	✓	✓	✓	July 17/76	✓	3	July 22/76
1606	CM	T, C, P, S, D	OT	✓	✓	✓	✓	July 17/76	✓	3	July 22/76
333	CM	T, S, D	OT	✓	✓	✓	✓	July 17/76	✓	3	July 22/76
T63/17	TC	10 x T	U	✓		✓			✓	2	July 14/76
T93/18	TC	11 x T	U	✓		✓			✓	2	July 14/76
T93/19	TC	11 x T	OT	✓					✓	2	Sept 7/76
D85/8	A	T, S, D	OT	✓							
D86/8	A	T, S, D	OT	✓							
D85/9	A	T, S, D	OT	✓							

[1] CM - current meter
TC - thermistor chain
A - anemometer

[2] T - temperature
C - conductivity
P - pressure
S - speed
D - direction

[3] OT - instrument on time
U - end time unknown

time series it was evident that the missing data records were dropped within 2 days of the start of data recording for this meter. In further analyses of this data set missing data was accounted for.

It was noted that even though meter #642 was on time two sections of data within the record were bad. These two sections were replaced by zero data values. From the temperature and conductivity records time series of salinity in parts per thousand and sigma-t were computed. These calculations were based on Bennett's (1967) and Knudsen's formulae, respectively. Knudsen's formulae is that quoted by Fofonoff (1962). The calibrated time series of north-south components of velocity, of east-west components of velocity, of pressure, of temperature and of salinity were plotted for each of the current meters.

The subsequent analysis of the current meter data divides into 4 paths: the examination of low frequency variations in the data, the examination of two 25 hour sections of the current meter data, the evaluation of tidal energy, and the computation of power spectra.

2. Examination of Low Frequency Variation in the Current Meter Data

In order to examine its low frequency variations the data was first operated on by the low pass filter $A_{144}\, A_{149}^2$. The operator A_i is described by Godin (1972). If $\{x_t\}$ is the original sequence of discrete data values and $\{X_t\}$ is the filtered data sequence such that:

$$\{X_t\} = A_i\{x_t\}$$

then:

$$X_t = \frac{1}{i} \sum_{\ell=1}^{i} x_{t-i/2\ell-\frac{1}{2}}$$

If one considers a discrete data series of sampling interval Δt which has been operated on by A_i the amplitude attenuation of a variation having frequency f is given as:

$$G(f) = \frac{\sin 2\pi\, if\, \Delta f}{i \sin 2\pi\, f\, \Delta t}$$

The amplitude attenuation of the filter $A_{144}\, A_{149}^2$ is shown in Figure 8a as the "low pass filter". This filter causes a 50% amplitude attenuation at a frequency corresponding to a period of 3 days. At periods of 1 lunar day or less very little energy is passed by the filter.

The filtered time series of temperature, salinity and 2 components of velocity from the current meter were plotted as in Figure 10. Even though only one data point for each parameter was plotted per day (the values which occurred at midnight), very little of higher frequency energy would occur because this energy should be effectively removed by the filter. It should be noted that on these plots the velocity has been resolved into components

in directions along Haro Strait (V) and transverse to the strait (U). Transverse to the strait will be defined as 55° true which is approximately the line along which the current meter moorings were positioned (see Figure 2); along the strait is considered to be perpendicular to the line of moorings, that is, -35° true.

3. Examination of Two 25-hour Sections of Current Meter Data

It was decided to examine in detail two 25-hour sections of current meter data. These two sections were chosen to coincide with Time Series #1 and Time Series #2 (CTD data) which were carried out during periods of relatively large and small tides, respectively. Since the raw data contained a considerable amount of high frequency variation (see Figure 9) it was low pass filtered prior to its presentation.

The filter used for this purpose was the digital filter A_4A_6. The explicit expression of this filtering operation is:

$$X_t = 0.042\ x_{t-4} + 0.083\ x_{t-3} + 0.125\ x_{t-2} + 0.167\ x_{t-1}$$

$$+ 0.167\ x_t + 0.167\ x_{t+1} + 0.125\ x_{t+2} + 0.083\ x_{t+3} + 0.042\ x_{t+4}$$

The filter amplitude attenuation function shown in Figure 8b indicates that 50% attenuation occurs at a frequency corresponding to a period of two hours. The filtered time series of 2 components of velocity and of salinity were plotted at ½ hour intervals (see for example Figure 20).

4. Evaluation of Tidal Energy

An evaluation of the energies in the M_2, K_1, O_1, S_2 and N_2 tidal components was accomplished by performing a Fourier transform on a section of data 28 days long. On a section of data this length the transform is incapable of resolving the K_1 and the P_1 components from each other hence the estimated K_1 component will include the contribution from the P_1 component.

Prior to its Fourier transformation the data was passed through a high pass digital filter to remove all the energy having periods greater than a lunar day. This operation consisted of subtracting data passed by the low pass filter $A_{144}\ A_{149}^2$ (see Section 2) from the original data series. Thus the high pass filter could be represented as:

$$\{X_t\} = (1-A_{144}\ A_{149}^2)\ \{x_t\}$$

The emplitude attenuations that this filter produces are shown in Figure 8a as the "high pass filter".

Fourier coefficients were computed on the filtered data from a single block of 4032 samples (28.00 days) using a Fast Fourier Transform (FFT) subroutine compiled by P. Chang of the Institute of Oceanography at the University of British Columbia. This subroutine, based on an algorithm by

R.C. Singleton (1969), computes coefficients which satisfy the relation:

$$x(t_i) = A_o + \sum_{n=1}^{N/2} A_n \cos 2\pi f_n t_i + \sum_{n=1}^{N/2} B_n \sin 2\pi f_n t_i$$

where:

$x(t_i)$ is the value of the data point at time t_i

A_n, B_n are the n'th cosine and sine coefficients respectively

N is the number of points in the data record

f_n is the positive n'th frequency harmonic

If T is the time duration of the data record then $f_n = \frac{n}{T}$. The cosine and sine coefficients are computed by the FFT as:

$$A_n = \frac{2}{N} \sum_{i=1}^{N/2} x(t_i) \cos 2\pi f_n t_i$$

and:

$$B_n = \frac{2}{N} \sum_{i=1}^{N/2} x(t_i) \sin 2\pi f_n t_i$$

The amplitude of a component having frequency f_n will be defined as:

$$D_n = (A_n^2 + B_n^2)^{\frac{1}{2}}$$

the phase as:

$$\phi_n = -\tan^{-1} (B_n/A_n)$$

The analysis of the tidal components of the salinity data will be described in terms of D_n and ϕ_n.

It has been shown in general that the tip of a two dimensional vector which has its two coordinates varying sinusoidally with frequency f_n traces out an ellipse which it traverses at frequency f_n. The lengths of the major and minor axes orientation and the phase of the ellipse can be derived from the cosine and sine coefficients of the two vector components (Mooers, 1973).

In the discussion of results tidal velocities will be presented using the ellipse description.

The tidal constituents derived here are based upon those FFT coefficients which have frequencies close to tidal frequencies. Table 6 shows the tidal frequencies and the centre frequency of the corresponding FFT

Tidal Constituent	Period (HRS)	Number of cycles in 28 days	Period of FFT harmonic used to estimate tidal energy	Number of cycles in 28 days
M_2	12.42	54.11	12.44	54.0
K_1	23.93	28.08	24.00	28.0
O_1	25.82	26.03	25.85	26.0
S_2	12.00	56.00	12.00	56.0
P_1	24.07	27.92	24.00	28.0
N_2	12.66	53.08	12.68	53.0

Table 6. Estimation of tidal constituents in current meter data.

coefficients. It should be noted that the bandwidth of each FFT coefficient is approximately 1/T or 0.0357 days^{-1}.

5. Estimation of Power Spectra and Coherences

Power spectra of two velocity components and of salinity were computed for 17 current meters. Also, coherences were computed between selected pairs of current meters.

Because it was anticipated that energy at tidal frequencies might "contaminate" the computation of power spectra and coherences at non-tidal frequencies, the data was passed through a tidal elimination digital filter. This filter, designated as S_{149}, is designed to remove all the harmonics (including the first) of frequencies having periods of 1 lunar day. S_i is defined as the operation of continuously taking the difference of observations $i\Delta t$ apart where Δt is the sampling interval (Godin, 1972). Thus,

$$\{X_t\} = S_i \{x_t\}$$

where:

$$X_t = \frac{1}{2} (x_t - x_{t+i})$$

The power attenuation factors of this filter are shown in Figure 8c.

On successive blocks of 1008 samples (7days) Fourier coefficients were computed according to the definitions given previously. A set of coefficients was computed in this fashion on data passed by the tidal eliminator filter and on the equivalent section of unfiltered data. Next, the Fourier coefficients from the filtered data set were corrected for the filter attenuation. If the amplitude, at a given frequency, was attenuated by a factor greater than 20, the sine and cosine coefficients were simply replaced by those of the same frequency computed from the unfiltered data series.

The power, or energy per unit bandwidth, is defined as:

$$P(f_n) = \frac{T}{2} (A_n^2 + B_n^2)$$

The cospectrum between 2 data series is a measure of their "in phase" power. The cospectrum at a particular frequency f_n can be constructed from the Fourier coefficients of the 2 series. Let the coefficients from the first series be unprimed and those of the second be primed then the cospectrum is defined as:

$$C(f_n) = \frac{T}{2} (A_n A'_n + B_n B'_n)$$

Likewise a measure of the "90° out of phase" power is the quadrature spectrum given as:

$$Q(f_n) = \frac{T}{2} (A'_n B_n - A_n B'_n)$$

In order to obtain reliable spectra it is usually recommended that spectral estimates be averaged in some fashion. In this study the spectra are "smoothed" in 2 ways. First, the individual spectral estimates were averaged over frequency bands of width Δf such that $\frac{\Delta f}{f_c} \simeq 0.26$, f_c being the centre frequency in the band.
The band averaged power spectrum is thus:

$$\overline{P(f_c)} = \frac{1}{m} \sum_{n=c-m/2}^{c+m/2} P(f_n)$$

where m is the number of harmonics in the band. The first 6 bandwidths (after 0) were too far apart to be averaged with this bandwidth. The smoothed spectra for each block were then averaged over the number of blocks, B, to produce a doubly smoothed spectrum.

$$\overline{\overline{P(f_c)}} = \frac{1}{B} \sum_{B} \overline{P(f_c)}$$

The double smoothing of co- and quad- spectral estimates were carried out in analogous fashion. The smoothed co-, quad-, and power spectra can be combined to produce a coherence spectrum. This coherence is just a measure of the proportion of power coherent between 2 data series. At frequency f_c it is defined as:

$$K(f_c) = \left(\frac{\overline{\overline{C(f_c)}}^2 + \overline{\overline{Q(f_c)}}^2}{\overline{\overline{P(f_c)}} \cdot \overline{\overline{P'(f_c)}}} \right)^{\frac{1}{2}}$$

The phase of the coherent power can also be computed:

$$\phi(f_c) = \tan^{-1} \left(\overline{\overline{Q(f_c)}} / \overline{\overline{C(f_c)}} \right)$$

For each meter power spectra of salinity, longitudinal velocity and transverse velocity are presented. As before, longitudinal velocity and transverse velocity are defined as -35 degrees true and 55 degrees true, respectively. The power spectra are all plotted as $f \cdot P(f)$ versus log f. It can easily be shown that $f \cdot P(f)$ is proportional to the energy contribution in the logarithmic frequency band $\Delta \log f$.

The coherence spectra between 2 current meters were estimated from blocks of coincidental operation. Both coherences and phases are plotted on linear axes versus log f. Jenkins and Watts (1968) derive the expected coherence between 2 noise sources as $L^{-\frac{1}{2}}$ where L is the product of the number of blocks and the number of frequency harmonics averaged in each block for a given coherence calculation. On each plot of coherence the level of the expected noise coherence for each situation is indicated (see Figure 36).

Thermistor Chain Data

The data from the thermistor chains was translated and calibrated by G. Kamitakahara of Coastal Zone Oceanography. The raw data was of sufficiently good quality that it was not considered necessary to follow any data conditioning procedures such as removing spikes. From each of the three installations of thermistor chains a calibrated plot of the time series of temperatures at the different depths was produced.

Further data analysis procedures follow those carried out on the current meter data. For the data sets T63/17 and T93/18 the data from the thermistors at the depths of 10m, 30m and 55m are considered because for one of the chains the data from 5m depth had been lost. In addition to the examination of the low pass filtered time series and of two 25-hour sections of data coinciding with Time Series #1 and #2, power spectra were computed from the data from the 3 depths. Also, coherences and phases between corresponding depths on the two chains were computed.

For the data set T93/19 which utilizes a shorter sampling interval of 1.25 minutes a somewhat different procedure was followed. Aside from the plotting of the calibrated time series, power spectra only were computed from the data from 5m, 30m and 55m depths. No filtering was carried out prior to the computation of these spectra.

CTD Data

The raw data from the CTD, available on 9 track tape, was first calibrated. Temperatures were calculated in degrees centigrade, pressures in decibars, conductivities in mmhos/cm^2. From conductivities and temperatures salinities were computed using Bennett's formula. Sigma-t's were computed using Knudsen's formula from salinities and temperatures. The computed sigma-t's and calibrated pressures were used to calculate the depths of the observations by an incremental process from the surface using the hydrostatic relationship between depth, pressure and density.

The calibrated CTD data were first used to plot salinity versus pressure for each of the individual drops in the four CTD time series. We decided that further processing of the CTD data would be facilitated by averaging the data over 5m depths, so this was done. Using the averaged data T,S plots were determined for each time series. Since the interval between CTD drops on a given time series was quite irregular we felt the construction of an interpolated set of CTD drops would simplify their interpreation. The actual data from the CTD was used to estimate what the CTD would have observed if it had been dropped at regular intervals. For example for Time Series #1 a hypothetical CTD drop for 1200 Pacific Standard Time (PST) was computed from a linear interpolation of data from a given depth from the two actual CTD drops which bracket it in time, that is, from the one which preceded it at 1145 PST and from the one which followed it at 1215 PST. This interpolation procedure was carried out for Time Series #1, #2 and #4 but not for Time Series #3 because the latter was incomplete. In the case of Time Series #1 and #2 interpolation was carried out at hourly intervals for 24 consecutive hours. The interpolated profiles were plotted for salinity only. The average profile shown on each plot (see Figure 54) was determined for each

time series by simply averaging the 24 interpolated profiles. For Time Series #4 which had only 7 CTD drops per station over the 25-hour period, salinity profiles were interpolated for each station to intervals of 4 hours. In the latter case, because the interpolated times were chosen to be the same for all 6 stations, it was possible to construct "instantaneous" longitudinal profiles of the salinity structure in Haro Strait at 4-hour intervals over the period of a day (see Figure 55).

Anemometer Data

Only the data from the first two anemometer installations, namely D85/8 and D86/8, were reduced. Using programs developed by Coastal Zone oceanography these data sets were first calibrated and then plotted as time series of wind speed, wind direction and air temperature. Aside from calibration no data conditioning procedures were followed for the anemometer data.

DISCUSSION AND PRESENTATION OF DATA

In the following presentation of data all salinities will be expressed in parts per thousand (PPT), all temperatures in degrees centigrade (°C) and, except where noted, all velocities in cm/sec. Time will be understood to be Pacific Standard Time (PST).

Results of Current Meter Analysis

1. Current Meter Time Series

Only the calibrated time series of current meter data, from meter #338 which was situated at a depth of 100m on the eastward end of the current meter array, is included in this report. This time series (shown in Figure 9) exhibits many features common to all the time series. The water movements are seen to be strong, being dominated by the tides which are of the mixed, strongly semi-diurnal type. At current meter #338 current velocities over 2m/sec were observed on occasion. Although this meter was situated in that part of Haro Strait where the tidal currents were to prove to be the strongest, at all the current meters, the currents were observed to exceed 1m/sec at times. As expected, a pattern of relatively strong tidal currents and relatively weak tidal currents which repeats itself every 2 weeks is evident. The pressure record of meter #338 indicates that the meter underwent significant changes in depth when the currents were strong. At times of the peak tidal currents this particular meter increased its depth by more than 100m. The mooring which contained meter #338 was supported by a subsurface buoy. Under conditions of strong current such a mooring system can begin to lay over due to the effects of frictional drag on the mooring components. All the moorings using subsurface buoys appeared to lay over to a certain extent during periods of strong current. The current meters on the two most western moorings did not change depth by more than 5m at any time whereas those on the eastern side of the strait were more affected. Current meters #731, #337 and #639 changed depth by up to 60m, 50m and 30m respectively when currents were strong. However, the remaining meters did not change depth by more than 30m.

W. Bell of Coastal Zone Oceanography has modelled numerically the behaviour of the mooring in which meters #731, #337 and #639 are positioned, (Static Analysis of Single Point Moorings, In Preparation). Using estimates of the frictional drag coefficients on the mooring line, on the flotation buoy and on the current meters he predicts the configuration of the mooring in various current conditions. When the current is 1.5m/sec the model predicts an increase in depth of meter #731 of nearly 40m and an angle of tilt of the mooring line at the bottom meter #639 of 35°. In reality, in currents of this size, increases in depth of meter #731 were observed to be of the order of 60m which implies that at meter #639 the mooring line likely achieves tilt angles greater than 35°. Since the gimbals on the meters can accomodate 23° of mooring line tilt and the meter itself can tilt 12°, the compass will perform satisfactorily if the line angle is not greater than 35°. At meter #639 and also at the lowest meters on other moorings angles greater than 35° are probably attained during periods of the highest current.

Both the time series of salinity and temperature for meter #338 appear to have strong tidal variations. The dominance of tidal influences is common to the records from the other current meters also. Although the details of the long and short term changes in temperature and salinity in Haro Strait will be examined later it is worthwhile pointing out here that the variance in these parameters at tidal frequencies and higher appears to go through a cycle over a period of 2 weeks. These variances tend to be largest during periods when the tidal ranges are still building to their maxima and smallest immediately following the largest tides. Evidently, intense mixing associated with large tidal ranges tends to destroy temperature and salinity stratification.

2. Low Frequency Current Meter Results

Figures 10 to 17 show the results of passing the current meter data through the low pass filter $A_{144}\ A_{149}^2$ which smooths out variations of periods less than several days. Each data point on these plots is the value of the filtered time series which occurred at 0000 on the data.

What is striking about the low frequency variations in temperature, salinity, and velocity are their periodic natures. Although not more than several cycles are represented on any plots these variations probably have a period of two weeks corresponding to the cycle of spring and neap tides.

The temperature and salinity variations are mirror images of one another indicating a linear relationship between the two parameters. In fact the analysis of CTD data showed that this relationship was quite linear, hence the following discussion of low frequency water property variations will be restricted to salinity alone. The low frequency variations in salinity at meters 40m and deeper were in phase with one another whereas meters #643 and #1022 at 20m near the centre of the current meter array were 180° out of phase with the others. The magnitudes of these variations were smallest at 40m; both at deeper and shallower depths the magnitudes increased in size. The net effect of this behaviour is that the vertical salinity gradients also go through a two weekly cycle which is in phase with the salinity cycle at the deeper meters. High salinity gradients, high salinities in the deeper water and low salinities in the surface water appear to coincide with the period between neap and spring tides whereas low salinity gradients, high surface salinities and relatively low salinties in the deeper water occur in the period following spring tides. It would appear that spring tides are associated with considerable interchange between relatively fresh surface water and deeper more saline water. Figures 18a and 19a show the salinities in cross sections of Haro Strait at 0000 July 14 and 0000 July 22 which are times following a set of spring and neap tides respectively. On neither of these two occasions are the horizontal salinity gradients sufficiently great that they could be regarded as significant in view of possible errors in the depths of the meters and in the meters' determination of salinity. The longitudinal flow in Haro Strait, that is, the component perpendicular to the current meter array, appeared to divide into two layers; the top flowing approximately south and the bottom flowing into Haro Strait approximately towards the north. The dividing line between the two directions of flow varied somewhat during the period of study, but an average would lie between 40m and 100m on the east side of the strait deepening to greater than 100m on the west side of the strait. The longitudinal velocities were of the

order of 10cm/sec where there were observations in the upper layer. At meter #638 at a depth of 250m on the east side of Haro Strait a filtered longitudinal velocity of 64.5 cm/sec flowing towards the north was observed. This meter did not record longitudinal velocities less than 25 cm/sec. Although not as regular as those of temperature and salinity the two components of velocity showed a repetitive two weekly cycle. It seems that the velocity gradients are largest during that period of the tidal cycle. At this time the surface flow towards the south and the subsurface flow towards the north are both relatively strong while the opposite situation occurs when the salinity gradients are near their minima. Figures 18b and 19b show the distribution of longitudinal velocity across Haro Strait at 0000 July 14 and 0000 July 22, respectively.

3. Results of the Analysis of Two 25-hour Sections of Current Meter Data

Two 25-hour sections of current meter data are presented in Figures 20 to 26 primarily to complement the interpretation of the data from the CTD Time Series #1 and #2. These two sections of data were passed through the filter A_4A_6 which removes fluctuations having periods less than an hour. The first section of data lies between 1200 July 26 and 1300 July 27 whereas the second lies between 1030 August 3 and 1130 August 4. The first section lies near the middle of the spring tides and is labelled "large tides" on the plots. The second section occurs during the periods of neap tides and is labelled "small tides". The filtered time series are all plotted at ½ hour intervals. Each plot shows the results from current meters on the same mooring. It is evident from these sections of data that the water properties in Haro Strait are very dependent on the phase of the tide. Also the phase of the components varies markedly with depth.

4. Results of the Analysis of Tidal Components of the Current Meter Data

Estimates of the magnitudes and phases of the major tidal constituents of velocity and salinity were computed using a Fourier transform. The results for the major semi-diurnal and diurnal components (M_2 and K_1 components respectively) are presented in Tables 7 and 8. As explained before, the K_1 component calculated here actually consists of the contribution of the true K_1 component of period 23.93 hours together with the P_1 component of period 24.07 hours. The difference in frequency between these two components will cause a beat phenomenom to occur with period of about ½ year. At Race Rocks in the Strait of Juan de Fuca (see Figure 1) the magnitude of the P_1 component of current velocity is estimated to be of the order of a third of the K_1 component (A. Douglas, private communication). The magnitudes of the tidal velocity components are provided in terms of the lengths of the semi-major and semi-minor axes of the tidal ellipses. The sense of rotation of the velocity vector is either clockwise or anti-clockwise, the direction of the major axis is defined relative to the angle -35° and the phase is the temporal phase of the tidal ellipse. The results of the tidal analysis for the one dimensional scalar salinity are presented as magnitudes and phases. The calculation of phases considers time zero as being 1040 July 12, 1976. Several of the calculations for tidal constituents started 5 days later (see Table 5) but their phases were corrected for the change in starting time. In the block of data analysed for tidal constituents for current meter #642 there were 2 missing sections which would affect the results of the calculation.

Current meter	Rotary Velocity Components					Salinity	
	Semi-major axis (cm/sec)	Semi-minor axis (cm/sec)	Sense[1] of rotation	Direction of major axis	Phase	Magnitude (PPT)	Phase
338	68.6	3.5	C	-10.1	309.0	0.28	- 10.1
731	67.9	8.5	A	3.2	285.7	0.089	36.8
639	43.9	0.0		- 0.3	336.0	0.17	- 15.0
337	58.0	0.0		- 6.1	306.2	0.21	- 6.7
643	52.3	17.0	A	- 2.1	293.7	0.19	115.8
333	35.4	4.2	A	4.5	23.6		
739	53.7	1.4	A	-10.2	311.7	0.17	- 5.6
644	53.7	9.9	A	10.8	300.3	0.071	21.3
738	56.6	11.3	A	4.7	292.9	0.093	109.1
730	62.2	9.9	A	0.6	287.7	0.080	52.8
335	43.1	5.0	A	1.0	344.8		
336	52.3	1.4	A	- 7.6	320.0	0.12	- 22.7
642			A	3.5	342.2		- 38.8
1459	42.4	18.4	A	- 1.6	318.2	0.22	121.6
1458	43.1	10.6	A	9.3	1.2	0.045	64.6
1606	42.4	14.1	A	- 8.1	344.8	0.24	135.7
1460	43.1	16.3	A	-14.7	342.7	0.34	132.0

Table 7. Summary of tidal analysis -M_2 component. [1](C - clockwise, A - anti-clockwise)

Current meter	Rotary Velocity Components					Salinity	
	Semi-major axis (cm/sec)	Semi-minor axis (cm/sec)	Sense[1] of rotation	Direction major axis	Phase	Magnitude (PPT)	Phase
338	41.7	2.1	C	-10.6	204.5	0.25	-106.1
731	58.0	0.0		5.5	183.5	0.093	- 81.5
639	31.8	0.7	A	8.5	191.5	0.13	-101.3
337	41.0	1.4	C	- 0.5	190.7	0.18	-110.9
643	50.2	5.0	C	3.8	175.1	0.27	25.0
333	12.2	1.2	A	4.9	299.8		
739	36.8	0.0		- 2.5	194.4	0.16	-102.4
644	38.2	7.1	C	12.6	184.9	0.10	33.2
738	47.4	5.0	C	5.7	181.6	0.11	21.0
730	52.3	1.4	C	3.2	180.4	0.073	- 60.6
335	19.1	2.1	A	15.5	206.0		
336	29.0	0.7	C	- 1.5	201.5	0.14	-109.6
642			A	17.1	195.6		-136.6
1459	25.5	4.2	C	16.3	192.9	0.25	34.7
1458	15.2	1.8	A	32.1	268.0	0.076	228.2
1606	15.4	3.0	A	2.5	243.4	0.25	46.0
1460	19.1	3.5	A	16.3	194.7	0.44	40.5

Table 8. Summary of tidal analysis $-K_1$ component. [1](C - clockwise, A - anti-clockwise)

Since we anticipated that magnitudes of the tidal constituents would be affected more than their phases the former are excluded from Tables 7 and 8 but tha latter are included.

Figure 27a shows the distribution across Haro Strait of the length of the semi-major axis of the M_2 tidal velocity ellipse. Velocities are highest in the top 100m of the eastern side of the strait where magnitudes reach almost 70 cm/sec. At current meters deeper and at current meters further west the magnitudes decrease to the order of 40 cm/sec. The magnitude of the semi-minor axis of the M_2 velocity ellipse is considerably smaller than the magnitude of the semi-major axis of the ellipse indicating that the M_2 tidal motion is predominantly back and forth. The velocity ellipses from several current meters on the western side of the strait have semi-major axis of size approaching 1/3 the size of the semi-major axes.

The phases of the M_2 velocity ellipses across Haro Strait are shown in Figure 27b. These phases are less than 300^o in the top 40m from the middle of the current meter array to the eastern side of the strait. At increasing depths the phases increase to over 340^o. Likewise, the phases show a considerable increase towards the western side of the strait. Meter #333 at 100m on the most western mooring has a phase almost 100^o ahead of meter #731 at 40m on the opposite side of the strait.

As anticipated the magnitudes of the K_1 fluctuations of velocity are less than the M_2 magnitudes. Like the M_2 component of tidal velocity, the K_1 tidal ellipses have their largest semi-major axes and their smallest phase values in the surface layer of the eastern side of the strait where magnitudes of over 50 cm/sec are attained. Figure 28 shows the distribution of the semi-major axes and phases of the K_1 tidal component in the cross section of Haro Strait. The relative magnitudes of the M_2 and K_1 velocity components and phases at a given location are seen to be not all constant over the cross section of the strait.

5. Current Meter Power Spectra

The results of the power spectral analysis of longitudinal velocity, of transverse velocity and of salinity are presented in Figures 29 to 35. In each case the log of the frequency multiplied by the energy density (or power) is plotted versus the log of frequency (i.e., log $f \cdot P(f)$ is plotted versus log f). It should be noted that the spectral analysis was based on blocks each 7.00 days long. Therefore, the K_1 component which has a period of 23.93 hours (close to 24 hours), should be fairly well represented by the analysis. Conversely, the M_2 component of period 12.42 hours which has 13.53 cycles in each 7 day block has a frequency which lies approximately halfway between 2 Fourier harmonics and so will be poorly represented in this analysis. Furthermore the application of the S_{149} filter prior to the analysis will effectively remove most of the energy at the M_2 frequency and its harmonics. Chang (1976) in an analysis of current meter records in Haro Strait has shown that the magnitudes of the tidal harmonics of current velocity, temperature and conductivity are much diminished at frequencies greater than 4 cycles per day. Hence, it is considered that the estimation of power spectra and coherences of current meter records by the spectral analysis technique used in this study should be appropriate to frequencies above 4 cycles per day (or log f = 0.6).

5a. Spectra of Longitudinal Velocities

The spectra of longitudinal velocity from the different current meters show a considerable degree of similarity at frequencies above 4 cycles per day. They all show a steady decrease with increasing frequency which has an approximately power law form. Although the slopes of the spectra vary somewhat an average relationship between power and frequency would be something near $P(f) \alpha f^{-2}$.

The levels of this high frequency part of the spectrum seem to correlate with the magnitudes of the tidal constituents. Like the tidal constituents the highest spectral levels were observed to occur in data from current meters on the eastern side of Haro Strait. Spectral levels at meters #338 and #638 on the most eastern mooring in the strait were of the order of 5 times those at meters #1460, #1606 and #333 on the most western mooring.

5b. Spectra of Transverse Velocities

Like the spectra of longitudinal velocity the spectra of transverse velocity steadily decrease at frequencies above 4 cycles per day. On the western side of the strait the longitudinal and transverse velocity spectra are very similar to one another both in shape and in level; the transverse velocity power seems to decrease as f^{-2}. For the current meters in the middle of the strait and towards its eastern side the transverse velocity spectrum starts as $P(f) \alpha f^{-2}$ but at frequencies above about 50 cycles per day (or log f = 1.7) the spectrum begins to turn downwards. Meters #338 and #638 on the most eastern mooring have a somewhat different transverse velocity spectrum. Even though their longitudinal velocity spectra decrease as approximately $P(f) \alpha f^{-2}$ for f> 4 cycles per day the transverse velocity spectra start by decreasing as $P(f) \alpha f^{-1}$. However, at frequencies above 50 cycles per day the transverse velocity spectra for these 2 meters show a similar drop off to that exhibited by some of the other meters.

5c. Spectra of Salinities

Almost all of the plots of salinity spectra show a slow power law decrease in $f \cdot P(f)$ at frequencies above 4 cycles per day. From the plots an average relationship of salinity with frequency would be estimated as $P(f) \alpha f^{-1.3}$ in this part of the spectrum. The last 2 points on each plot "turn up" indicating the presence of aliased high frequency energy at the highest frequencies. The salinity spectrum for meter #1460 looks somewhat different from the others; P(f) for this meter decreases somewhat more slowly at frequencies above 4 cycles per day. Also, the greater "turn up" of the 2 spectral estimates at the highest frequencies would indicate that this spectrum is perhaps altered more than the others by aliased noise.

The levels of the salinity spectra vary somewhat between meters. Meter #638, the deepest meter on the most eastern mooring, shows the lowest spectral level of any meter while those meters nearest the surface show the highest levels. The range of spectral levels is of the order of a factor of 4.

5d. Current Meter Coherence Spectra

Figures 36 to 48 show the coherences and phases between longitudinal

velocities, transverse velocities and salinities for selected pairs of current meters in Haro Strait. The coherence, plotted on a linear scale versus the log of frequency, represents the coherence of energy between 2 time series rather than an amplitude coherence. On each plot is indicated the level of noise coherence for each frequency appropriate to the number of blocks analysed and the number of FFT harmonics in each frequency band. Two data sequences will be considered incoherent over a given frequency range if the coherence estimates lie scattered on both sides of the noise coherence level. Also, the phases between 2 incoherent data sequences tend to lie scattered between 180° and -180° in a random fashion. As an example, the longitudinal velocities for current meters #335 and #637 appear to be incoherent over most of the frequency range analysed (see Figure 42). Conversely, a pair of current meters which exhibits coherences which tend to lie above the noise coherence level and phases which are clustered near one another, might be considered to be coherent to a greater or lesser extent. The longitudinal velocities for current meters #738 and #335 are coherent between frequencies of 1 cycle per day (log f = 0.0) and 12 cycles per day (log f = 1.1). A positive phase between 2 current meters means that the second named current meter in the caption of the plot leads the first.

In the present study the coherences between current meters were observed to be highest between current meters around the diurnal and semi-diurnal frequencies, that is, near the prominent tidal frequencies. In fact, for cyclic deterministic processes such as the tide's, coherences should be high if long records are used for the analysis. The present analysis which uses only 7 day blocks and an M_2 tidal removal filter probably does not accurately represent the true coherences at the tidal frequencies. At higher frequencies all the coherences drop off at a rate similar to the decrease in level of the noise coherence. Some pairs of current meters become largely incoherent at frequencies little above the semi-diurnal frequency whereas others maintain significant coherences to fairly high frequencies even though these coherences are not necessarily large.

Results of Thermistor Chain Analysis

1. Thermistor Chain Time Series

Figure 49 shows 2 weeks of the time series from thermistor chain data sets T63/17 and T93/18 between July 20, 1976 and August 4, 1976. In each case the bottom trace represents the data from the deepest thermistor, located at 55m. The traces above provided the temperature data from progressively shallower thermistors. The data from each termistor is offset by $+1.0^{\circ}C$ with respect to the data from the thermistor immediately below. Thus the top trace for data set T63/17 gives the temperature data from 10m offset by $9.0^{\circ}C$, and the top trace on T93/18 gives data from 5m offset by $10.0^{\circ}C$.

Comparison of data from T63/17 and T93/18 indicates that temperatures at depths to 55m are higher by the order of $1^{\circ}C$ at station TA2 than they are at station TA1. This is consistent with the observation of lower surface salinities in the northern part of Haro Strait and of the occurrence of a negative T,S relationship during the summer months. Although neither thermistor chain exhibits large amounts of energy at the diurnal frequency the variances at higher frequencies show a pronounced diurnal cycle. Temperature changes occurring at the top thermistor are generally reflected

in changes at all the thermistors in a given chain even though the magnitudes of these changes are diminished with depth.

2. Results of the Analysis of Two 25-hour Sections of Thermistor Chain Data

Two 25-hour sections of data from thermistor chains T63/17 and T93/18 are presented in Figure 50. These sections of data which have been passed by the low pass filter A_4A_6 coincide with the CTD Time Series #1 and Time Series #2 on July 26, 27, 1976 and August 3, 4, 1976, respectively. Each plot includes data from the thermistors at 10m, 30m and 55m.

3. Temperature Power Spectra

The power spectra computed for data sets T63/17, T93/18 and T93/19 are shown in Figure 51. These power spectra are presented for 10m, 30m and 55m depths for the first two data sets and for 5m, 30 and 55m for data set T93/19. The temperature spectra are quite similar to the salinity spectra from the current meters. For temperature $f \cdot P(f)$ increases from low frequencies to reach a local maximum at the diurnal and semi-diurnal frequencies. At higher frequences $f \cdot P(f)$ slowly decreases as the Nyquist frequency is approached in the case of T63/17 and T93/18. The spectral analysis for T93/19 which carries the spectrum out to higher frequencies than for T63/17 or T93/18 indicates a downturn in $f \cdot P(f)$ at log f greater than 1.5 or equivalently greater than f equal to 30 cycles per day. The rate of decrease of P(f) at these higher frequencies appears to something like f^{-2}. A line for which $P(f) \alpha f^{-2}$ is indicated for T93/19 on Figure 51. It would seem probable that the other spectra of temperature and salinity would show a similar downturn at frequencies greater than 30 cycles per day if it were not for the effects of the aliasing of energy from frequencies above their Nyquist frequencies.

For thermistor chains T63/17 and T93/18 the level of the spectrum decreases slightly with depth, the level of the spectrum for T39/18 being similar to that of T63/17. In contrast, the spectral levels for T93/19 are highest for the thermistor at 5m depth and lowest for the middle thermistor at 30m. However, the spectral analysis of T93/19 covers only 2 days of data while the spectral analysis of T63/17 and T93/18 covers 14 days.

4. Coherences Between Thermistor Chains T67/17 and T93/18

Figure 52 shows the coherences and phases between thermistors at depths of 10m, 30m and 55m on thermistor chain data sets T63/17 and T93/18. There appear to be almost as many coherence values scattered below the noise coherence level as above. Also, the phases between the 2 chains are scattered between -180° and $+180^{\circ}$. One might have expected that the diurnal and semi-diurnal components would have reasonable coherences. At 55m, in fact, both these components have coherences somewhat above the noise coherence level yet the 10m semi-diurnal component and the 30m diurnal component are below the noise coherence level.

Results of CTD Time Series

1. T,S Diagrams

Figure 53 shows a comparison of the T,S relationships observed in the CTD Time Series #1 and Time Series #4 on July 26, 27 and September 8, 9, respectively. The data points on this plot were selected to include the range of temperatures and salinities encountered on each time series. The T,S relationship for both time series is fairly linear which allows the use of salinity alone to define water properties over short periods of time. The line: T (in deg C) = 0.79 S (in PPT + 33.6^{o}C is provided as a possible fit to the data from Time Series #1. The slope of the T,S relationship observed for Time Series #2 and #3 (not shown) becomes less steep until for Time Series #4 the slope is reduced to approximately -0.73^{o}C/PPT. For the period of operation of the thermistor chains T63/17 and T93/18 the T,S relationship of Time Series #1 is considered the most appropriate whereas CTD Time Series #4 coincides with the last deployment of a thermistor chain, that is, T93/19.

2. Time Series #1

Figure 54a shows the interpolated Time Series #1 plotted with the average interpolated profile for comparison. This time series collected on July 26-27, 1976 coincides with a period when the tides in Haro Strait are relatively large (see Figure 9). It is evident that large changes in the water structure from the surface to the bottom occur over a 24-hour period. On average the salinity increases smoothly with depth from 30.3 PPT at the surface to 32.6 PPT at 300m. Most striking perhaps is the occurrence of what appears to be a mixed layer of salinity about 30.9 PPT and of thickness 250m at 1600 on July 26. Figures 20 to 26 are plots of the current meter data during Time Series #1 showing that the phases of the current vary considerably across Haro Strait. However, in the eastern part of the strait where Time Series #1 was taken the currents at 1600 July 26 are near their maxima towards the north being over 100 cm/sec. The currents experience a local maximum towards the south at 2100 July 26 and a local maximum towards the north at 0200 July 27. Both of these maxima are of the order of 50 cm/sec. At these two times the salinity profiles are similar to the average profile. Later the current begins to flow towards the south to reach a maximum velocity of approximately 100 cm/sec at 0900 July 27. At this time salinities in the top 10m or so are lower than average, but below this depth salinities are higher than average by the order of 0.5 PPT. The last profile at 1100 July 27 is similar to the first in this time series at 1200 July 26.

3. Time Series #2

Figure 54b shows the interpolated Time Series #2 which was collected on August 3-4, 1976. The averaged profile for Time Series #2 is similar to that of Time Series #1. Time Series #2 shows lower salinities in the top 50m by less than 0.5 PPT and higher salinities below this depth. At 200m the difference in salinity of the two average profiles is of order 0.2 PPT. Like Time Series #1, Time Series #2 shows pronounced changes in salinity from the surface to the bottom during the 24-hour period. The plots of currents for this period (Figures 20 to 26) show pronounced phase shifts with depth hence it is difficult to define tidal phases for these currents. However, one might consider the two maximum northerly and southerly currents as occurring at 1100 August 3, 1976 and at 0200 August 4, respectively and secondary maxima occurring in the northerly and southerly directions at 2100 August 3 and at 1600 August 3, respectively. Although Time Series #2 at no time exhibits a deep "mixed" layer as does Time Series #1 at times of the maximum

northerly set of the current the salinities are lower than average at all depths. Likewise when the current achieves its maximum towards the south salinities in the top 10m are lower than average whereas those below this depth are higher than average.

4. Time Series #4

Current meters were not operating in Haro Strait on September 8-9, 1976 when Time Series #4 was taken. However, tidal current predictions are available at Turn Point on Haro Strait to the north of the study area (see Figure 1 and Table 9). The maximum northward flowing currents, all of similar size, occur at 1505 September 8, 0325 September 9 and 1535 September 9. The maximum currents flowing in the southern direction which are also of similar size to one another occur at 0755 September 8, 2025 September 8 and 0840 September 9. The magnitudes of the maximum currents are less than those encountered on July 26, 27.

Figure 55 shows the longitudinal sections of the salinity structure along Haro Strait for Time Series #4 at intervals of 4 hours. Generally, the isohalines go deeper as one travels northward from F1 to F6. The depths of the isohalines have a "bumpy" character which is sometimes reflected in the depths of neighbouring isohalines and sometimes not. Many of the bumps are likely due to the influence of internal waves on individual CTD drops. It is evident that the salinity structure in the strait undergoes considerable variation during a 24-hour period. At 1630 September 8 which would be an hour or so after maximum northward current salinities of 32.5 PPT were observed at Station F1 only but at 0430 September 9, 12 hours later at a similar phase of the tide, the 32.5 PPT isohaline extended all the way from F1 to F6. The depth of the relatively low salinity isohalines near the surface exhibits a definite dependence on tidal phase. At 1230 September 8 and 0030 September 9, times near slack between southward and northward flowing current, the 30.0 PPT isohaline surfaces somewhere south of F1 while at the other times it surfaces north of F1.

Presentation of Anemometer Data

Figure 56 shows the time series for the anomometer D85/8, situated at Station TA2. The section of data presented lies between July 14, and August 19, 1976. On Figure 56 are plotted wind speed in cm/sec (x10), wind direction in degrees true and ambient air temperature in degrees centigrade.

TURN POINT (PST −8)

CURRENT TABLES

1976

JULY-JUILLET

Turns		Maximum		Renverse		Maximum	
Day	Time	Time	Rate/kn	Jour	Heure	Heure	Vit/n
1		0000	−0.8	16		0045	−1.2
	0305	0500	+0.4		0445	0620	+0.2
TH	0650	1120	−1.8	FR	0800	1210	−1.1
JE	1455	1810	+1.5	VE	1515	1830	+1.1
	2150				2200		
2		0055	−1.1	17		0135	−1.4
	0415	0600	+0.3		0610	0750	+0.1
FR	0755	1225	−1.4	SA	0930	1310	−0.8
VE	1535	1845	+1.3	SA	1545	1900	+0.9
	2225				2240		
3		0145	−1.5	18		0215	−1.5
	0535	0720	+0.3		0745	0955	+0.2
SA	0935	1325	−1.1	SU	1140	1405	−0.5
SA	1610	1920	+1.2	DI	1610	1920	+0.7
	2305				2315		
4		0230	−1.8	19		0300	−1.6
	0655	0945	+0.4		0840	1105	+0.5
SU	1150	1425	−0.9	MO	1315	1455	−0.3
DI	1645	2000	+1.0	LU	1635	1930	+0.6
	2345				2355		
5		0320	−2.1	20		0335	−1.8
	0805	1105	+0.8		0920	1155	+0.7
MO	1330	1525	−0.6	TU		1540	*
LU	1720	2055	+0.9	MA		1940	+0.5
6	0025	0405	−2.4	21	0025	0415	−1.9
	0900	1205	+1.1		0955	1240	+0.9
TU	1445	1620	−0.4	WE		1630	*
MA	1800	2225	+0.8	ME		2000	+0.5
7	0105	0450	−2.6	22	0100	0455	−2.1
	0945	1250	+1.4		1020	1315	+1.1
WE		1710	*	TH		1720	*
ME		2340	+0.8	JE		2040	+0.4
8	0150	0535	−2.8	23	0140	0530	−2.2
	1030	1335	+1.7		1050	1350	+1.3
TH		1800	*	FR		1800	*
				VE		2140	+0.4
9		0030	+0.8	24	0220	0610	−2.3
	0235	0620	−2.8		1115	1420	+1.4
FR	1110	1415	+1.8	SA		1850	*
VE	1740	1900	−0.3				
	2050						
10		0120	+0.8	25		0110	+0.5
	0320	0705	−2.8		0300	0650	−2.4
SA	1150	1455	+1.9	SU	1140	1450	+1.5
SA	1820	1955	−0.4	DI	1800	1930	−0.4
	2230				2135		
11		0210	+0.8	26		0150	+0.6
	0405	0750	−2.6		0345	0735	−2.4
SU	1230	1535	+1.9	MO	1210	1525	+1.6
DI	1900	2055	−0.5	LU	1830	2020	−0.5
					2305		
12	0005	0255	+0.7	27		0235	+0.7
	0450	0835	−2.4		0435	0820	−2.3
MO	1305	1610	+1.8	TU	1245	1555	+1.6
LU	1935	2200	−0.7	MA	1900	2115	−0.7
13	0115	0340	+0.7	28	0025	0320	+0.7
	0535	0925	−2.1		0520	0905	−2.1
TU	1340	1645	+1.7	WE	1315	1625	+1.6
MA	2010	2300	−0.8	ME	1935	2210	−1.0
14	0225	0430	+0.6	29	0135	0405	+0.7
	0620	1020	−1.8		0615	1000	−1.9
WE	1415	1720	+1.5	TH	1350	1655	+1.5
ME	2045	2355	−1.0	JE	2005	2310	−1.2
15	0330	0520	+0.4	30	0240	0500	+0.7
	0705	1115	−1.4		0715	1100	−1.6
TH	1445	1800	+1.3	FR	1425	1730	+1.4
JE	2125			VE	2045		
				31		0010	−1.5
					0345	0600	+0.6
				SA	0825	1205	−1.2
				SA	1500	1805	+1.3
					2120		

AUGUST-AOUT

Turns		Maximum		Renverse		Maximum	
Day	Time	Time	Rate/kn	Jour	Heure	Heure	Vit/n
1		0105	−1.7	16		0130	−1.5
	0455	0715	+0.6		0600	0900	+0.4
SU	1005	1310	−0.9	MO	1130	1340	−0.4
DI	1540	1840	+1.1	LU	1540	1825	+0.6
	2205				2155		
2		0200	−2.0	17		0215	−1.6
	0610	0915	+0.6		0715	1030	+0.5
MO	1200	1410	−0.7	TU	1300	1435	−0.3
LU	1615	1915	+0.9	MA	1610	1840	+0.5
	2250				2235		
3		0250	−2.2	18		0300	−1.7
	0720	1045	+0.9		0815	1125	+0.7
TU	1330	1510	−0.5	WE		1520	*
MA	1655	2005	+0.8	ME		1900	+0.4
	2345				2325		
4		0340	−2.4	19		0340	−1.8
	0825	1145	+1.2		0900	1205	+0.9
WE		1600	*	TH		1610	*
ME		2205	+0.6	JE		1940	+0.3
5	0040	0430	−2.5	20	0020	0425	−1.9
	0920	1230	+1.4		0935	1245	+1.1
TH	1535	1700	−0.4	FR		1650	*
JE	1845	2330	+0.7	VE		2340	+0.3
6	0130	0515	−2.5	21	0115	0505	−2.0
	1010	1315	+1.6		1005	1320	+1.2
FR	1620	1750	−0.4	SA	1605	1735	−0.4
VE	2000			SA	1940		
7		0030	+0.7	22		0025	+0.4
	0225	0600	−2.5		0210	0545	−2.1
SA	1050	1355	+1.7	SU	1035	1350	+1.3
SA	1655	1840	−0.5	DI	1635	1820	−0.6
	2140				2055		
8		0120	+0.8	23		0110	+0.6
	0315	0645	−2.4		0300	0630	−2.2
SU	1130	1430	+1.7	MO	1105	1420	+1.4
DI	1730	1930	−0.7	LU	1705	1905	−0.8
	2305				2210		
9		0205	+0.9	24		0150	+0.8
	0405	0730	−2.2		0350	0715	−2.1
MO	1205	1505	+1.7	TU	1140	1450	+1.4
LU	1805	2020	−0.8	MA	1730	1950	−1.0
					2320		
10	0005	0250	+0.9	25		0235	+0.9
	0450	0815	−2.0		0440	0800	−2.0
TU	1240	1540	+1.6	WE	1210	1520	+1.4
MA	1835	2110	−1.0	ME	1800	2040	−1.3
11	0105	0335	+0.8	26	0020	0320	+1.0
	0540	0900	−1.7		0535	0850	−1.8
WE	1310	1615	+1.4	TH	1245	1550	+1.4
ME	1905	2205	−1.1	JE	1830	2130	−1.5
12	0200	0420	+0.8	27	0120	0405	+1.1
	0625	0950	−1.4		0630	0940	−1.5
TH	1345	1645	+1.3	FR	1320	1620	+1.3
JE	1940	2300	−1.2	VE	1905	2225	−1.7
13	0250	0505	+0.6	28	0215	0455	+1.1
	0715	1045	−1.1		0735	1040	−1.2
FR	1415	1715	+1.1	SA	1355	1655	+1.2
VE	2010	2350	−1.3	SA	1940	2325	−1.9
14	0350	0555	+0.5	29	0315	0555	+1.0
	0815	1145	−0.8		0855	1150	−0.9
SA	1440	1745	+0.9	SU	1450	1730	+1.1
SA	2045			DI	2020		
15		0045	−1.4	30		0025	−2.0
	0450	0700	+0.4		0420	0705	+0.9
SU	0940	1245	−0.6	MO	1030	1300	−0.7
DI	1510	1805	+0.7	LU	1515	1805	+0.9
	2120				2105		
				31		0125	−2.1
					0525	0845	+0.9
				TU	1200	1400	−0.6
				MA	1605	1850	+0.7
					2200		

SEPTEMBER-SEPTEMBRE

Turns		Maximum		Renverse		Maximum	
Day	Time	Time	Rate/kn	Jour	Heure	Heure	Vit/n
1		0220	−2.2	16		0220	−1.6
	0635	1015	+1.1		0630	1040	+0.8
WE	1315	1500	−0.5	TH	1330	1505	−0.4
ME	1700	1945	+0.5	JE	1705	1840	+0.2
	2305				2120		
2		0315	−2.2	17		0305	−1.7
	0740	1115	+1.3		0730	1125	+0.9
TH	1410	1555	−0.5	FR	1410	1550	−0.4
JE	1810	2215	+0.5	VE	1805	1930	+0.2
					2335		
3	0015	0405	−2.2	18		0355	−1.7
	0840	1205	+1.4		0820	1205	+1.0
FR	1455	1645	−0.6	SA	1440	1635	−0.6
VE	1940	2335	+0.6	SA	1920	2335	+0.3
4	0125	0455	−2.1	19	0100	0440	−1.8
	0935	1245	+1.5		0900	1240	+1.1
SA	1530	1735	−0.8	SU	1510	1715	−0.8
SA	2115			DI	2035		
5		0030	+0.8	20		0025	+0.5
	0225	0540	−2.0		0205	0525	−1.8
SU	1020	1325	+1.5	MO	0940	1310	+1.2
DI	1605	1820	−0.9	LU	1540	1800	−1.1
	2225				2140		
6		0120	+0.9	21		0105	+0.7
	0320	0625	−1.9		0305	0610	−1.6
MO	1100	1400	+1.5	TU	1015	1340	+1.2
LU	1635	1900	−1.1	MA	1605	1840	−1.4
	2315				2230		
7		0205	+1.0	22		0150	+1.0
	0410	0710	−1.7		0400	0655	−1.7
TU	1135	1435	+1.4	WE	1050	1410	+1.2
MA	1705	1945	−1.3	ME	1635	1920	−1.6
					2320		
8	0000	0245	+1.1	23		0230	+1.2
	0500	0755	−1.5		0455	0740	−1.5
WE	1210	1505	+1.3	TH	1125	1440	+1.2
ME	1735	2025	−1.4	JE	1705	2010	−1.9
9	0045	0325	+1.1	24	0015	0315	+1.4
	0545	0840	−1.3		0550	0830	−1.3
TH	1240	1535	+1.1	FR	1205	1515	+1.2
JE	1805	2115	−1.5	VE	1735	2055	−2.1
10	0130	0410	+1.0	25	0105	0405	+1.4
	0635	0925	−1.0		0650	0925	−1.1
FR	1310	1605	+1.0	SA	1245	1545	+1.1
VE	1830	2200	−1.5	SA	1810	2150	−2.2
11	0215	0450	+0.9	26	0155	0450	+1.5
	0730	1020	−0.8		0800	1030	−0.8
SA	1340	1635	+0.8	SU	1325	1620	+1.0
SA	1900	2250	−1.5	DI	1845	2245	−2.2
12	0300	0535	+0.8	27	0250	0545	+1.4
	0830	1120	−0.6		0915	1145	−0.7
SU	1410	1655	+0.7	MO	1415	1700	+0.9
DI	1925	2345	−1.5	LU	1925	2350	−2.2
13	0350	0625	+0.7	28	0345	0650	+1.3
	0950	1225	−0.4		1040	1255	−0.6
MO	1445	1720	+0.5	TU	1510	1745	+0.7
LU	1950			MA	2010		
14		0040	−1.6	29		0050	−2.2
	0440	0740	+0.6		0445	0805	+1.2
TU	1120	1325	−0.3	WE	1150	1355	−0.6
MA	1525	1740	+0.4	ME	1615	1830	+0.5
	2015				2105		
15		0130	−1.6	30		0150	−2.1
	0535	0930	+0.7		0545	0930	+1.2
WE	1235	1420	−0.3	TH	1245	1450	−0.7
ME	1610	1805	+0.3	JE	1735	2000	+0.3
	2040				2230		

V-5

* WEAK AND VARIABLE, OR MINIMUM RATE / VITESSE MINIMUM, OU FAIBLE ET VARIABLE

+ FLOOD/FLOT DIRECTION 030–080 TRUE/VRAI – EBB/JUSANT DIRECTION 210–260 TRUE/VRAI

64

Table 9. Tidal current predictions for Turn Point (from Canadian Tide and Current Tables, Vol. 5, 1976, Environment Canada).

SUMMARY AND CONCLUSIONS

The physical oceanographic study of Haro Strait undertaken between July 5, 1976 and September 10, 1976 has pointed out several major features of the circulation through the strait at that time of year.

The study was consistent with previous observations that an estuarine type of circulation exists in Haro Strait; that is, a relatively fresh surface layer flows out of Haro Strait (towards the south) over more saline water flowing in. During the summer of 1976 the dividing line between the two flow regimes was observed to vary between 40m and 100m on the eastern side of the strait to greater than 100m on the western side. At each location average salinities, temperatures, longitudinal and transverse velocities were found to vary over a two weekly cycle presumably tied to the cycle of spring and neap tides. Following the period of spring tides vertical velocity, temperature and salinity gradients were found to be at their minima and following the neap tides they were at their maxima.

Water movements in Haro Strait were dominated by the tides; tidal currents were observed of strengths well over 1m/sec. The magnitudes of the 2 largest components, the M_2 and K_1, were largest in the top 100m on the eastern side of the strait and smallest on its western side. The tidal phases showed pronounced changes over the cross section of the strait. The smallest phases of both the M_2 and K_1 components occurred in the surface of the eastern side of the strait. Phases increased both with depth and towards the western side of the strait. In fact, for the M_2 component a phase difference of almost 100° was observed between 2 current meters in diagonally opposite positions in the strait's cross section.

Pronounced changes occur in the water characteristics in the whole water column of Haro Strait over the period of a day. Southward flowing tidal currents in the eastern side of the channel resulted in the appearence of lower than average salinities in the surface layer (compared to the average 24-hour profile) and higher than average salinities in deeper water. The change in surface salinities resulting from a southward current is consistent with the observation of a negative horizontal salinity gradient northwards along the axis of the strait but the increase in salinity in deeper layers seems anomalous. By contrast, northward flowing tidal currents in the strait seem to be associated with a lessening of vertical salinity gradients; the surface water is relatively saline while that below is realtively less aline compared to the average profile. On July 26, 1976, coinciding with the occurrence of spring tides, the maximum northward flowing tidal current was associated with the appearence of a 250m thick layer of almost uniform salinity in the southern end of the strait.

Above 4 cycles per day the power spectra of longitudinal and transverse velocities generally took on an approximately power law form, namely $P(f) \alpha f^{-2}$. At frequencies above 50 cycles per day there was usually a downturn in the transverse velocity spectra. Over that range of frequencies in which the power law form applied the spectra of longitudinal and transverse velocities were fairly similar in level to each another. From meter to meter, however, the velocity spectra varied in level, the highest levels being associated with the meters showing the largest tidal currents.

Like the velocity spectra, the salinity spectra all showed an approximately power law form above 4 cycles per day. In this case the power varied as $P(f) \alpha f^{-1.3}$ on average. However, the spectral analysis of data from a thermistor chain employing a sampling interval of 1.25 minutes instead of the 10 minutes used by the current meters indicated that above 30 cycles per day the temperature spectrum was closer to $P(f) \alpha f^{-2}$. The linear T,S relationship observed in the CTD data indicates that the temperature and salinity spectra should have almost the same shape. Hence, it would appear likely that the high frequency end of the salinity spectrum is adversely affected by aliased noise.

The primary purpose of this report is to point out major features of the circulation in Haro Strait in order to form a basis for interpretation and further analysis of the data. For example, we feel that important details of the momentum transfers and scales of events in Haro Strait could be derived from the construction of a turbulence model of the strait based upon the results of the spectral analysis and the analysis of coherence between current meters.

The effects on the results of current meters changing depths during periods of high current should be examined further. Unfortunately because the water characteristics in Haro Strait change considerably during the period when the meters are "pulled down" and because the tidal currents have different phases with depth the estimation of the effects on the data are not at all simple. In further field studies in Haro Strait we suggest that, if possible, the moorings be redesigned with lower drag and higher buoyancy. Another question which might be asked of the data is what is the nature and origin of the deep "mixed layer" which appeared in the southern part of Haro Strait when the current was flowing north on July 26, 1976? Does this phenomenon appear regularly during large spring tides? How does this body of water move during the tidal cycle? At least partial answers to these questions could be derived from further examination of the data as it already exists.

REFERENCES

Bennett, A.S. 1976. Conversion of *in situ* Measurements of Conductivity to Salinity. Deep Sea Research, Vol. 23, pp. 157-165.

Chang, P. 1976. Data Survey and Recommendations for an Oceanographic Study of Haro Strait, Report submitted to Coastal Zone Oceanography, Institute of Ocean Sciences, April, 1976, by Associated Engineering Services Ltd., Vancouver, B.C., Canada.

Fofonoff, N.P. 1962. Physical properties of sea water. The Sea, Vol. 1, edited by M.N. Hill. Interscience, New York - London, pp. 3-30.

Godin, G. 1972. The Analysis of Tides. University of Toronto Press, Toronto - Buffalo. 264 pp.

Jenkins, G.M. And D.G. Watts. 1968. Spectral Analysis and its Applications. Holden Day, San Francisco. 525 pp.

Mooers, C.N.K. 1973. A Technique for the Cross Spectrum Analysis of Pairs of Complex - Valued Time Series, with Emphasis on Properties of Polarized Components and Rotational Invariants. Deep Sea Research, Vol. 20, pp. 1129-1141.

Singleton, R.C. 1969. An Algorithm for Computing the Mixed Radix Fast Fourier Transform. IEEE Transactions on Audio and Electroacoustics, Vol. AU-17, pp. 93-103.

APPENDIX I - FIGURES 1 to 56

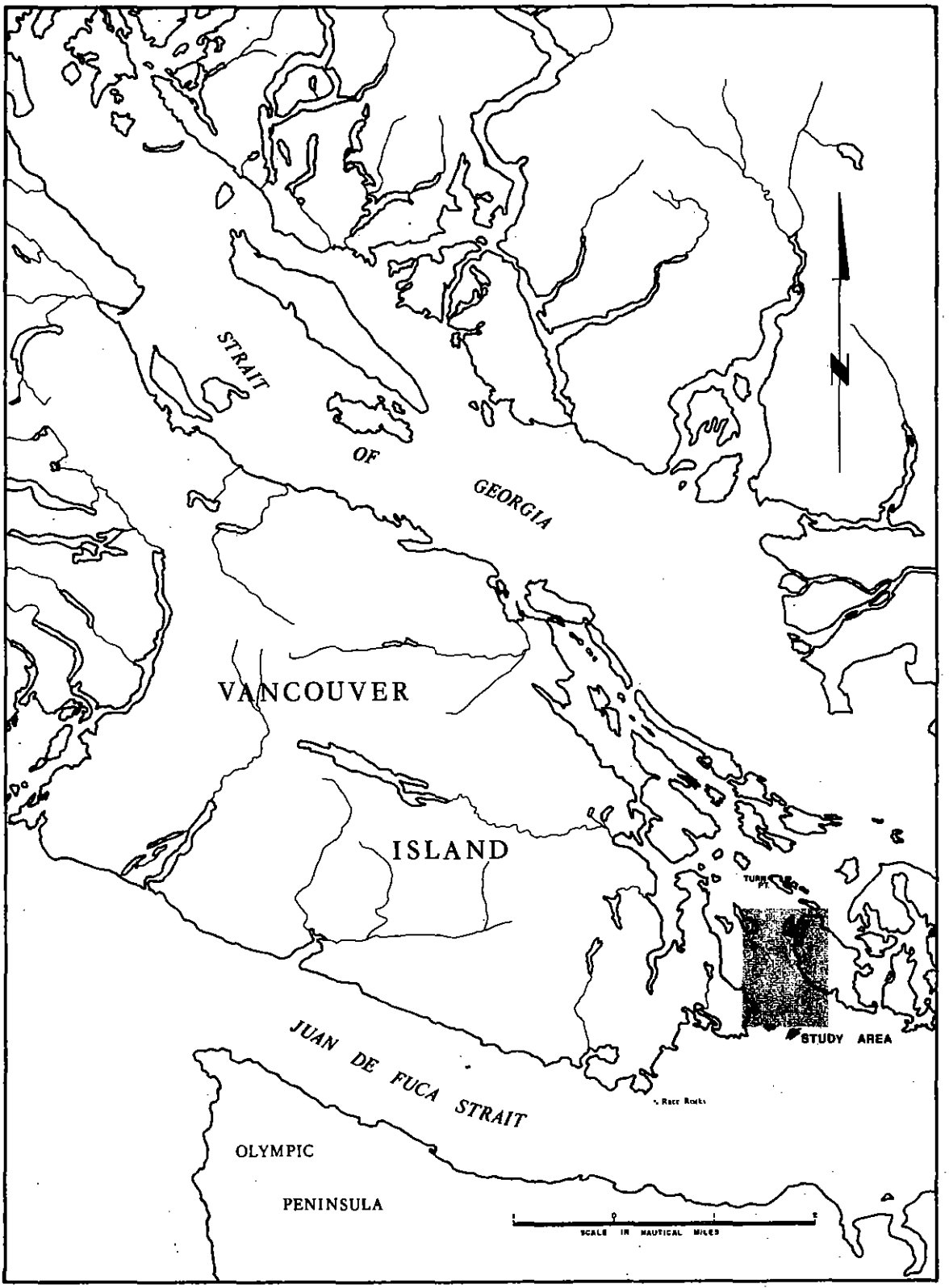

Figure 1. Map of southwestern British Columbia showing study area.

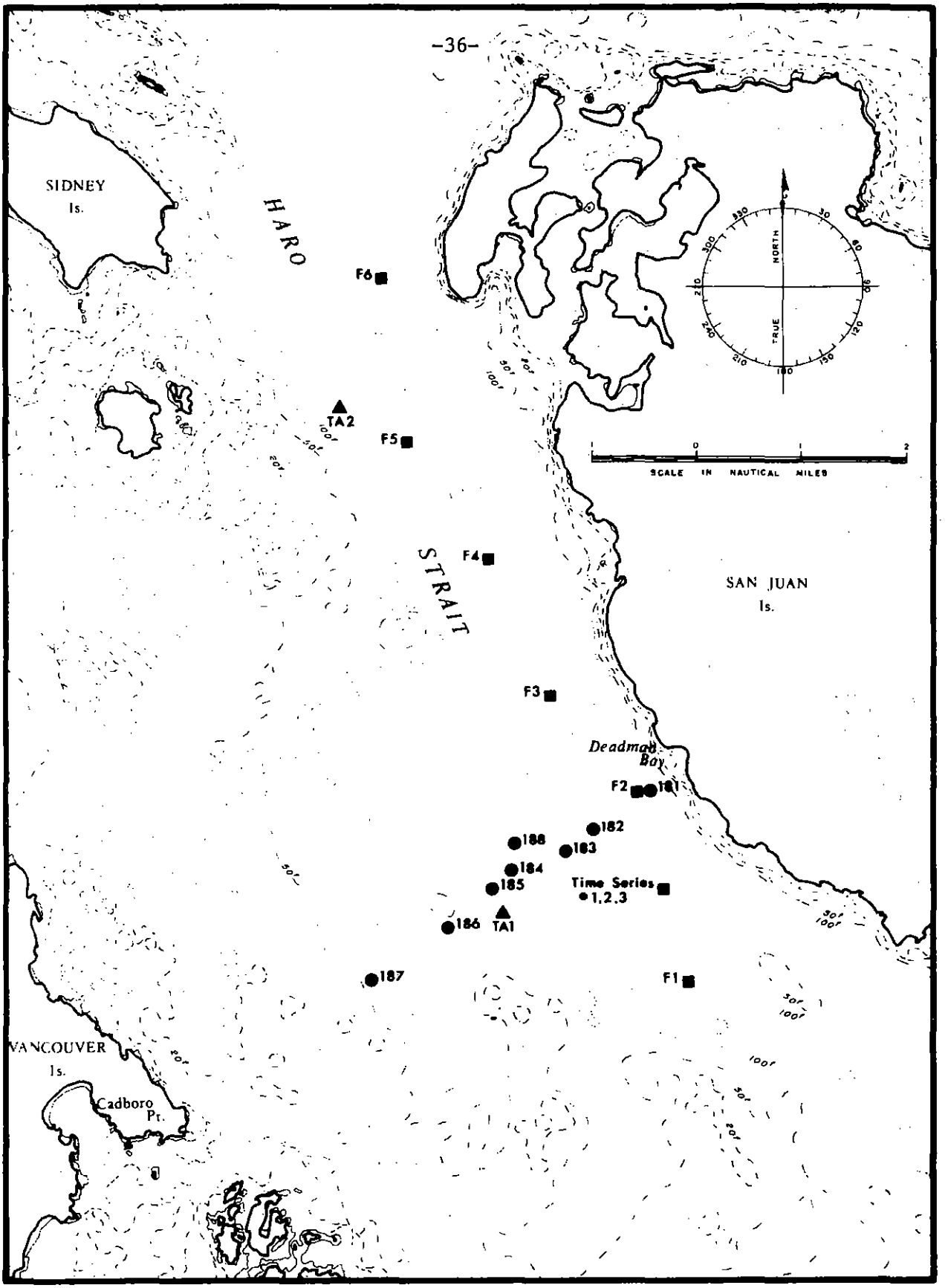

Figure 2. Map of Haro Strait showing locations of current meter moorings, thermistor chain anemometer moorings and CTD series.

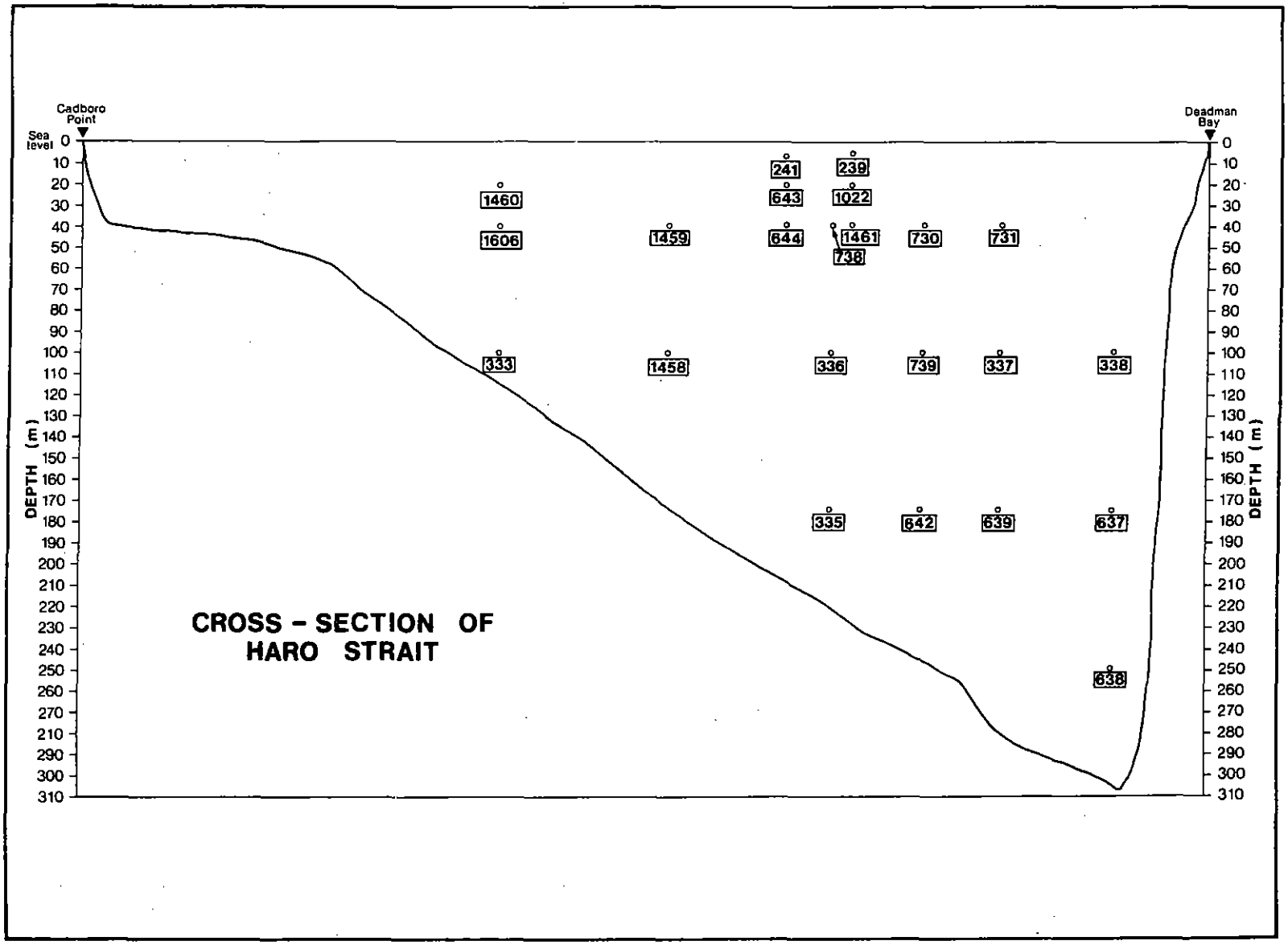

Figure 3. Cross section of Haro Strait between Cadboro Point and Deadman Bay with current meter location.

Figure 4. Schematic diagram of the mooring systems used in Haro Strait.

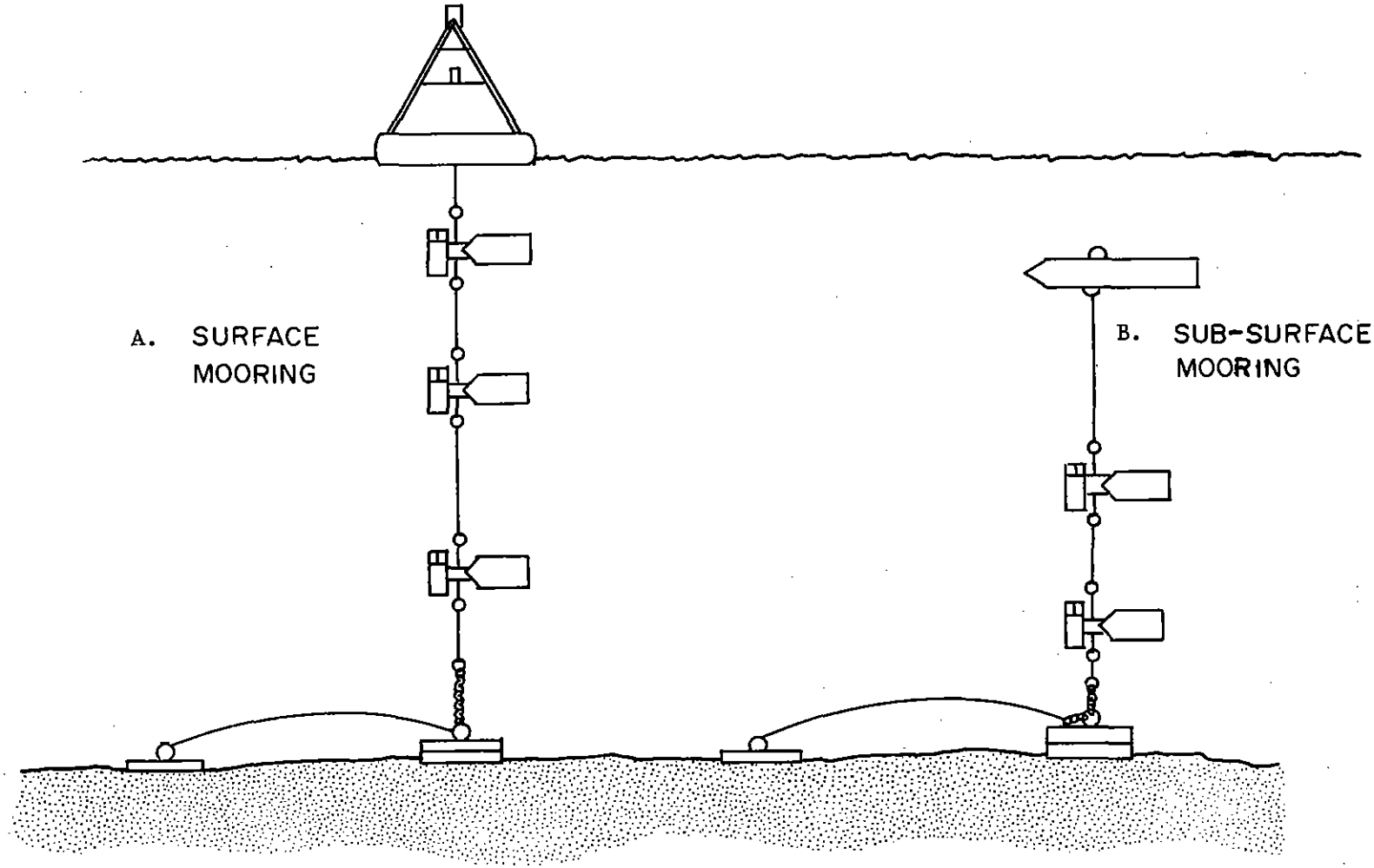

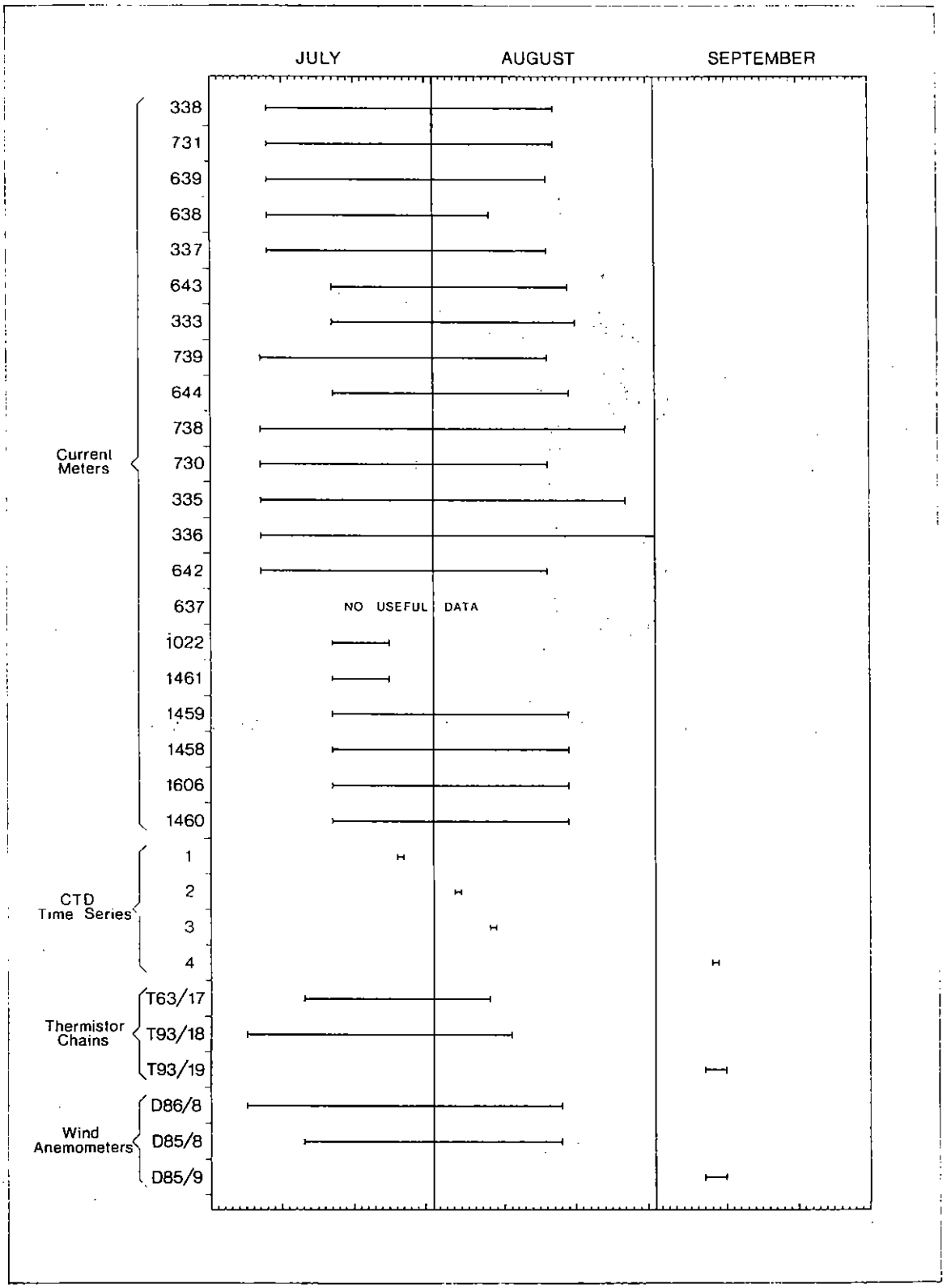

Figure 5. Bar graph showing periods of operation of the current meters, thermistor chains, anemometers and of the CTD time series.

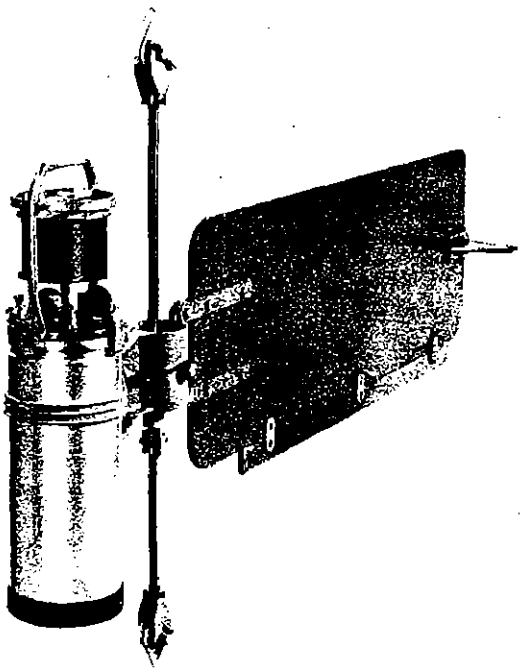

Figure 6. Photograph of an Aanderaa current meter (from Aanderaa Instruments Datasheet D147).

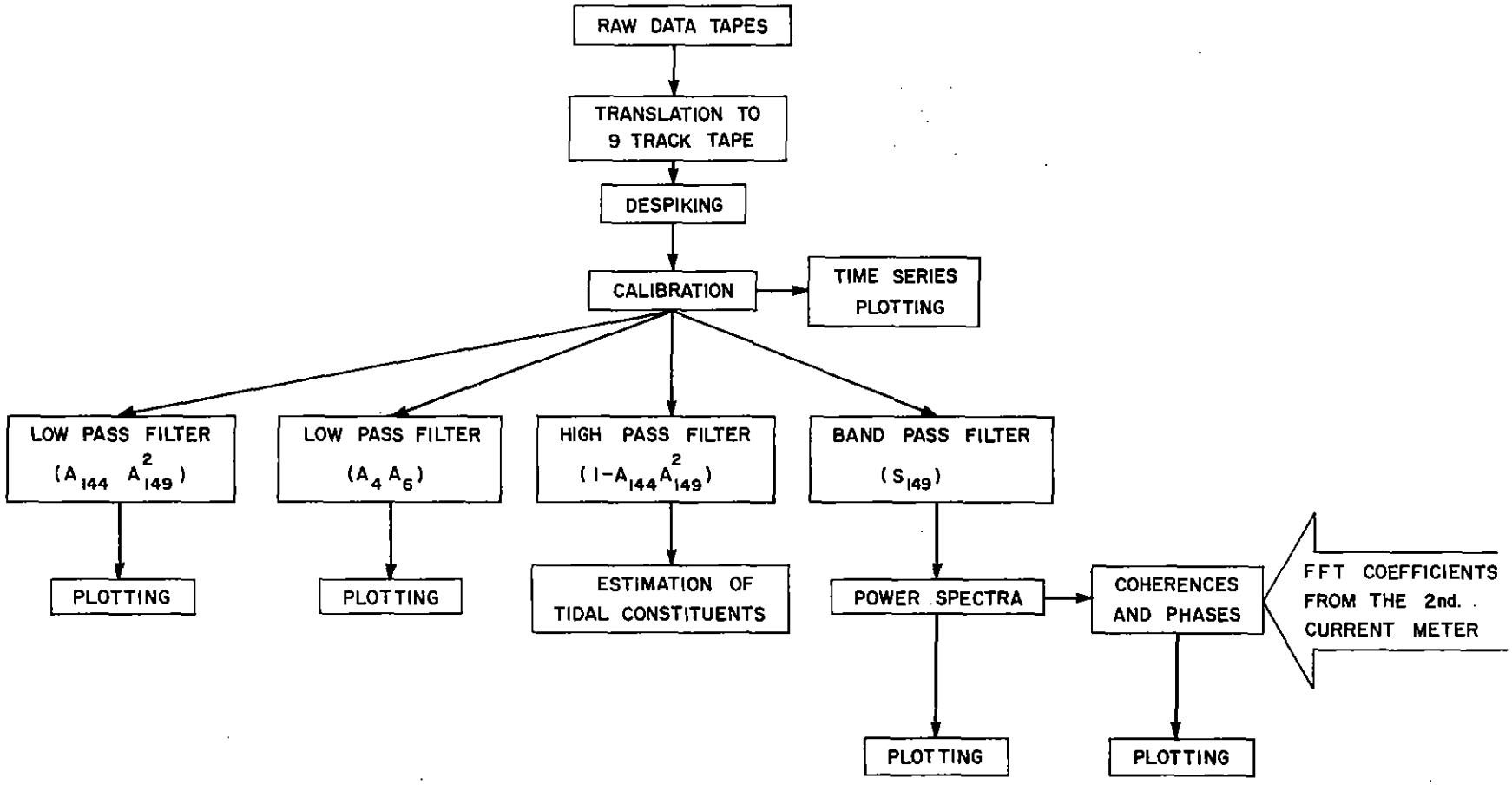

Figure 7. Schematic diagram of the analysis of current meter data.

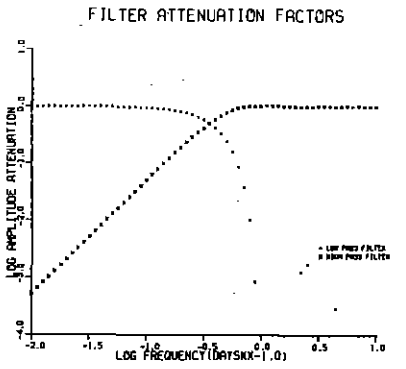

Figure 8a. Digital filter attenuation functions: $A_{144}\ A_{149}^2$ (low pass), $\{1-A_{144}\ A_{149}^2\}$ (high pass)

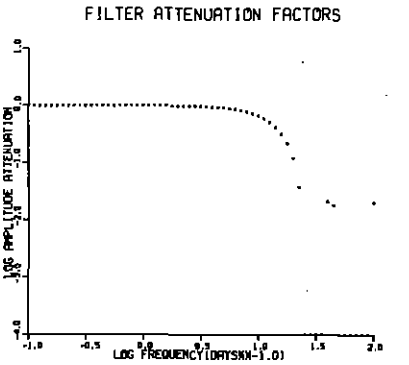

Figure 8b. Digital filter attenuation functions: $A_4\ A_6$ (low pass)

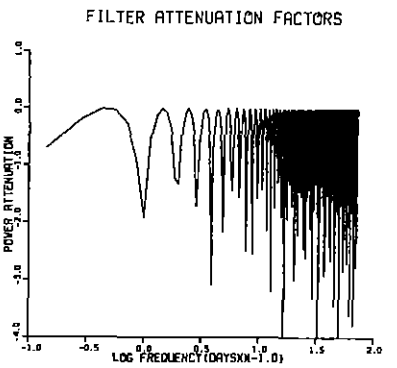

Figure 8c. Digital filter attenuation functions: S_{149} (M_2 tidal component removal).

Figure 9. Calibrated time series from current meter #338.

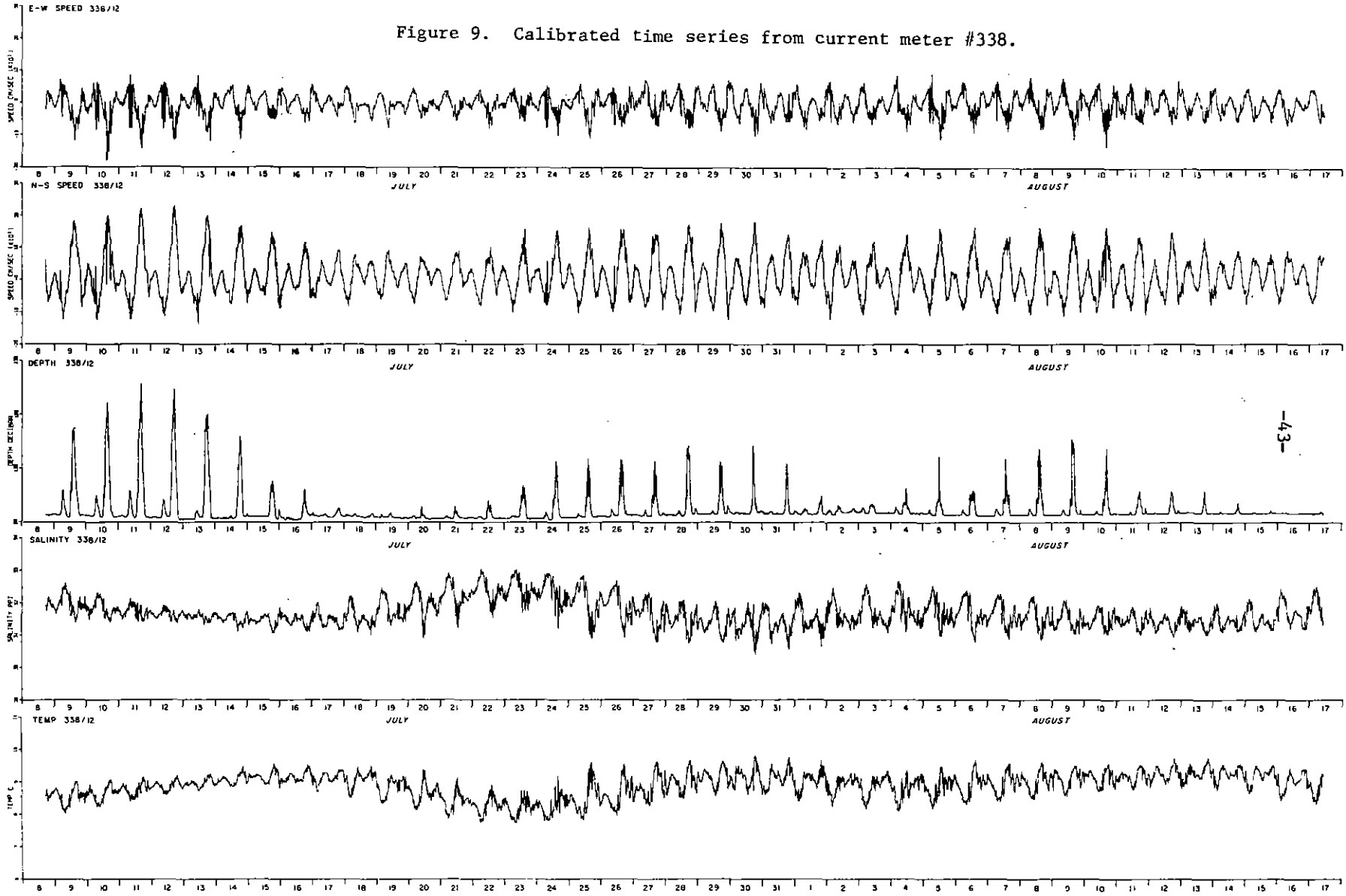

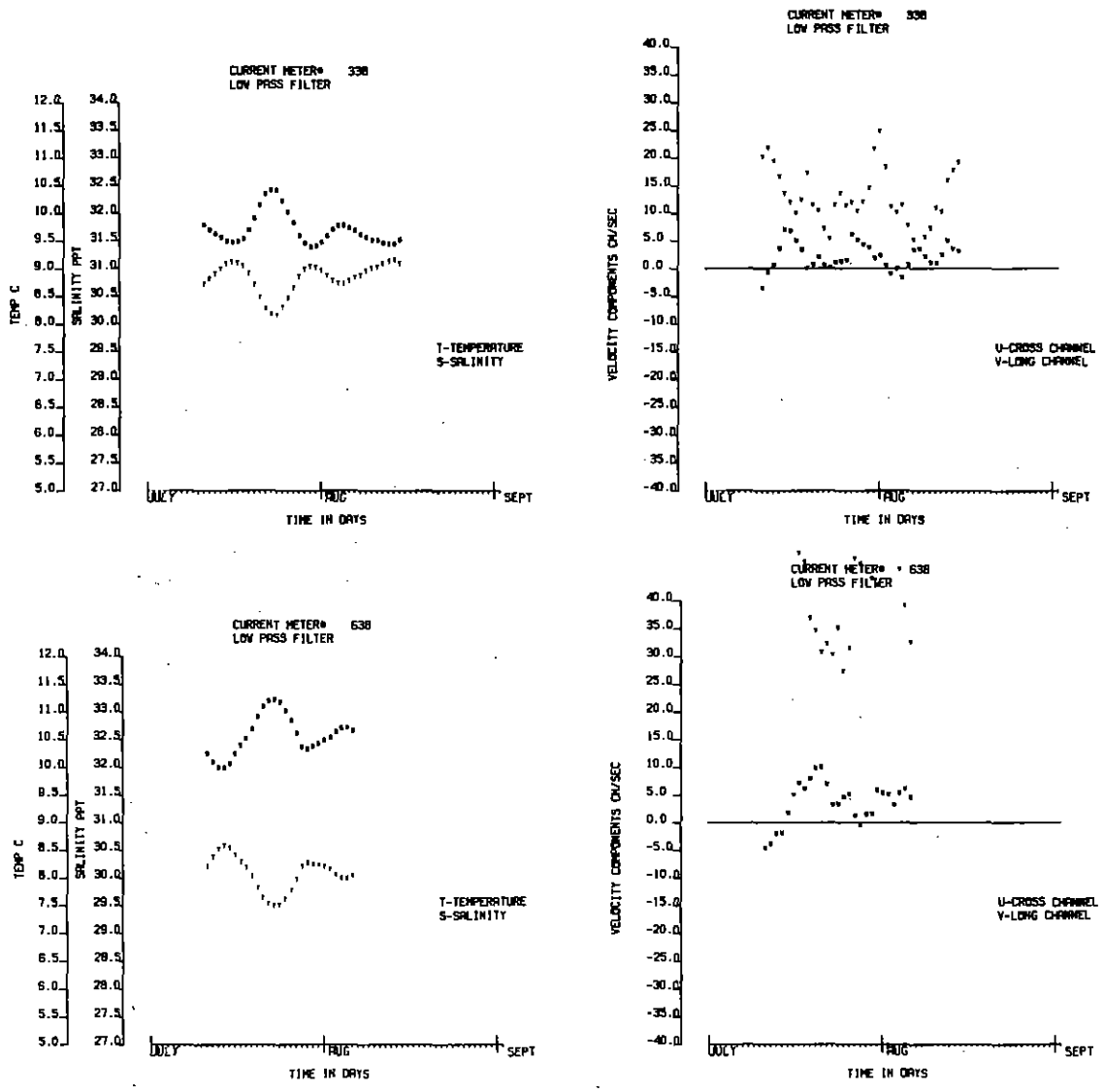

Figure 10. Low pass filtered time series from current meters #338 and #638.

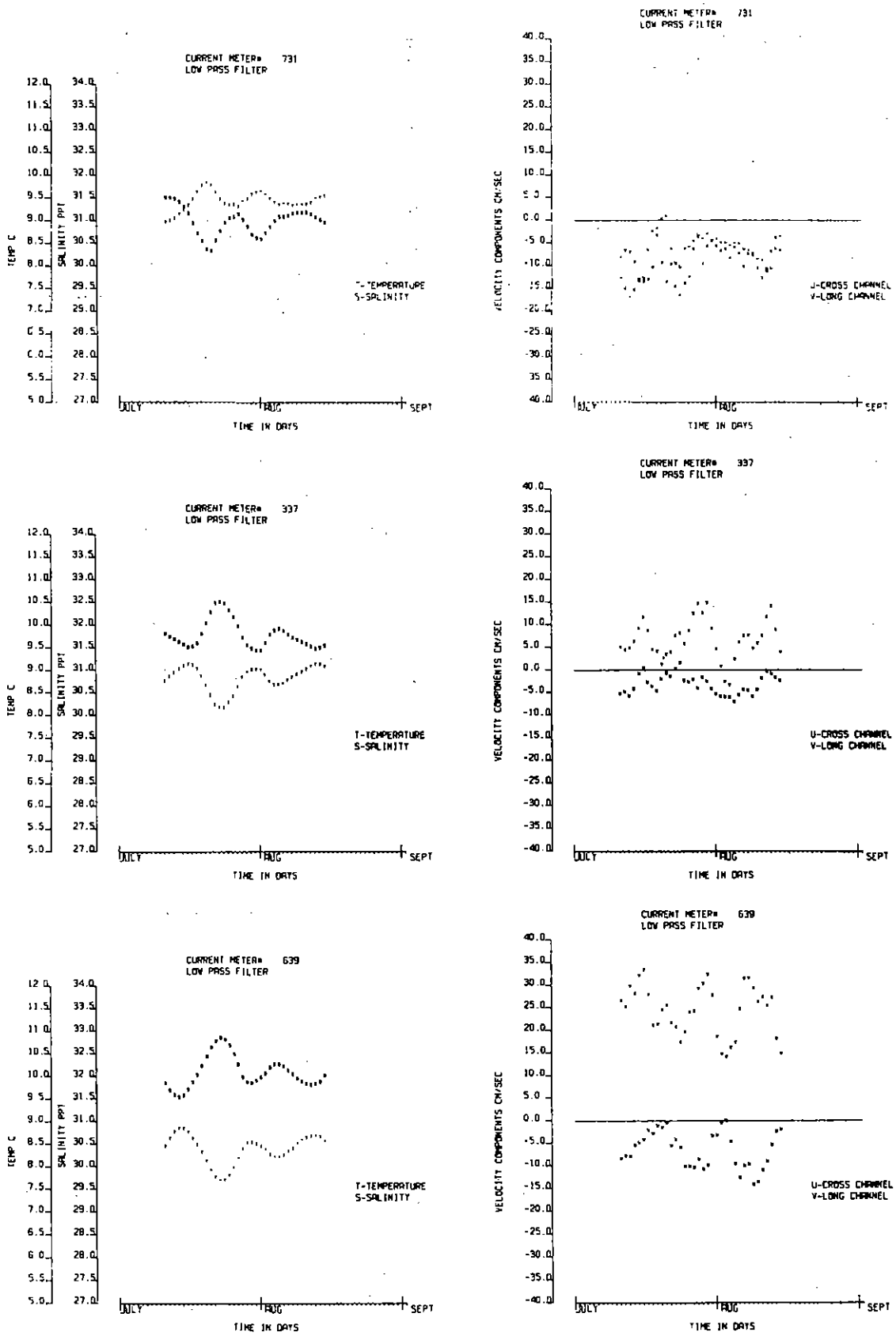

Figure 11. Low pass filtered time series from current meters #731, #337, and #639.

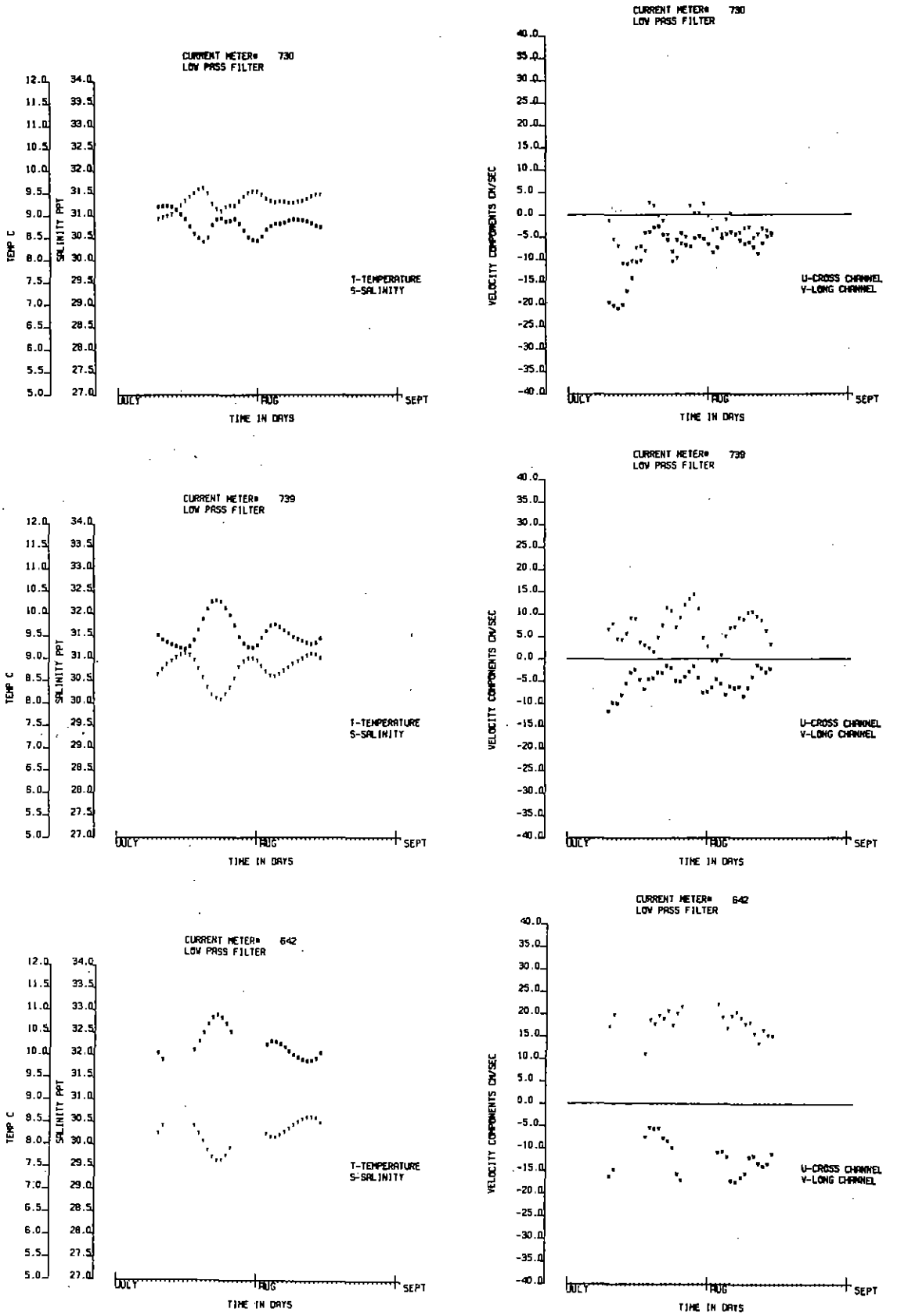

Figure 12. Low pass filtered time series from current meters #730, #739 and #642.

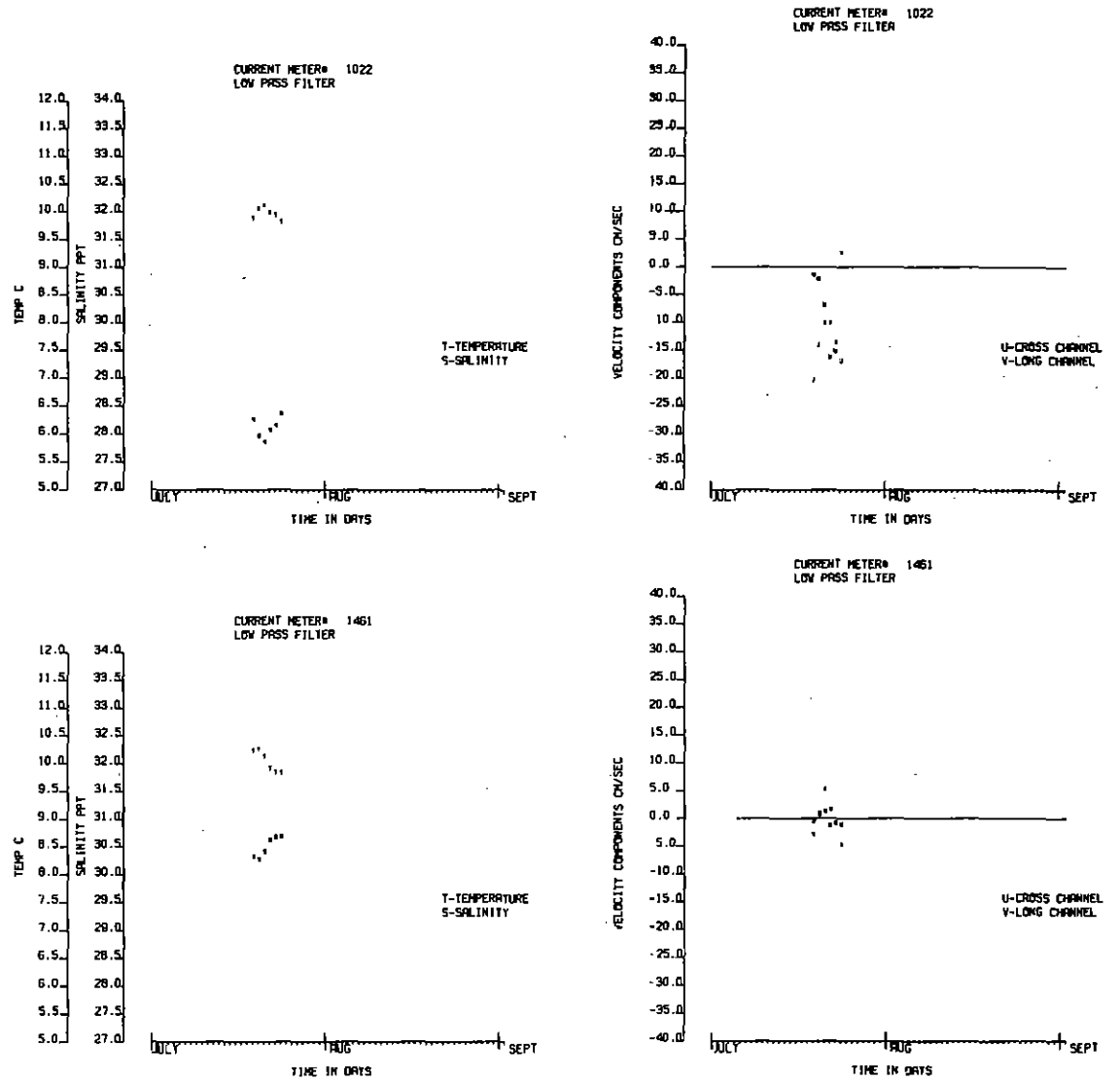

Figure 13. Low pass filtered time series from current meters #1022 and #1461.

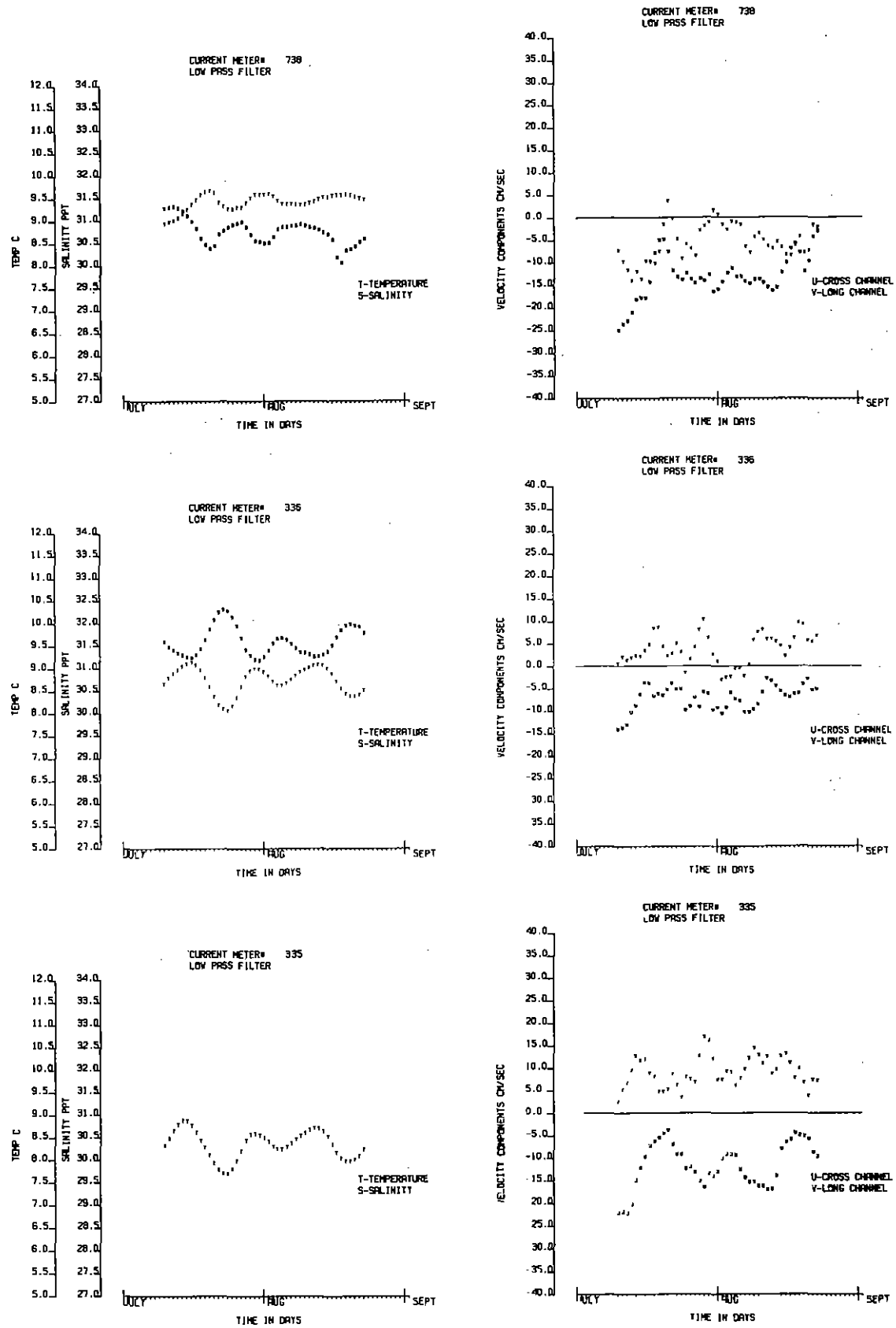

Figure 14. Low pass filtered time series from current meters #738, #336 and #335.

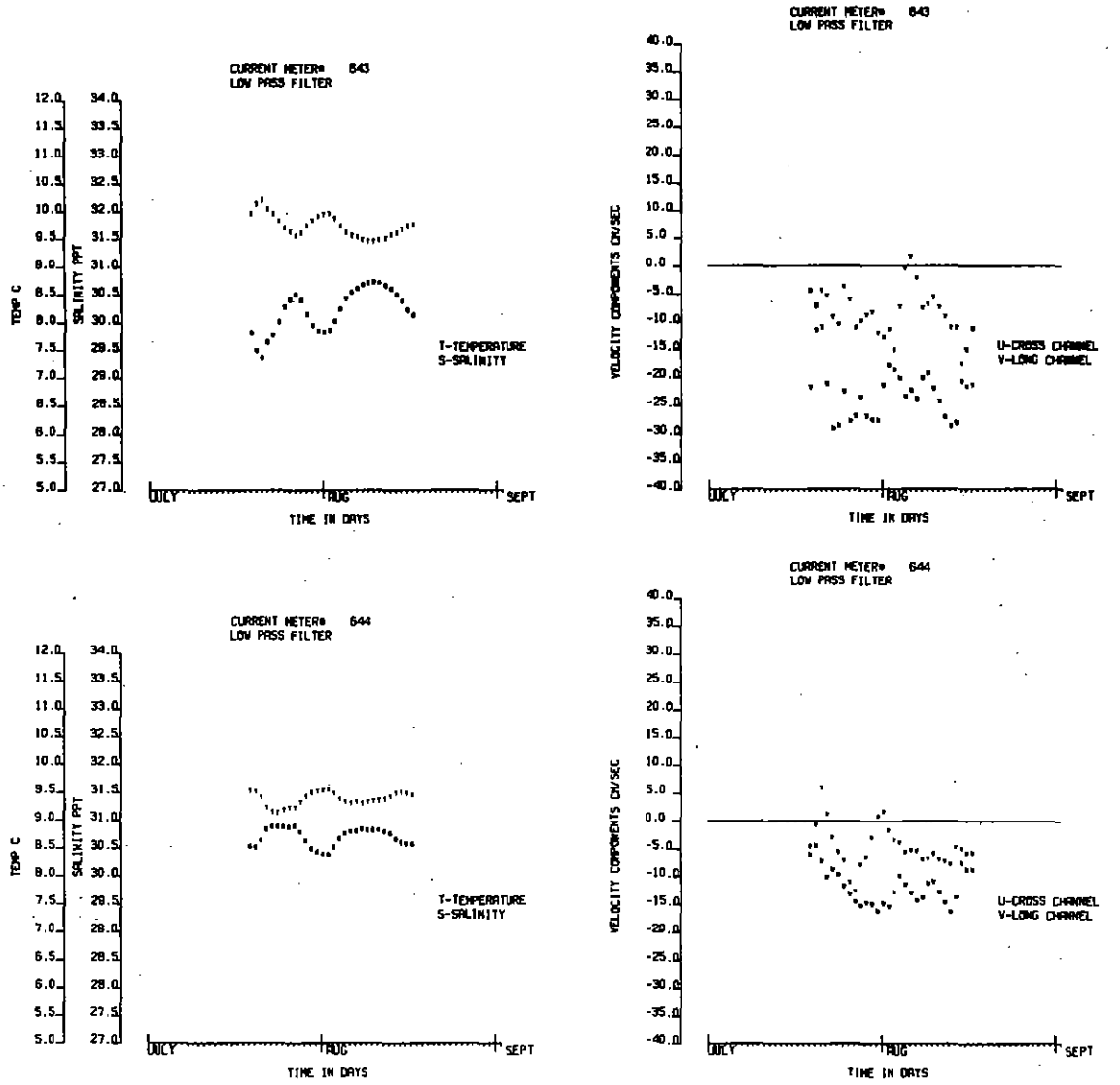

Figure 15. Low pass filtered time series from current meters #643 and #644.

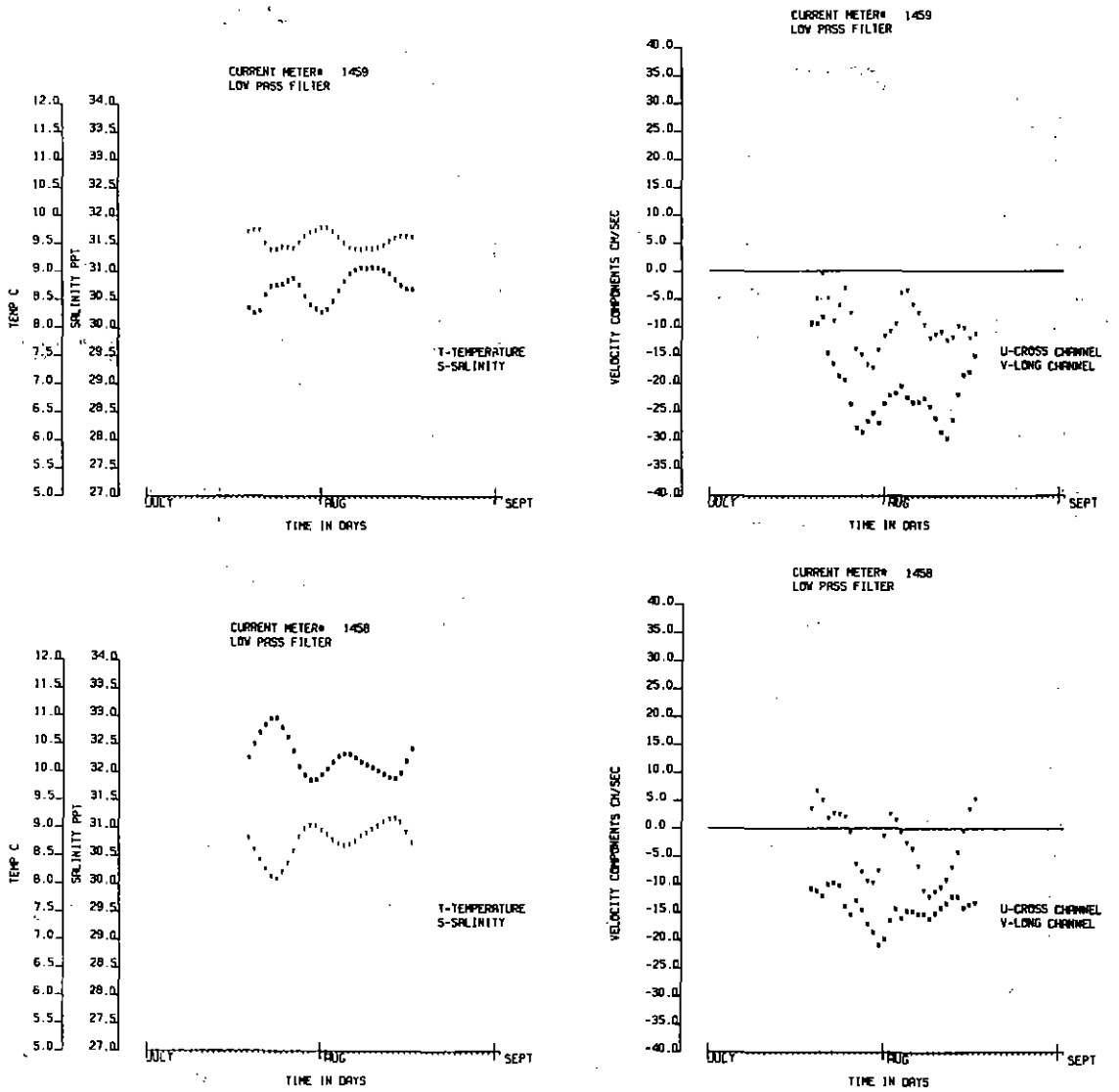

Figure 16. Low pass filtered time series from current meters #1459 and #1458.

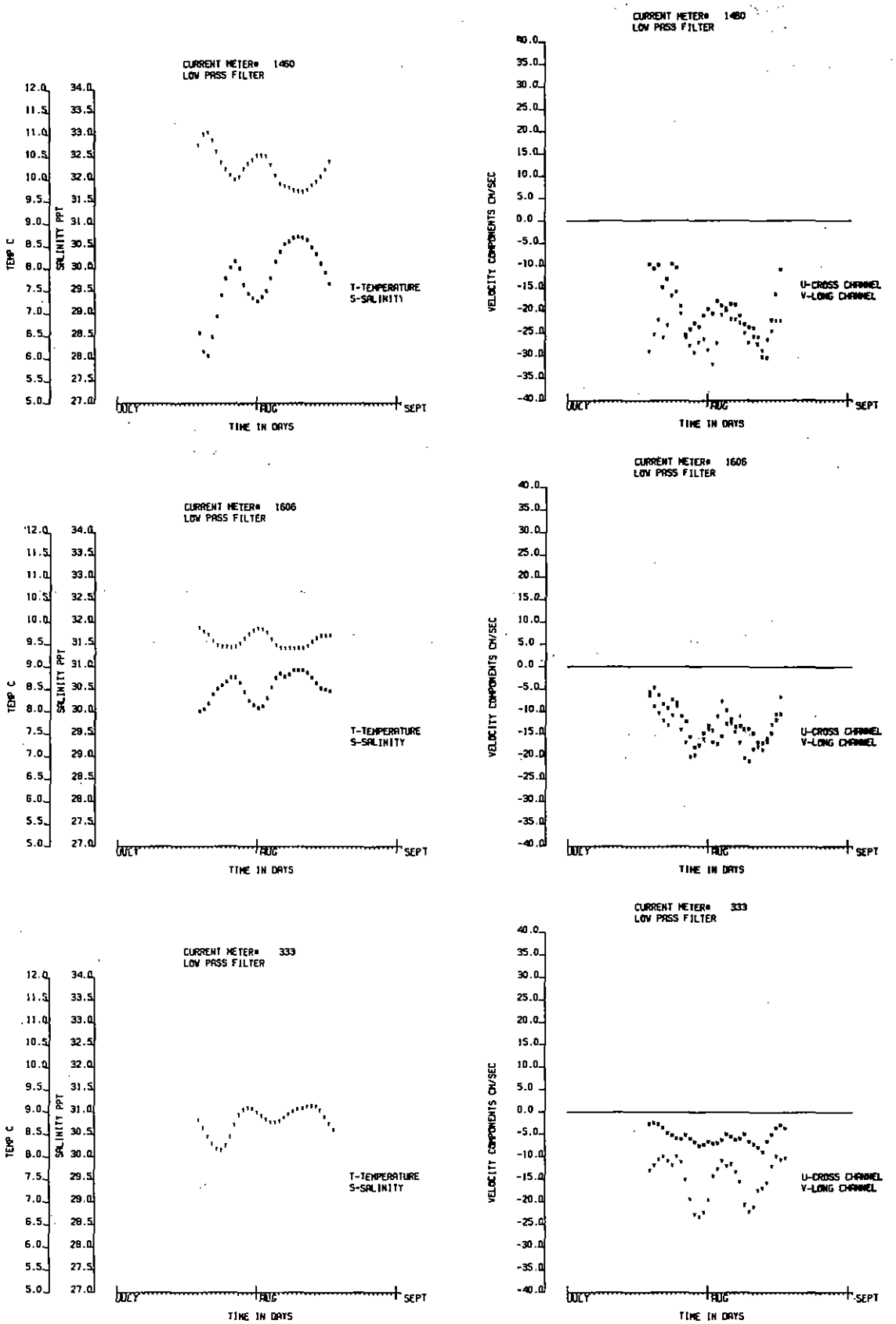

Figure 17. Low pass filtered time series from current meters #1460, #1606 and #333.

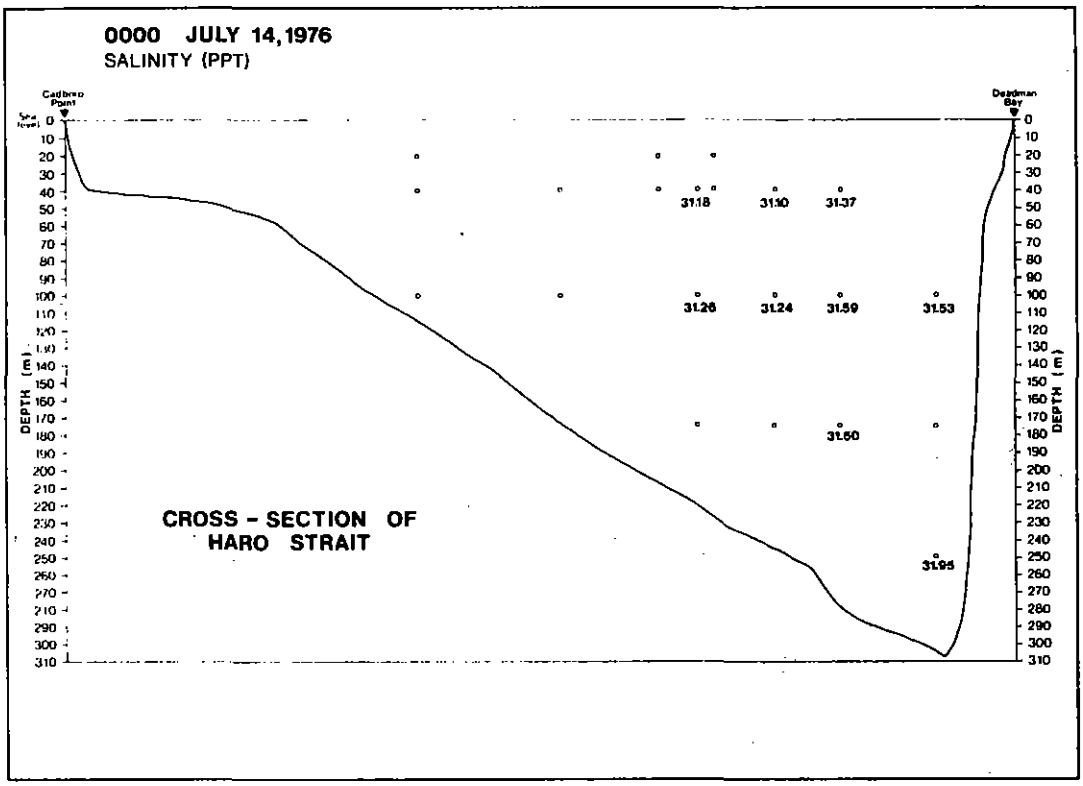

Figure 18a. Salinity low pass filtered data values for 0000 July 14, 1976.

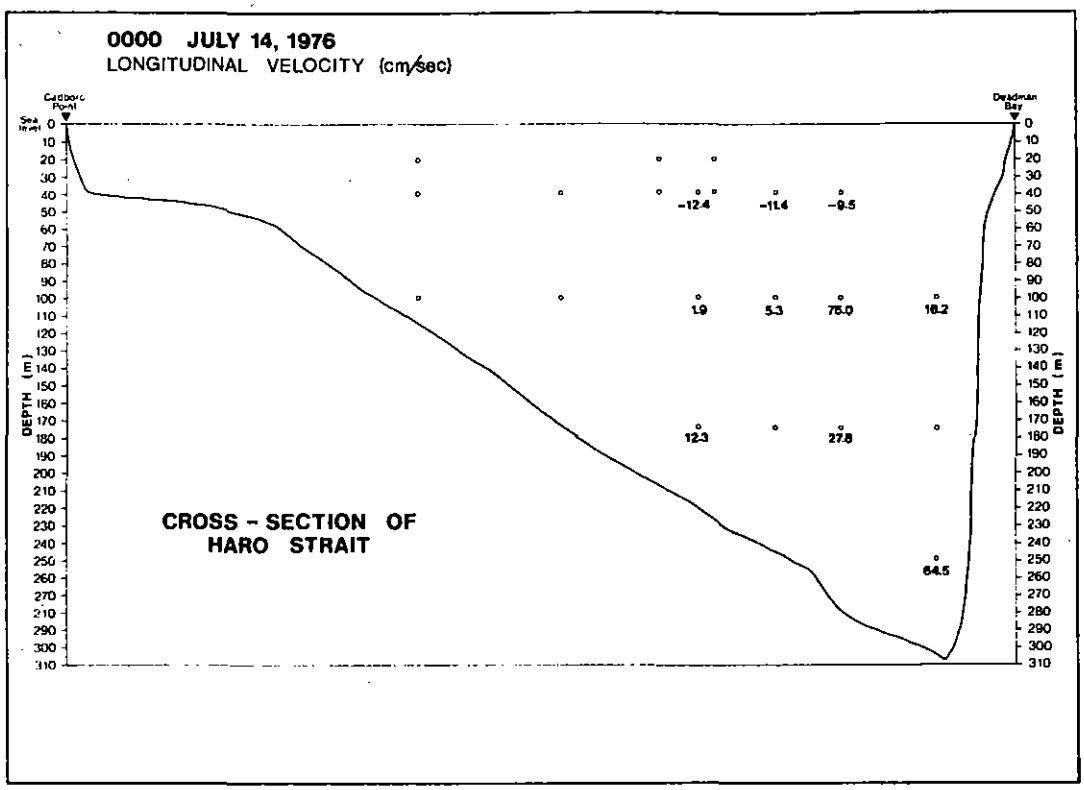

Figure 18b. Longitudinal velocity low pass filtered data values for 0000 July 14, 1976.

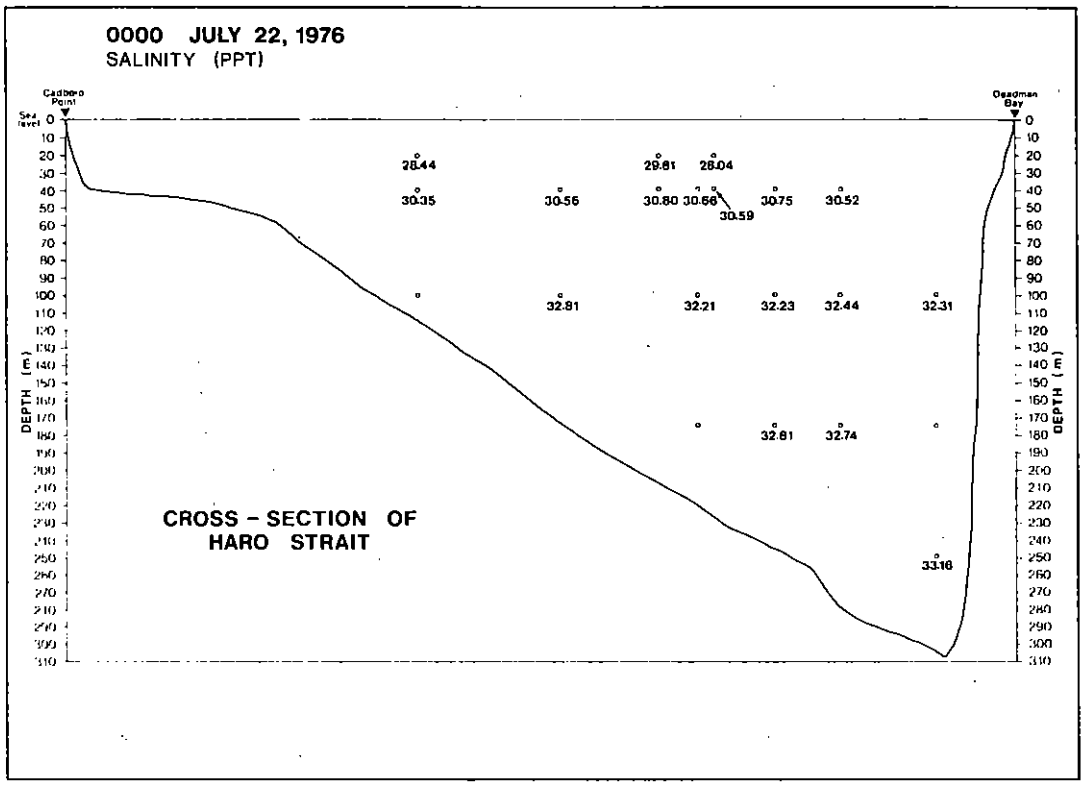

Figure 19a. Salinity low pass filtered data values for 0000 July 22, 1976.

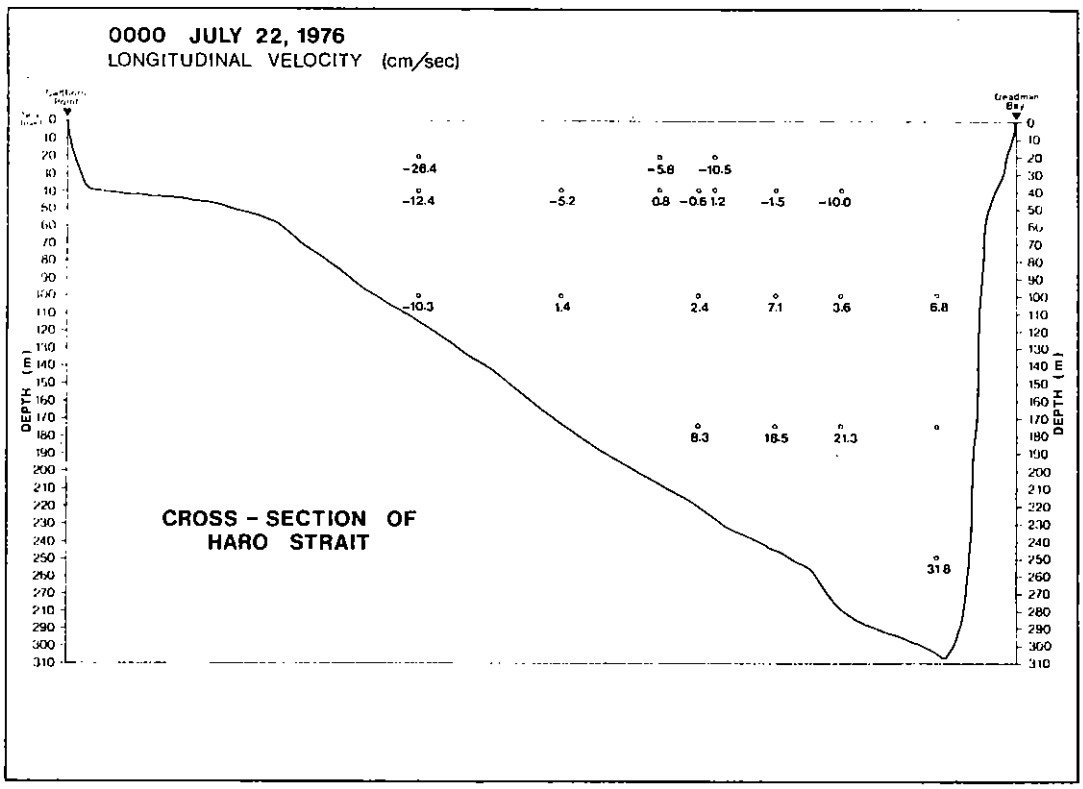

Figure 19b. Longitudinal velocity low pass filtered data values for 0000 July 22, 1976.

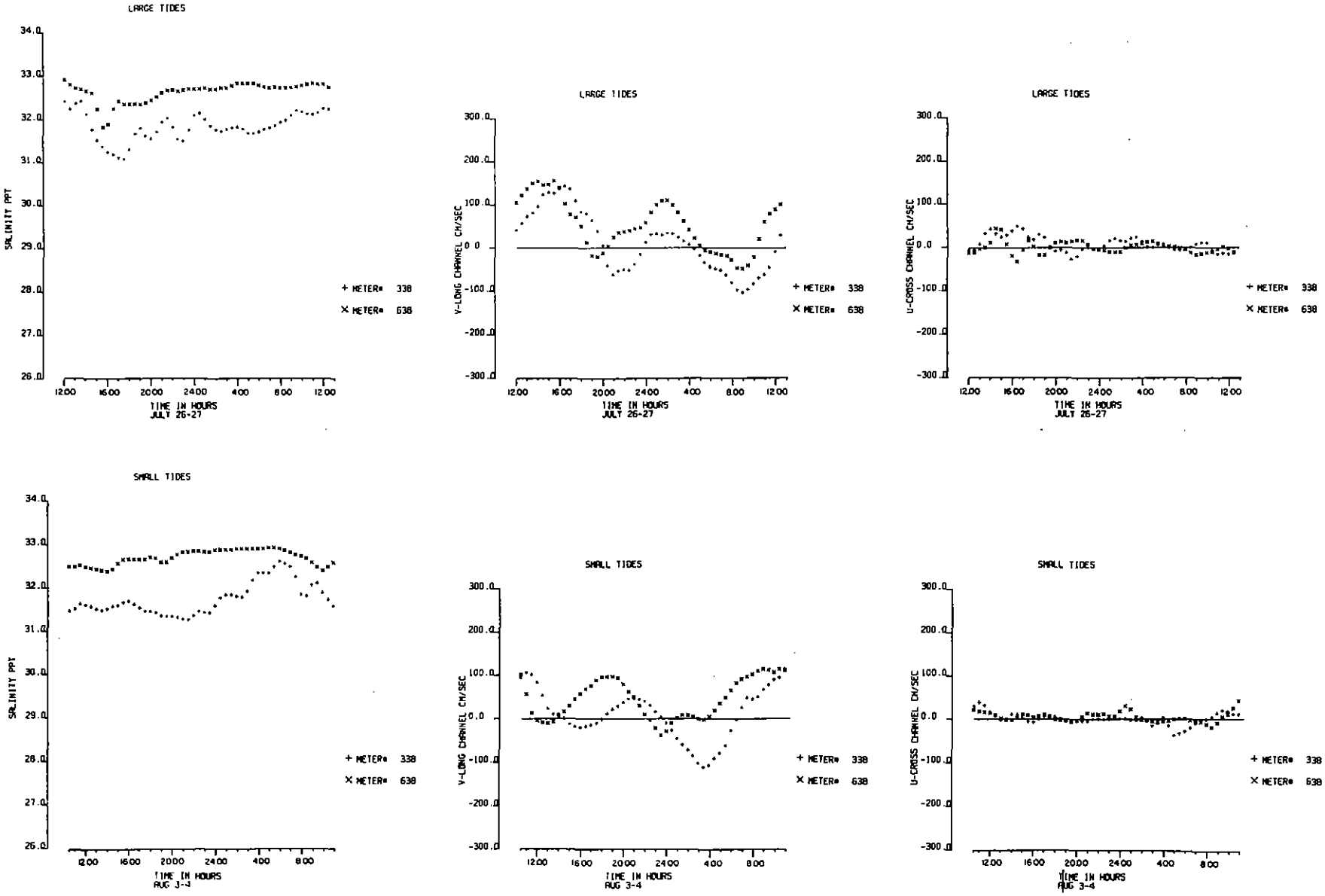

Figure 20. Two 25 hour sections of data from current meters #338 and #638.

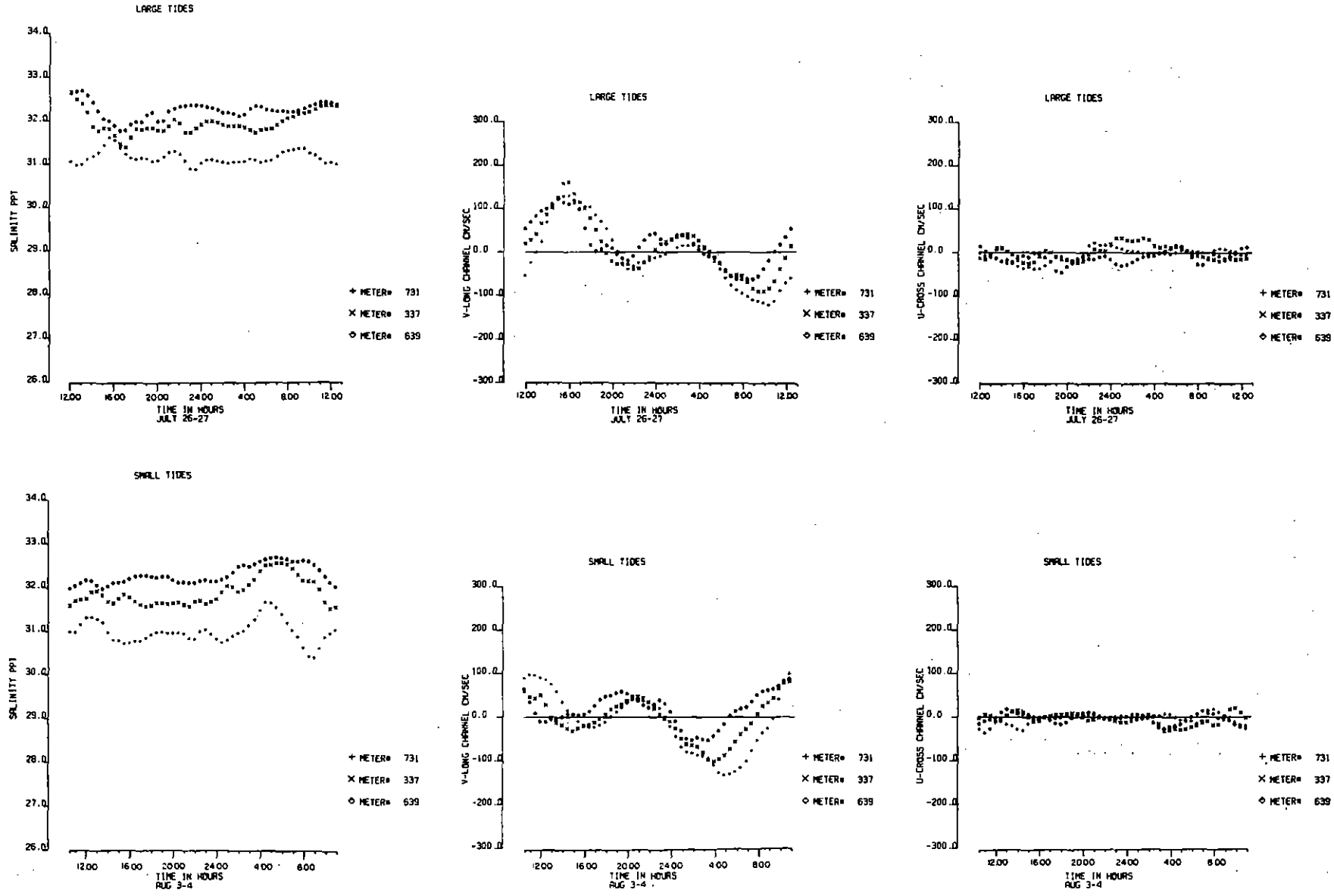

Figure 21. Two 25 hour sections of data from current meters #731, #337 and #639.

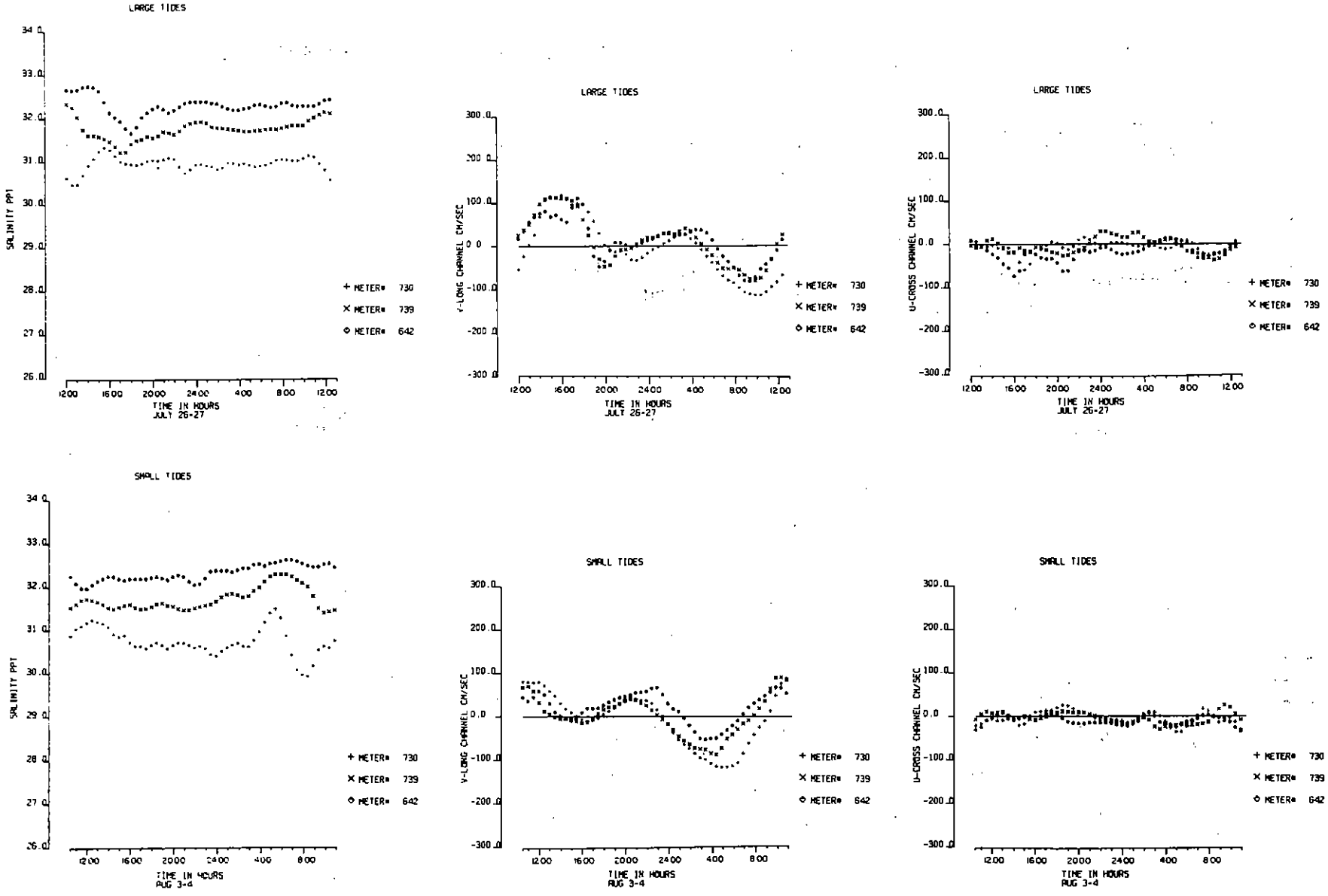

Figure 22. Two 25 hour sections of data from current meters #730, #739 and #642.

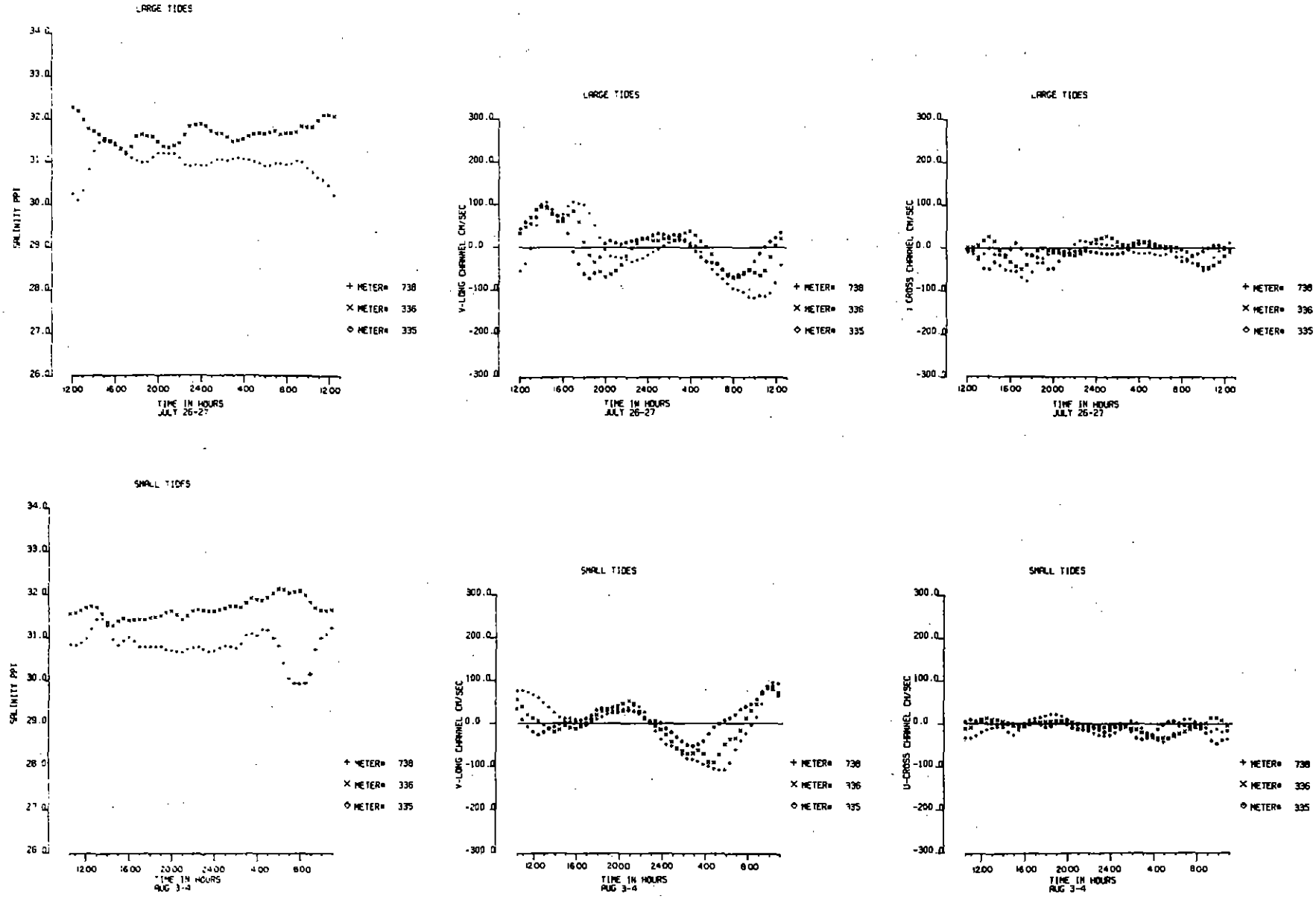

Figure 23. Two 25 hour sections of data from current meters #738, #336 and #335.

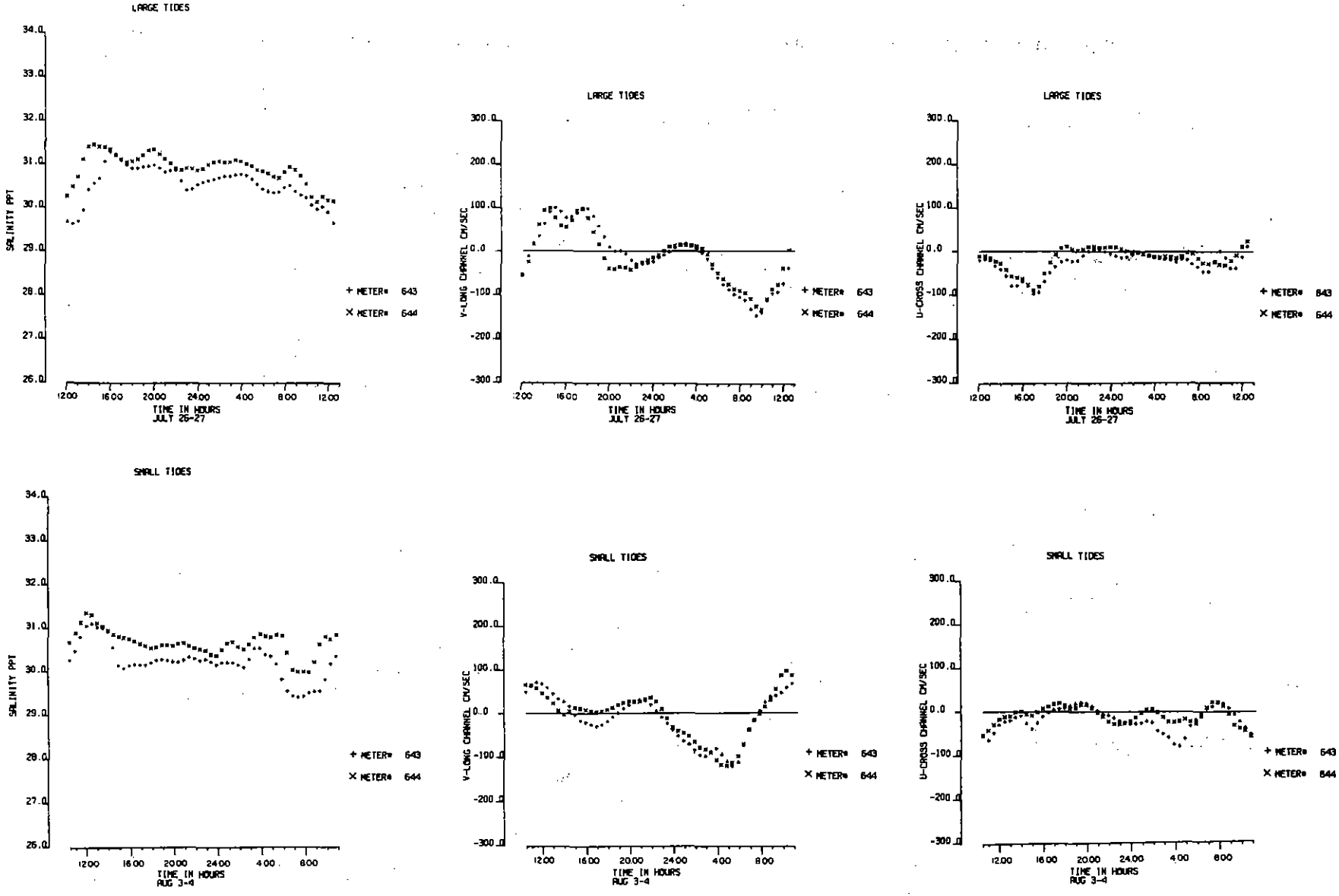

Figure 24. Two 25 hour sections of data from current meters #643, and #644.

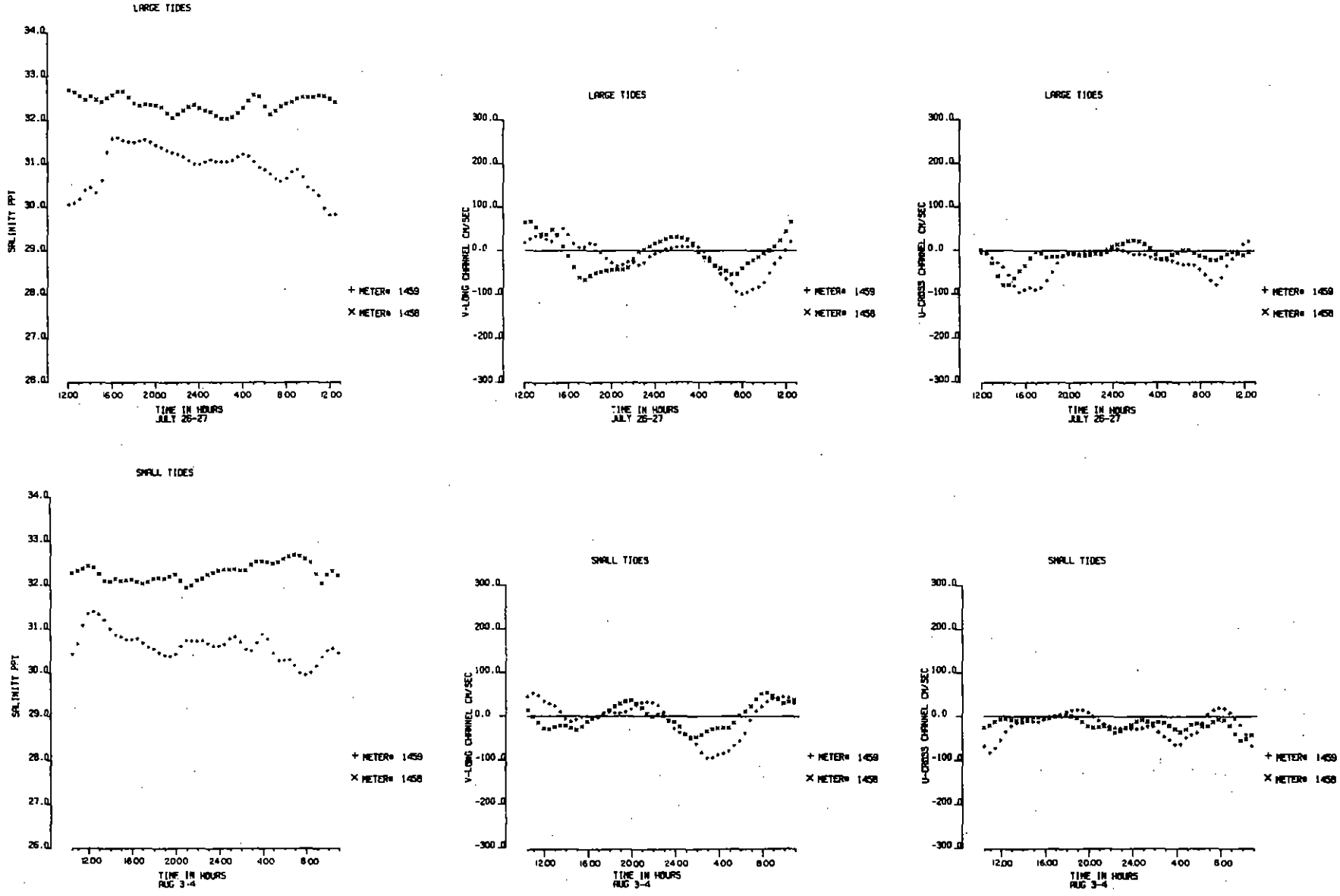

Figure 25. Two 25 hour sections of data from current meters #1459 and #1458.

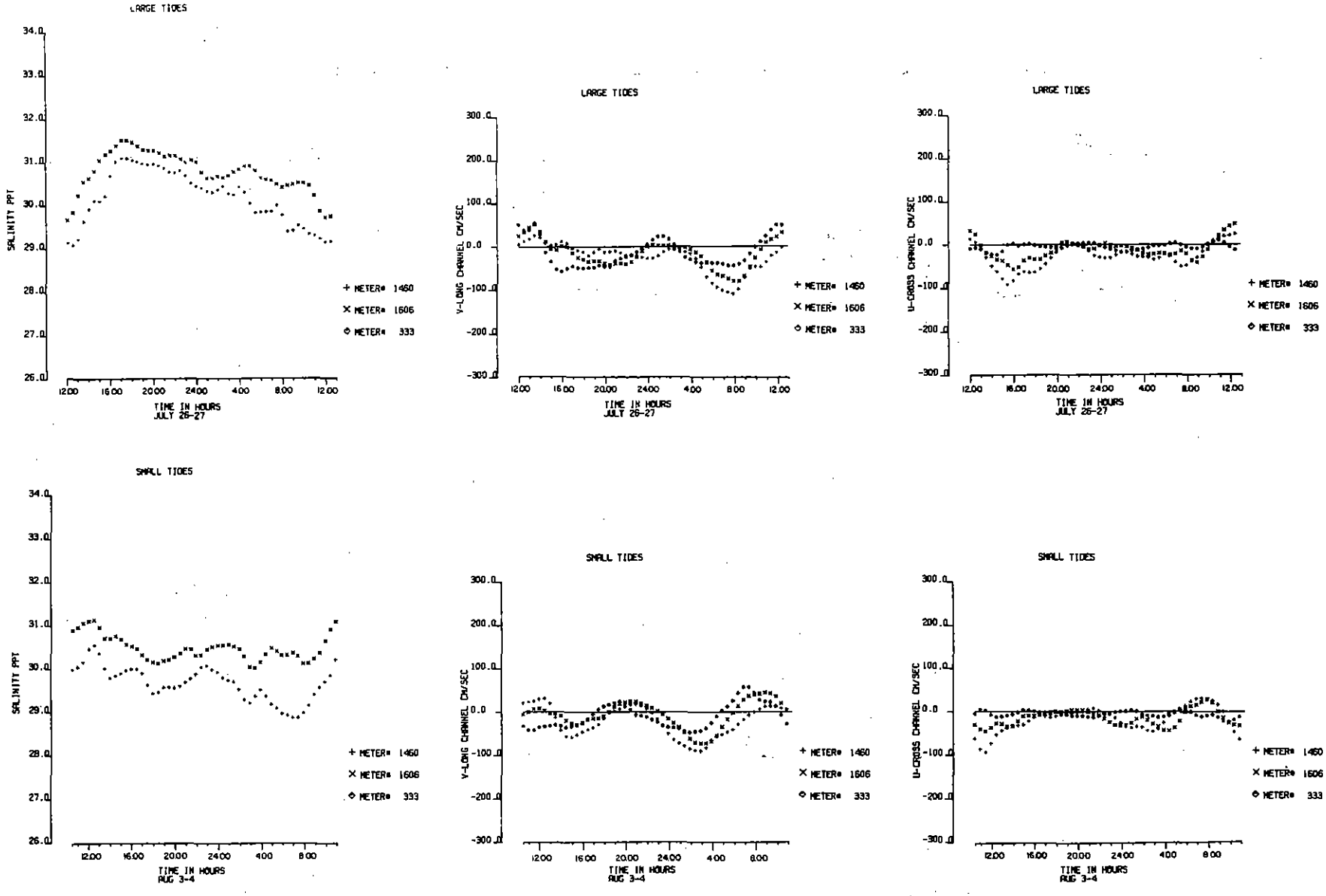

Figure 26. Two 25 hour sections of data from current meters #1460, #1606 and #333.

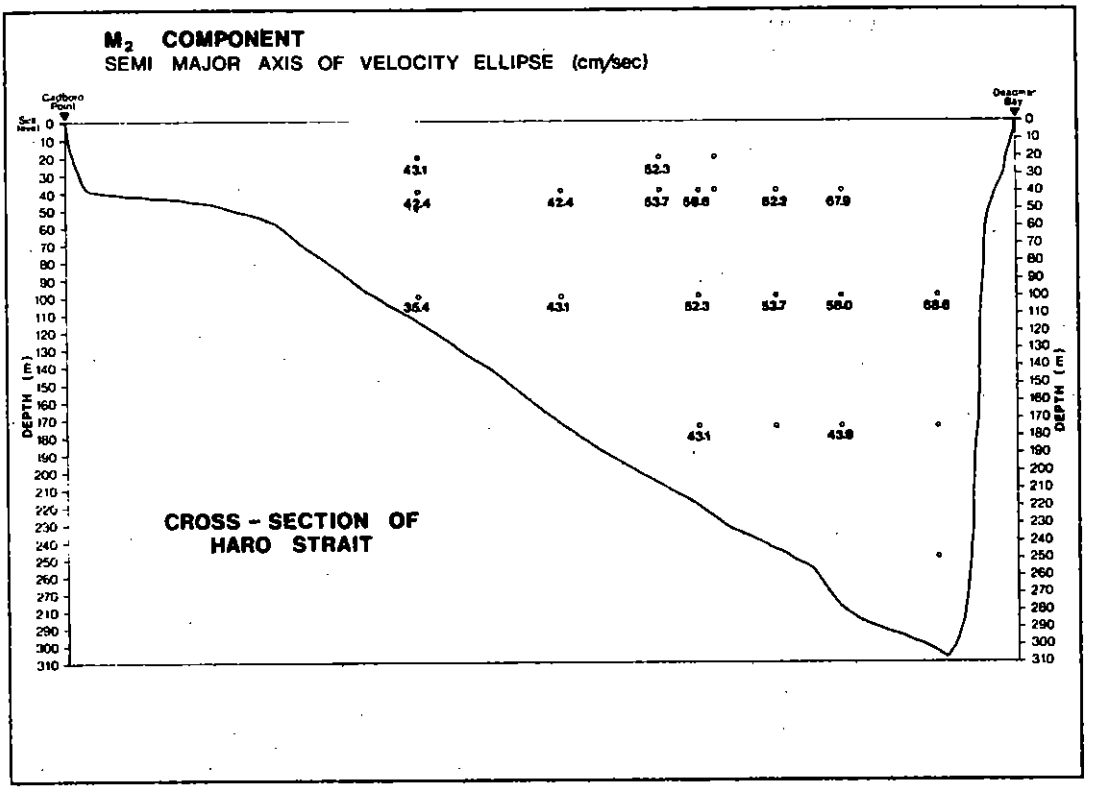

Figure 27a. Lengths of semi-major axes for M_2 velocity ellipse.

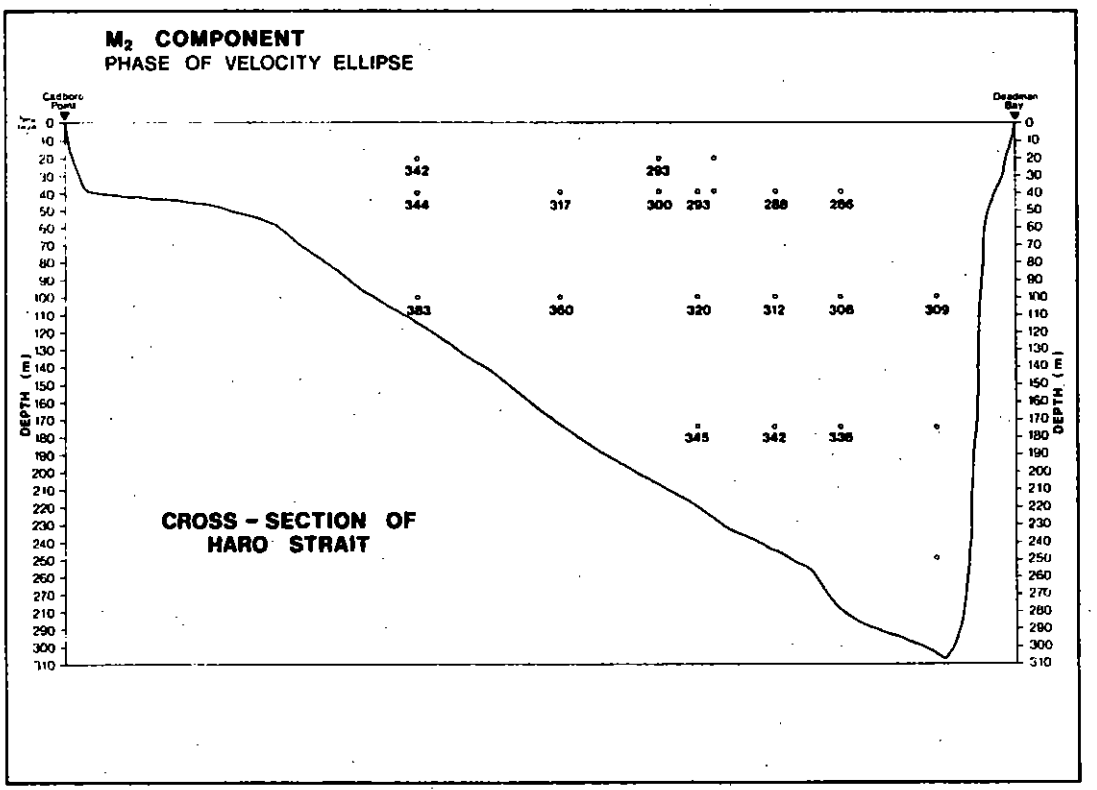

Figure 27b. Phases of M_2 velocity ellipses.

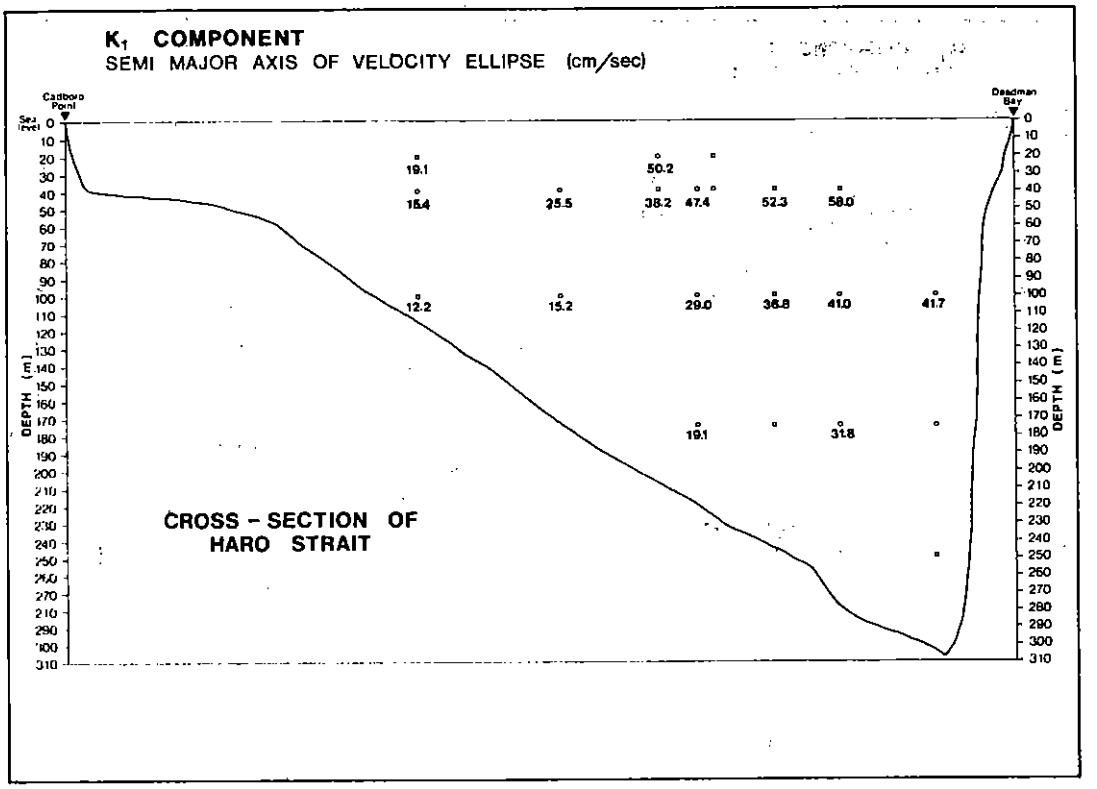

Figure 28a. Lengths of semi-major axes for K_1 velocity ellipse.

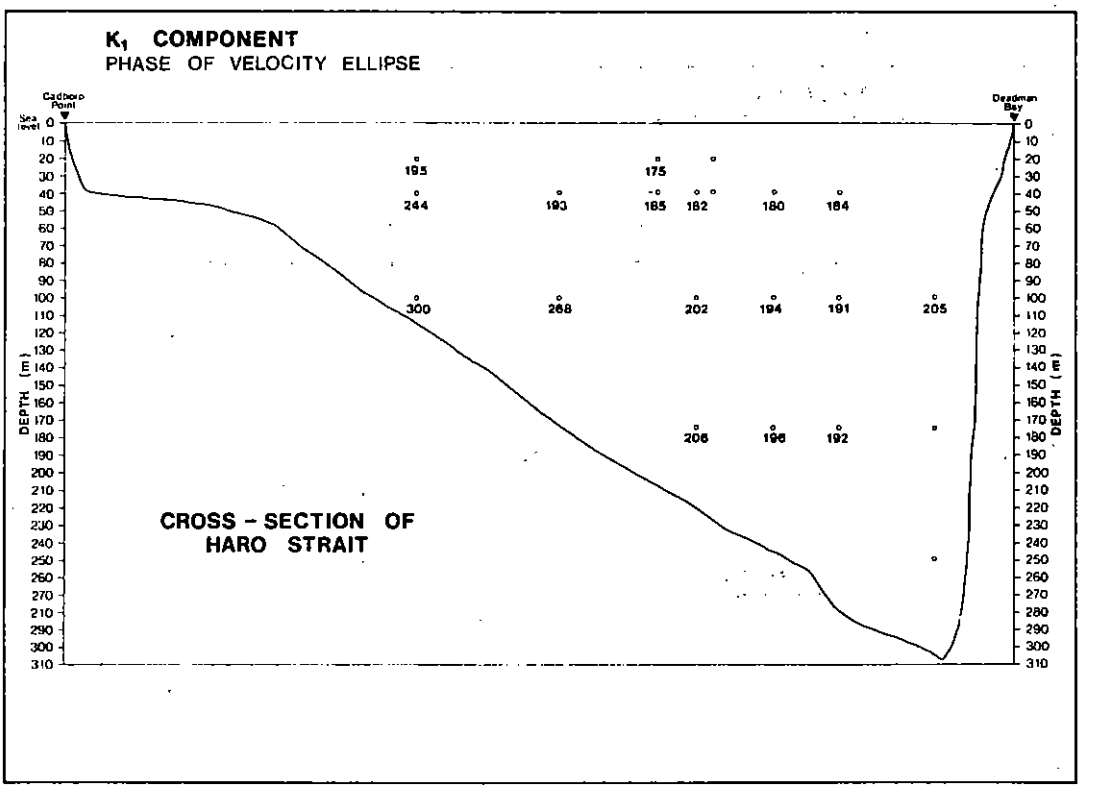

Figure 28b. Phases of K_1 velocity ellipse.

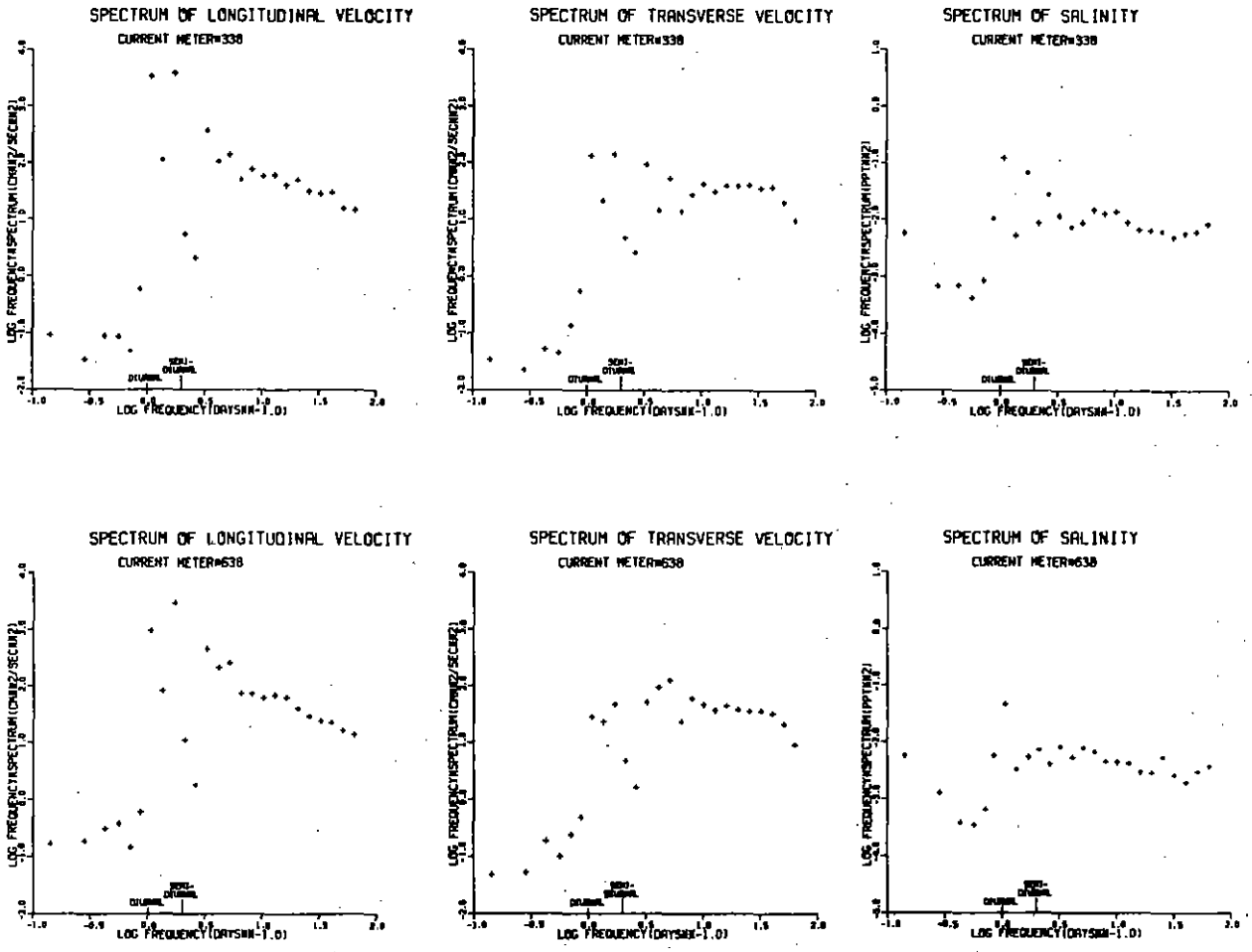

Figure 29. Power spectra current meters #338 and #638

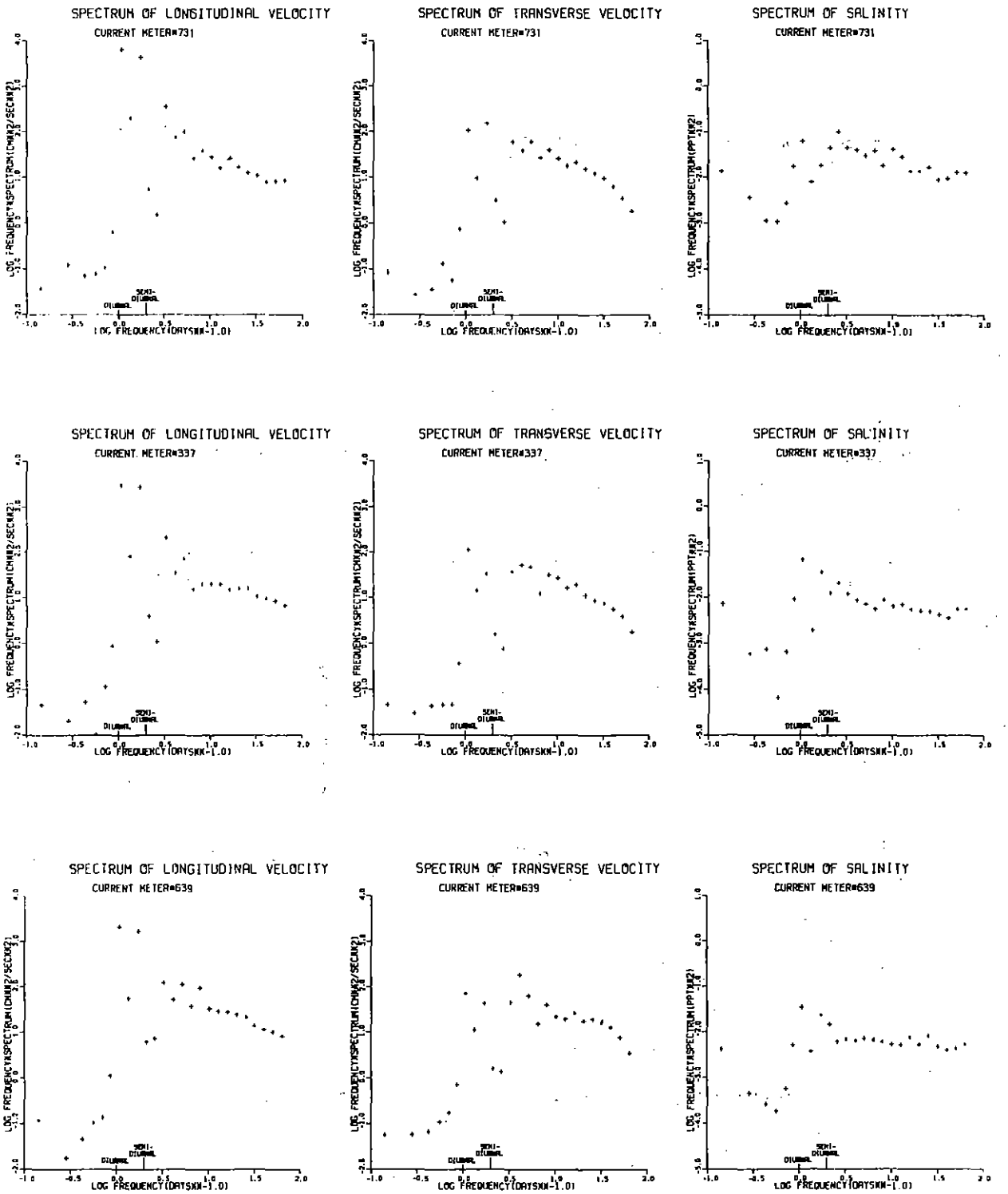

Figure 30. Power spectra current meters #731, #337 and #639.

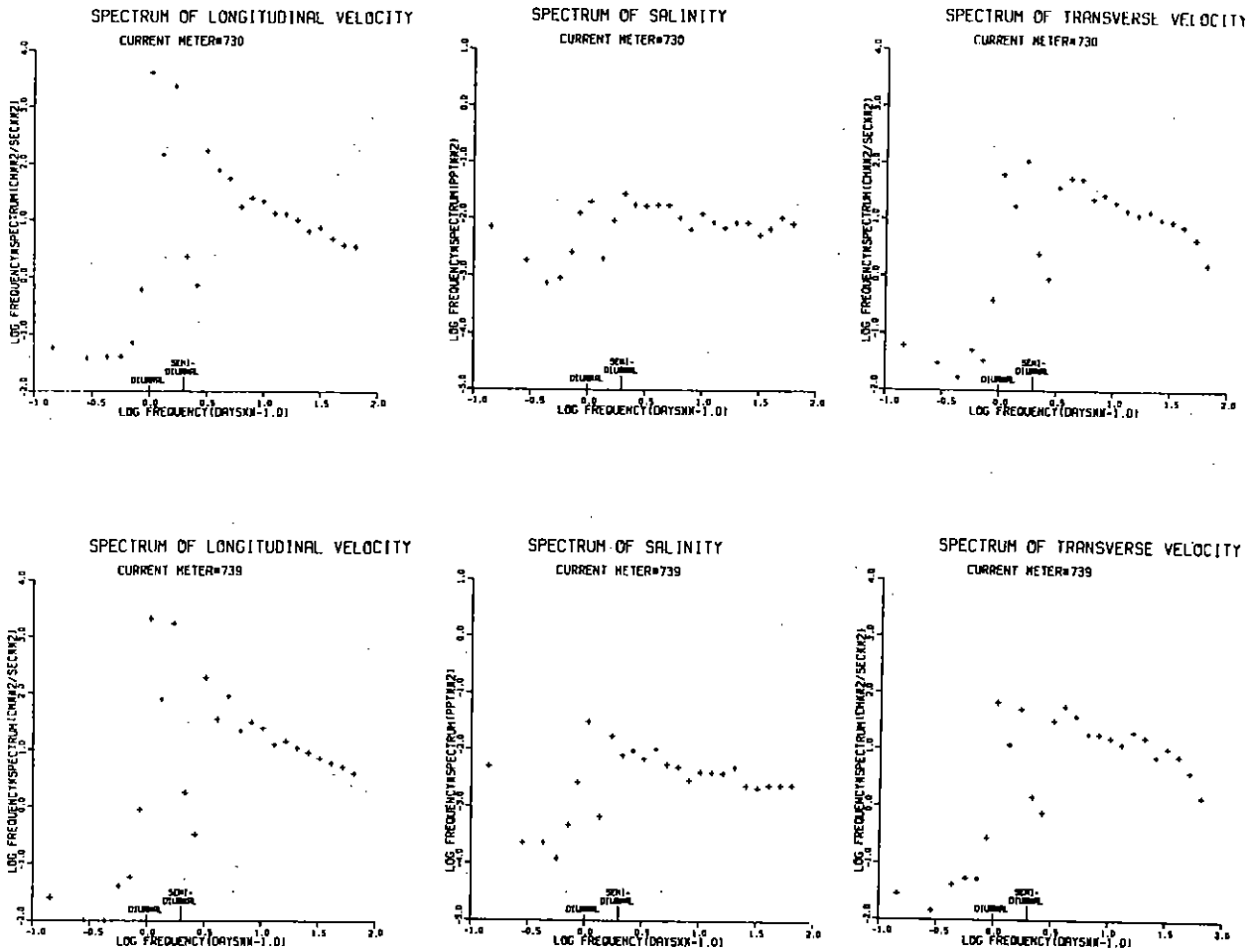

Figure 31. Power spectra current meters #730 and #739.

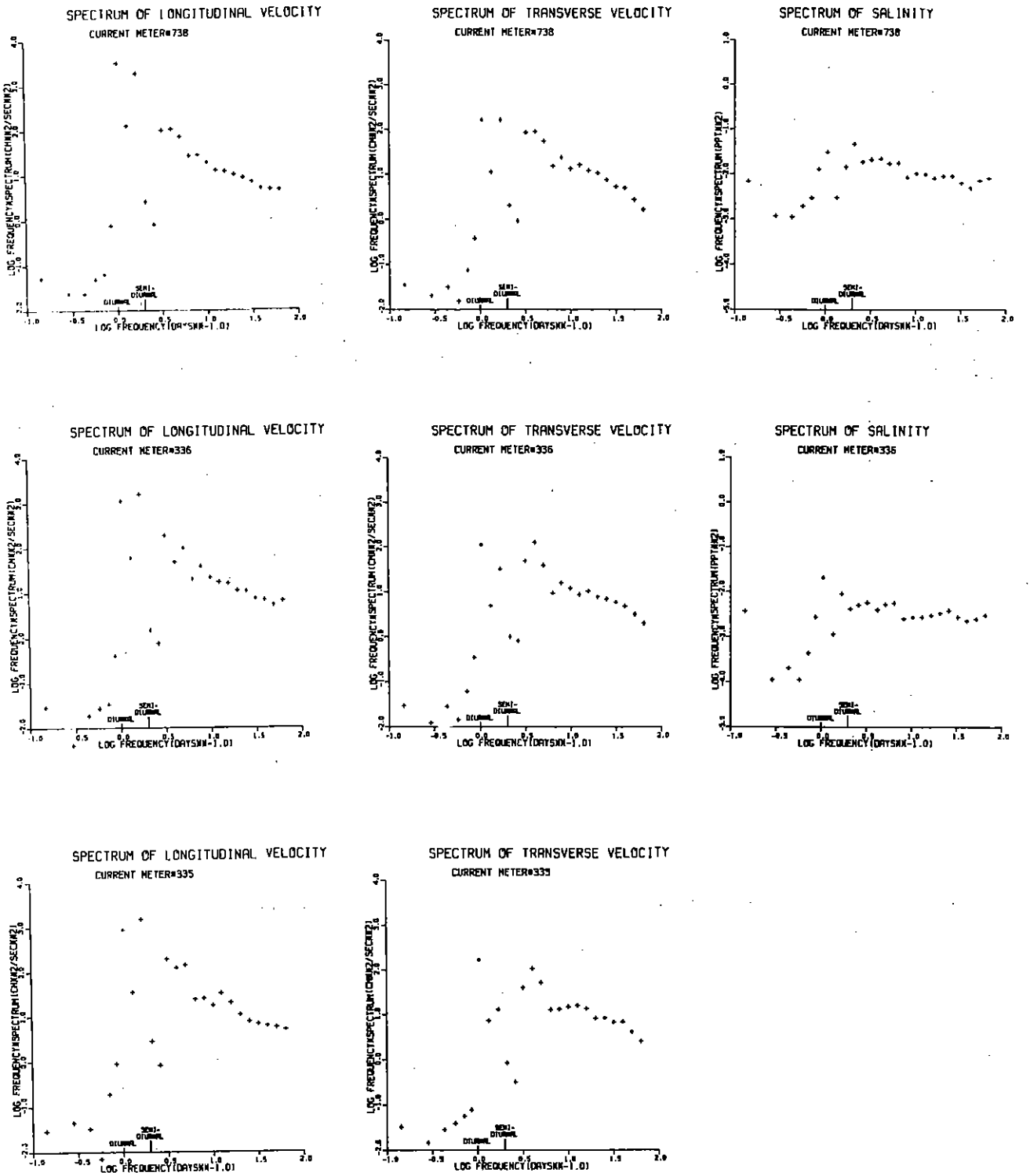

Figure 32. Power spectra current meters #738, #336, and #335.

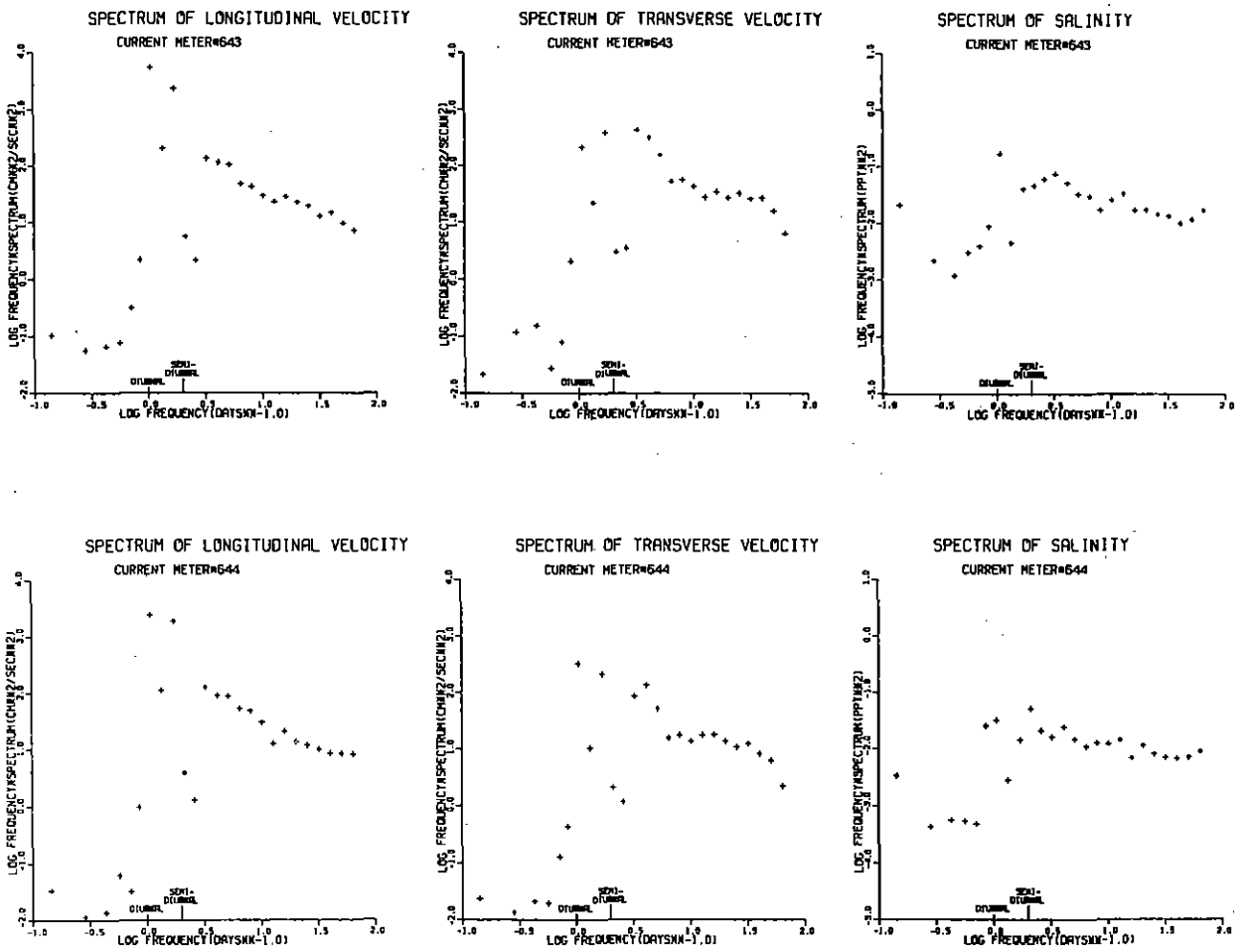

Figure 33. Power spectra current meters #643 and #644.

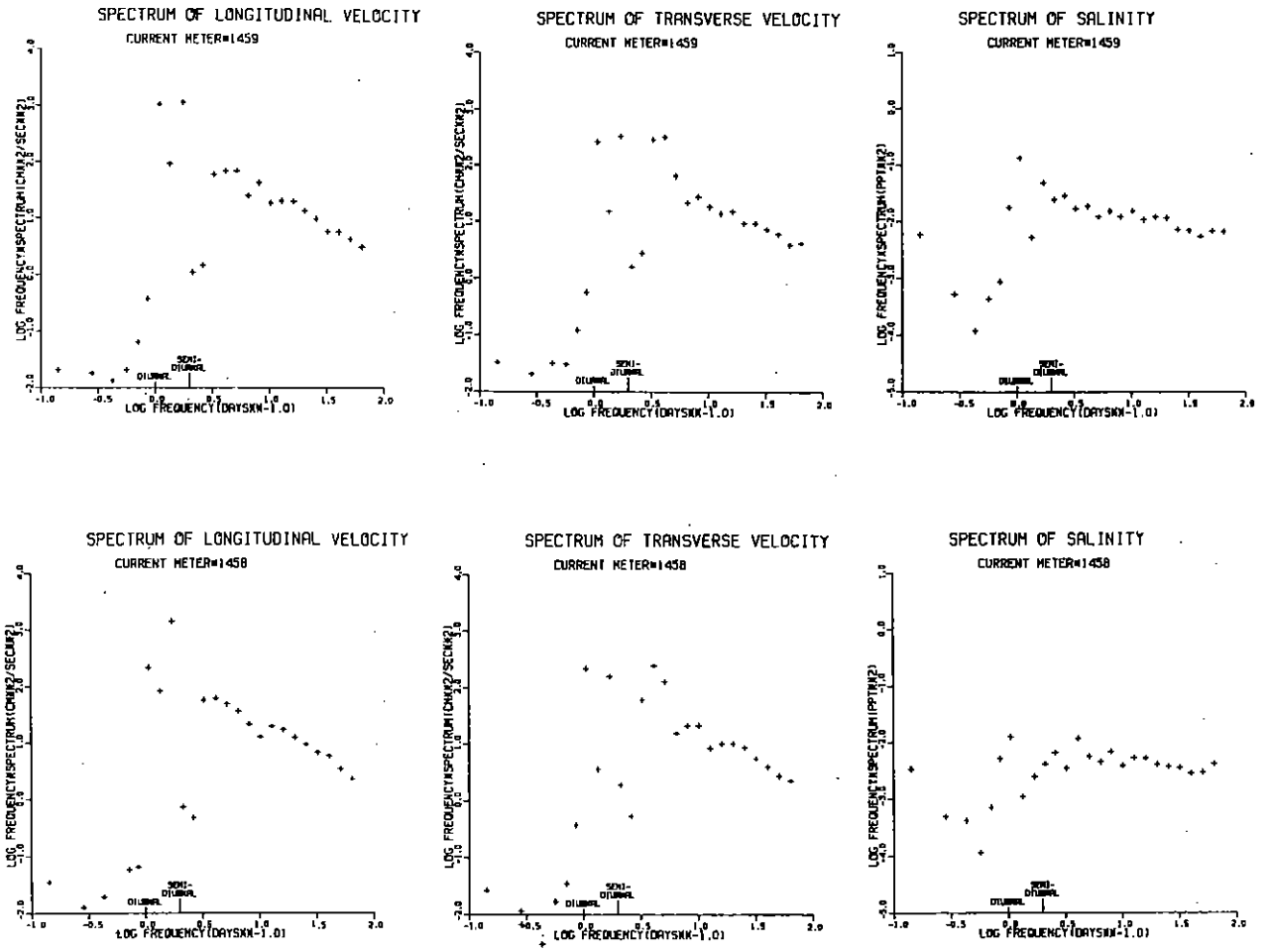

Figure 34. Power spectra current meters #1459 and #1458.

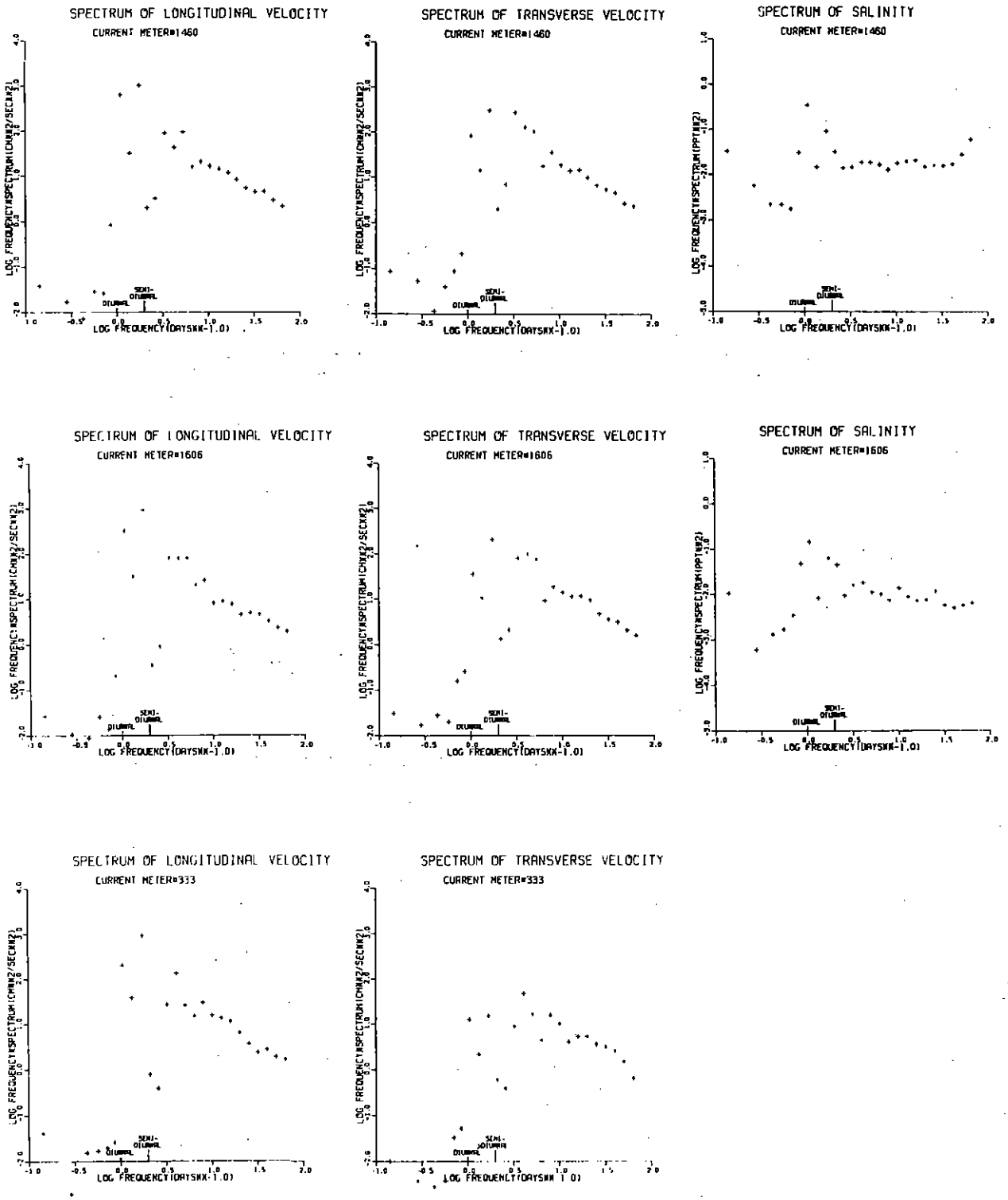

Figure 35. Power spectra current meters #1460, #1606 and #333.

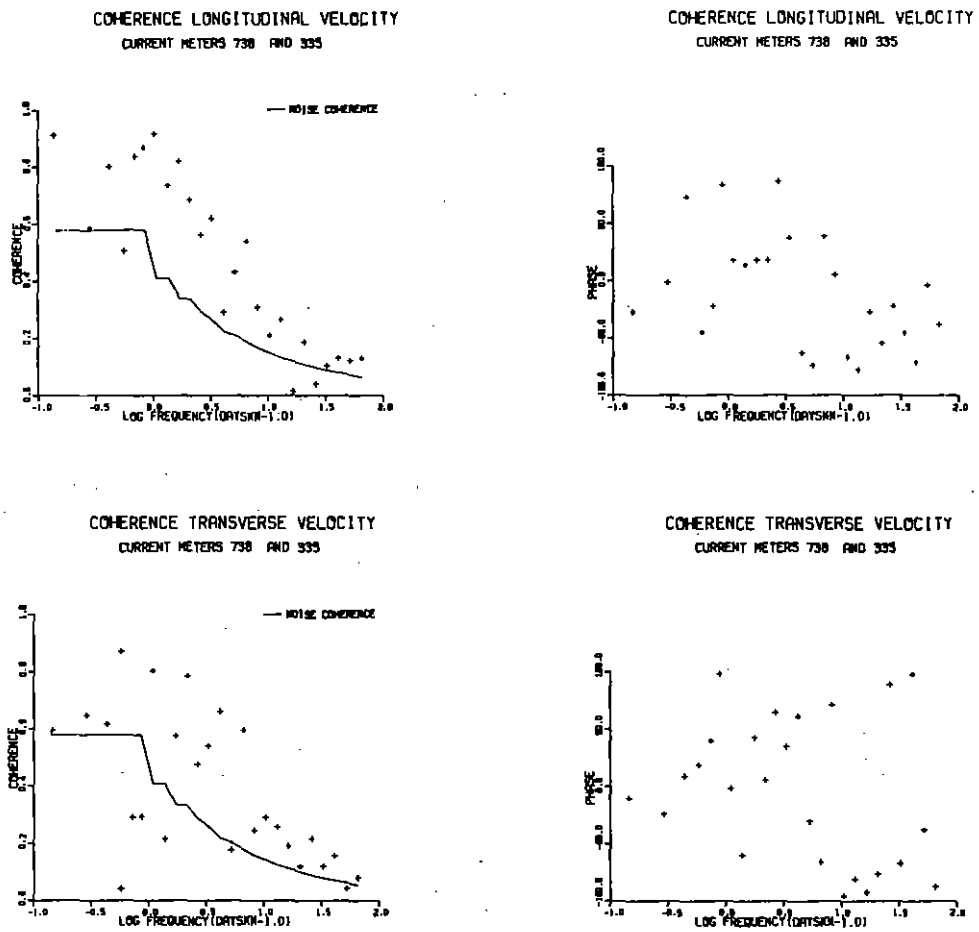

Figure 36. Coherences and phases between current meters #738 and #335.

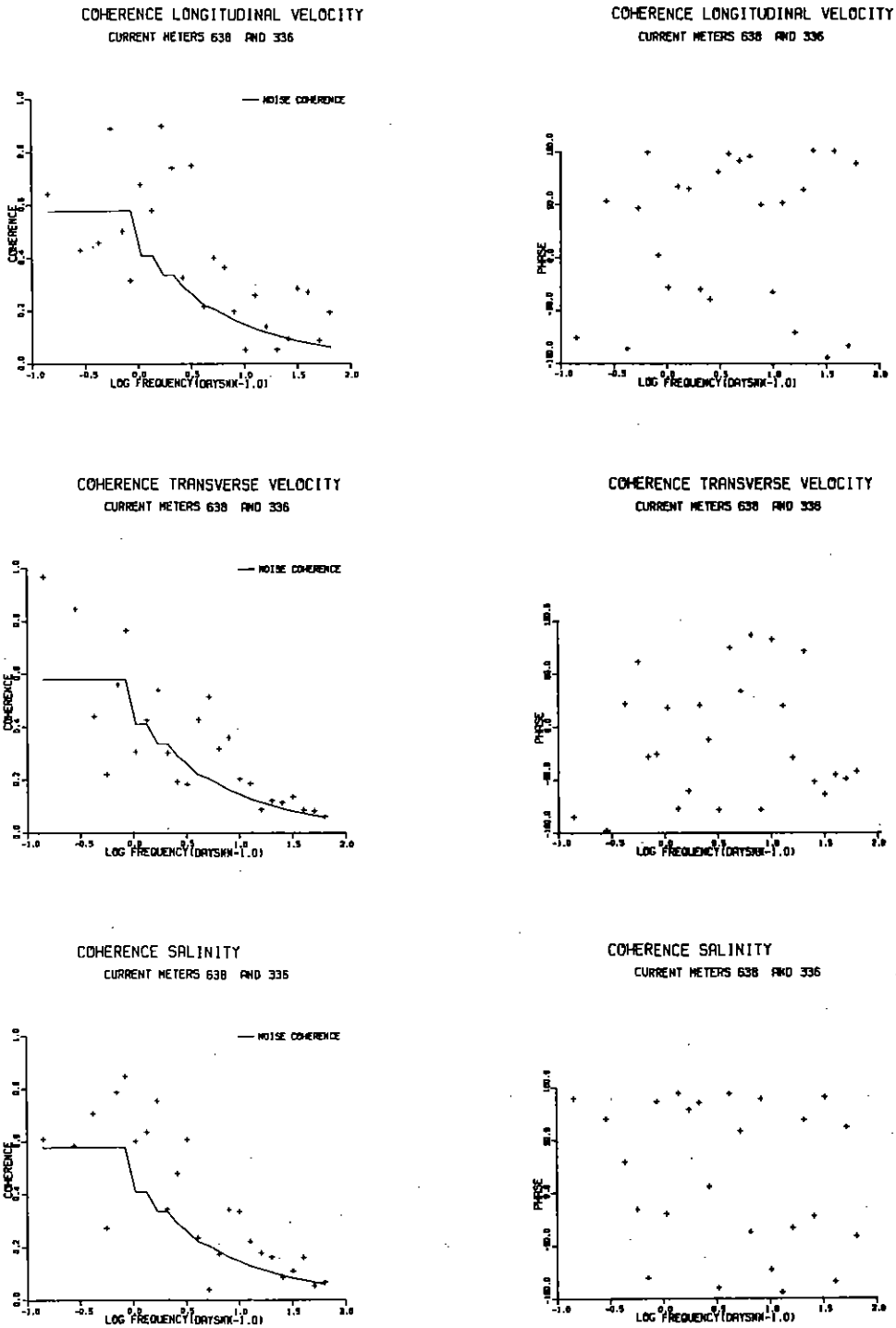

Figure 37. Coherences and phases between current meters #638 and #336.

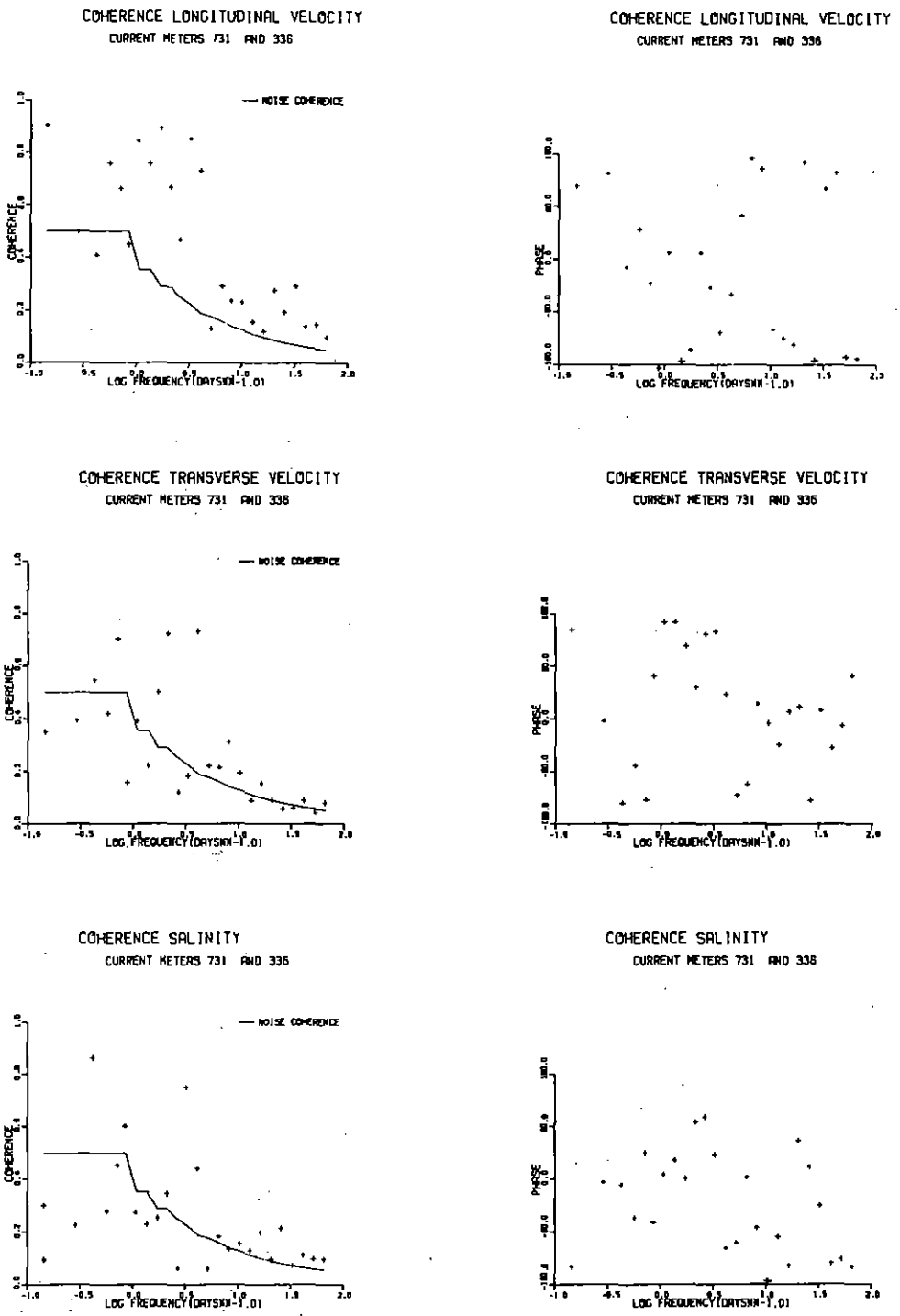

Figure 38. Coherences and phases between current meters #731 and #336.

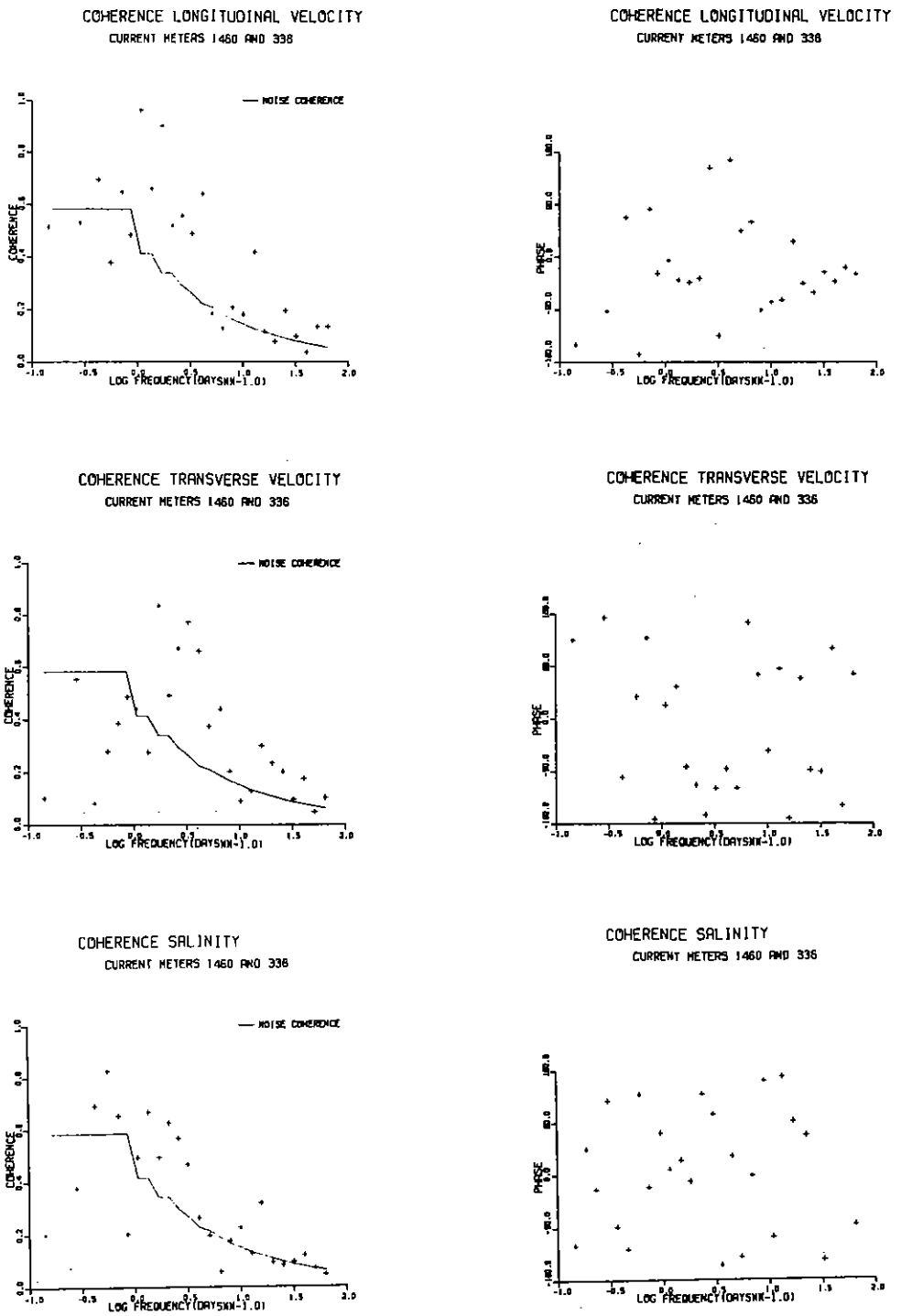

Figure 39. Coherences and phases between current meters #1460 and #336.

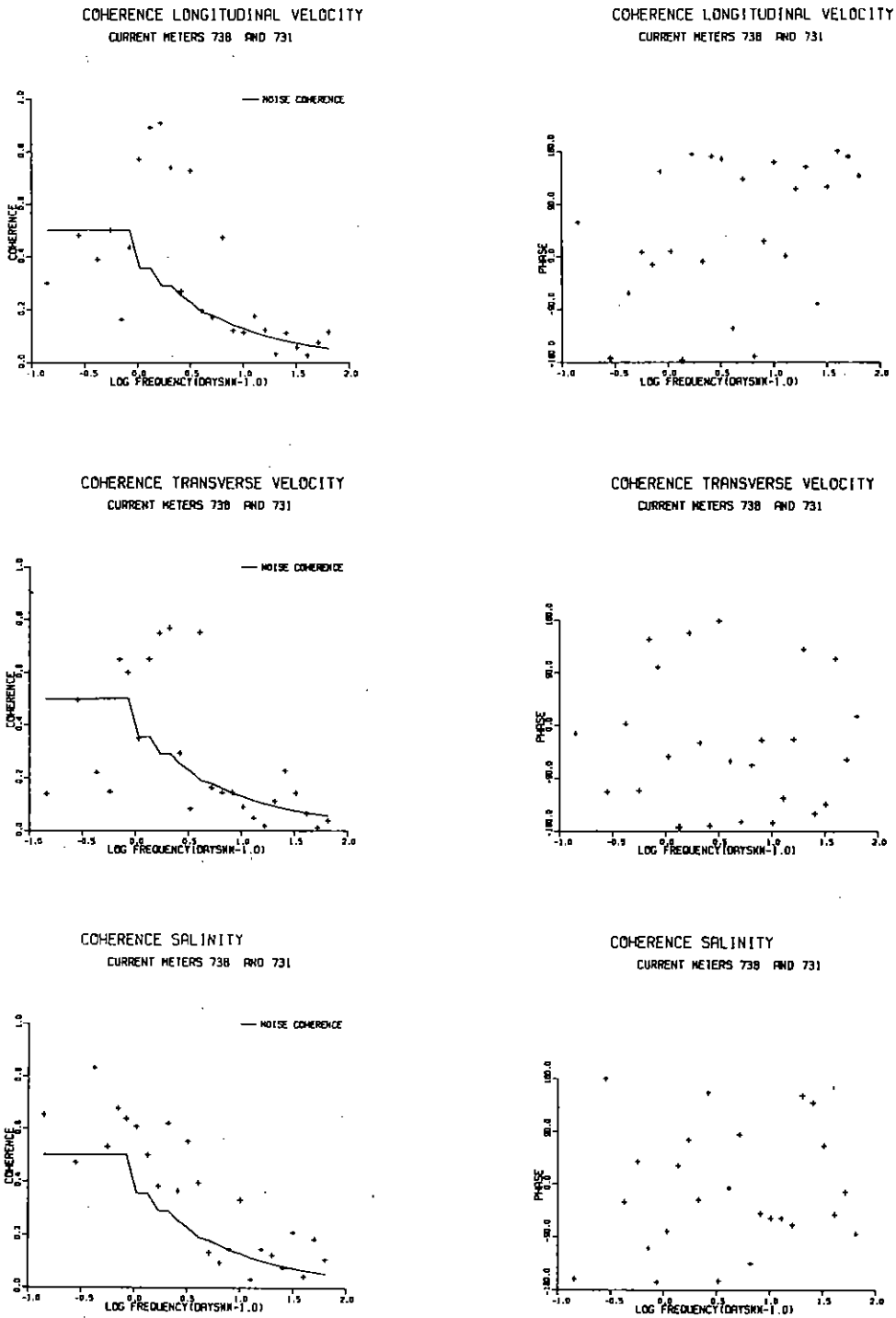

Figure 40. Coherences and phases between current meters #738 and #731.

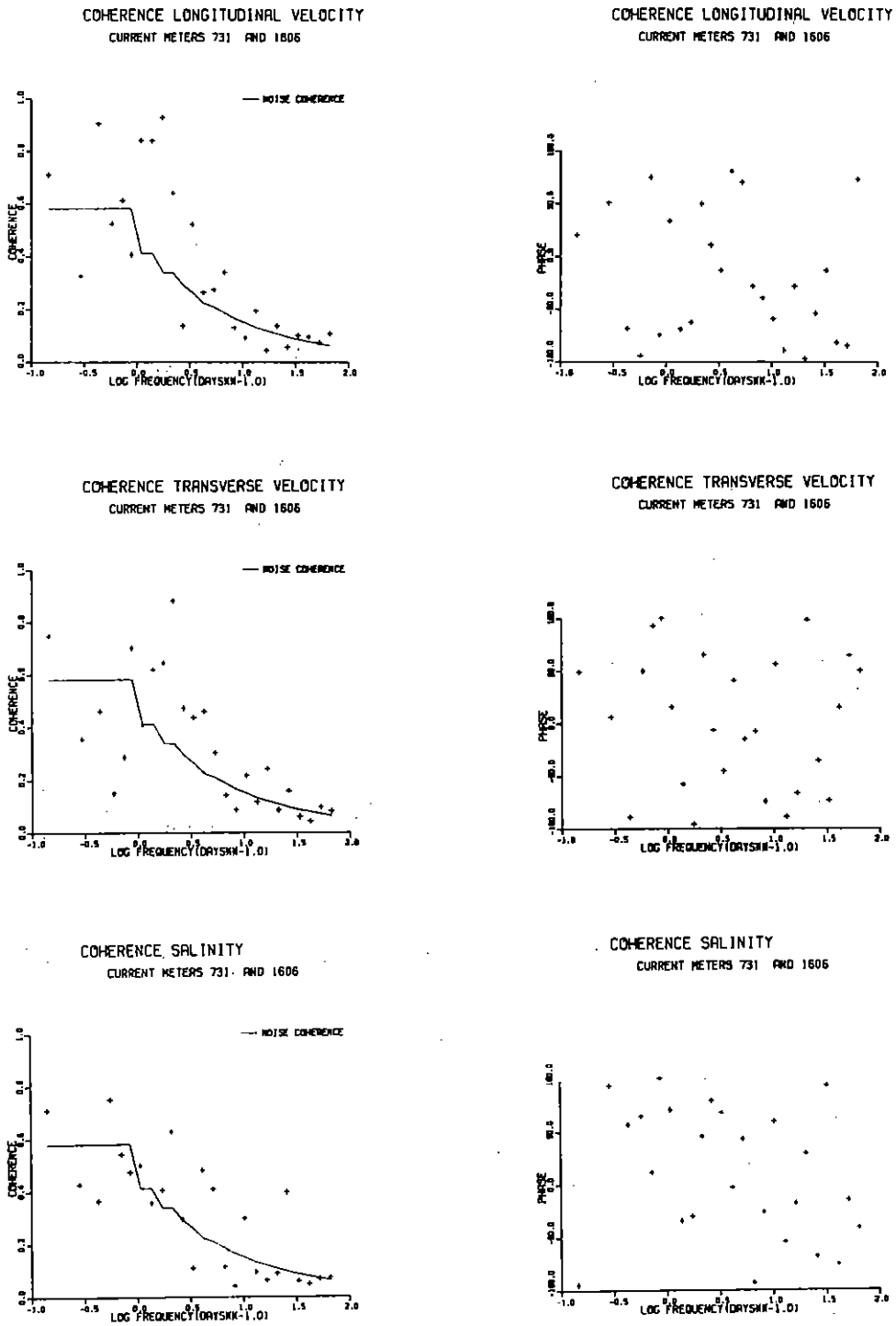

Figure 41. Coherences and phases between current meters #731 and #1606.

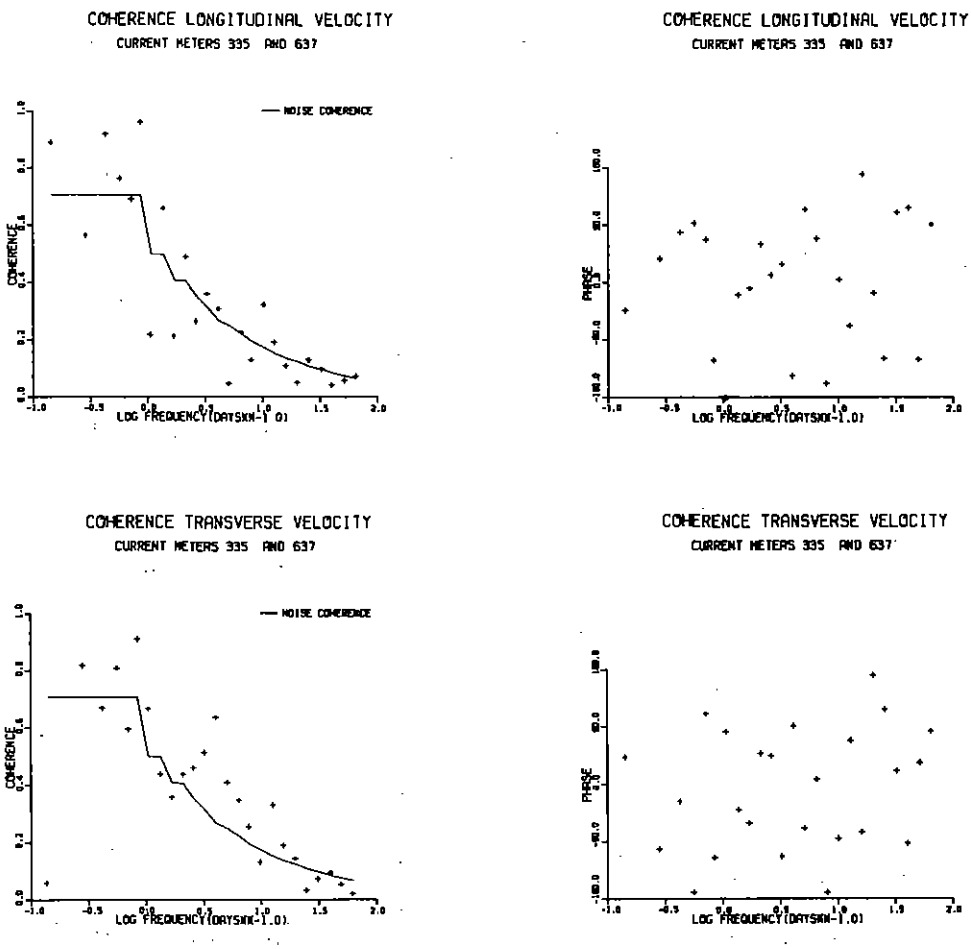

Figure 42. Coherences and phases between current meters #335 and #637.

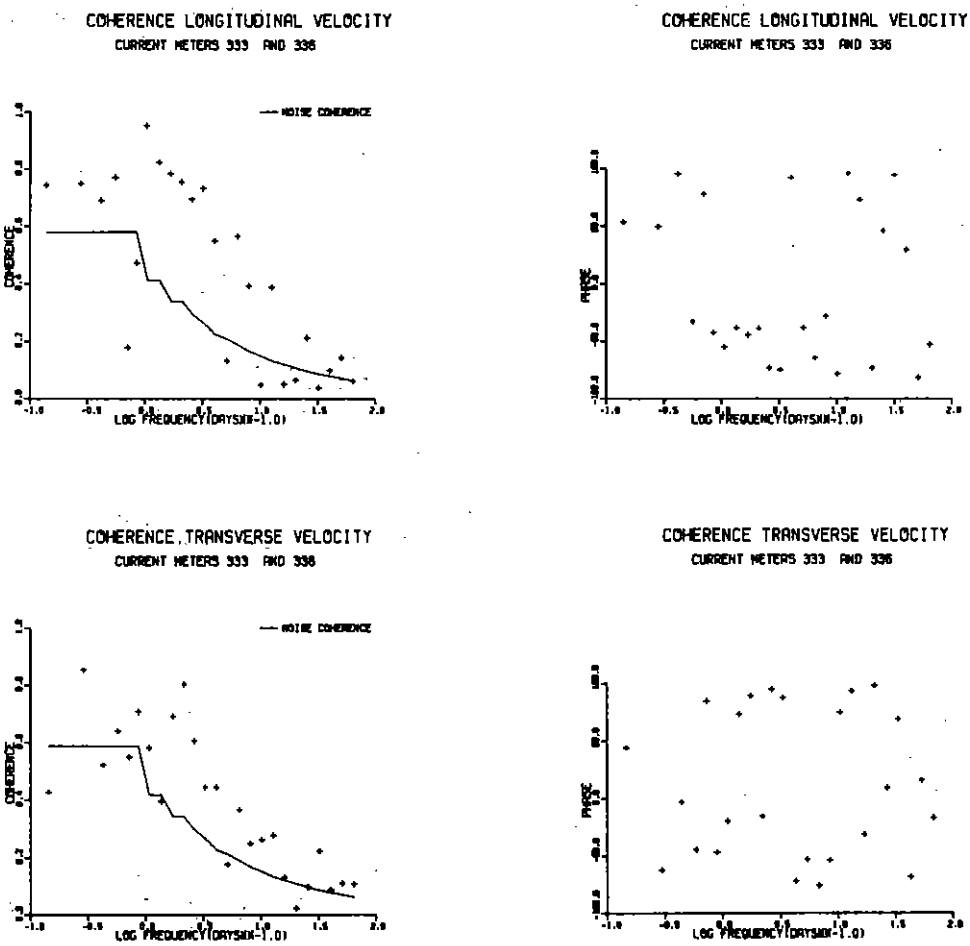

Figure 43. Coherences and phases between current meters #333 and #336.

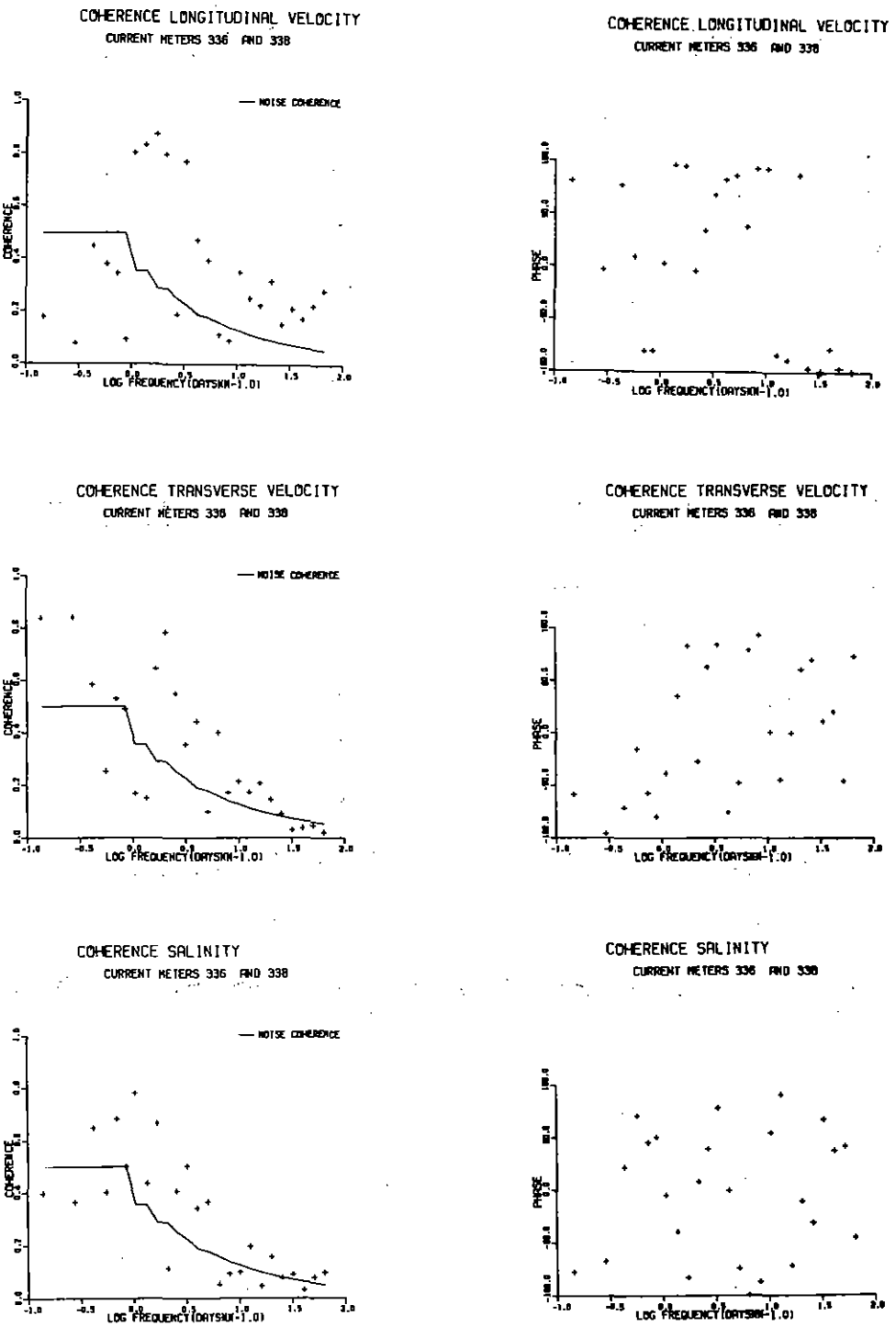

Figure 44. Coherences and phases between current meters #336 and #338.

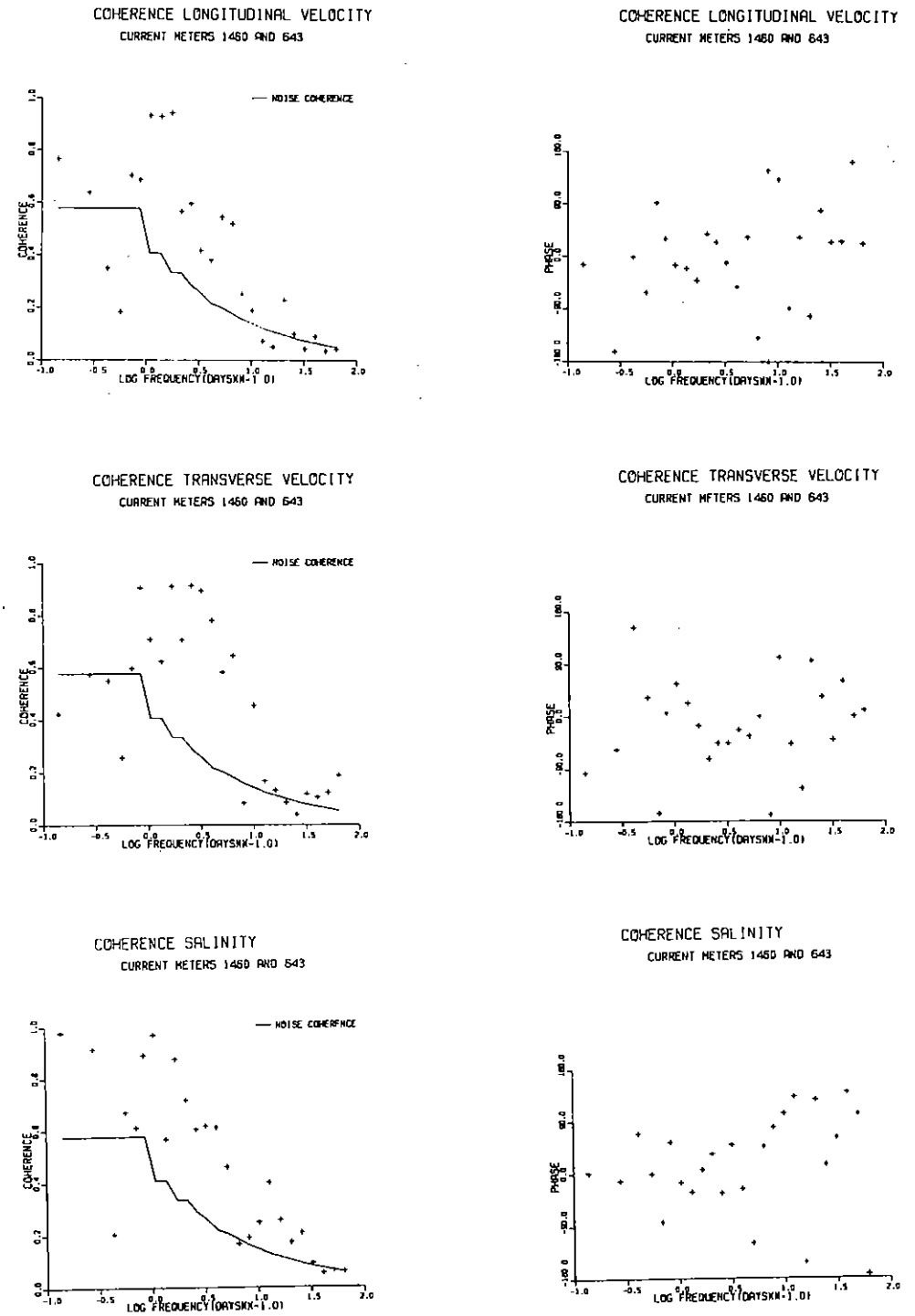

Figure 45. Coherences and phases between current meters #1460 and #643.

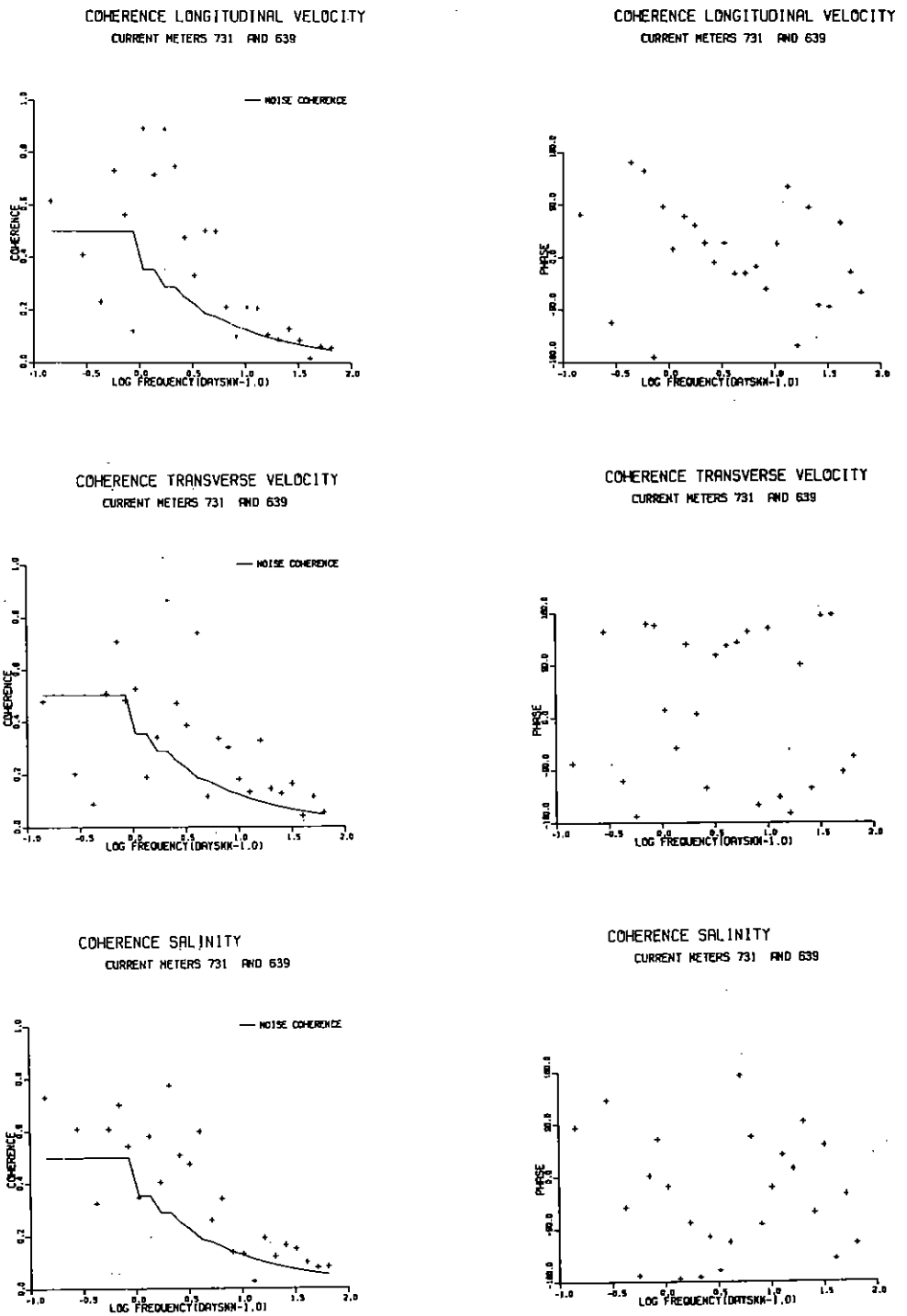

Figure 46. Coherences and phases between current meters #731 and #639.

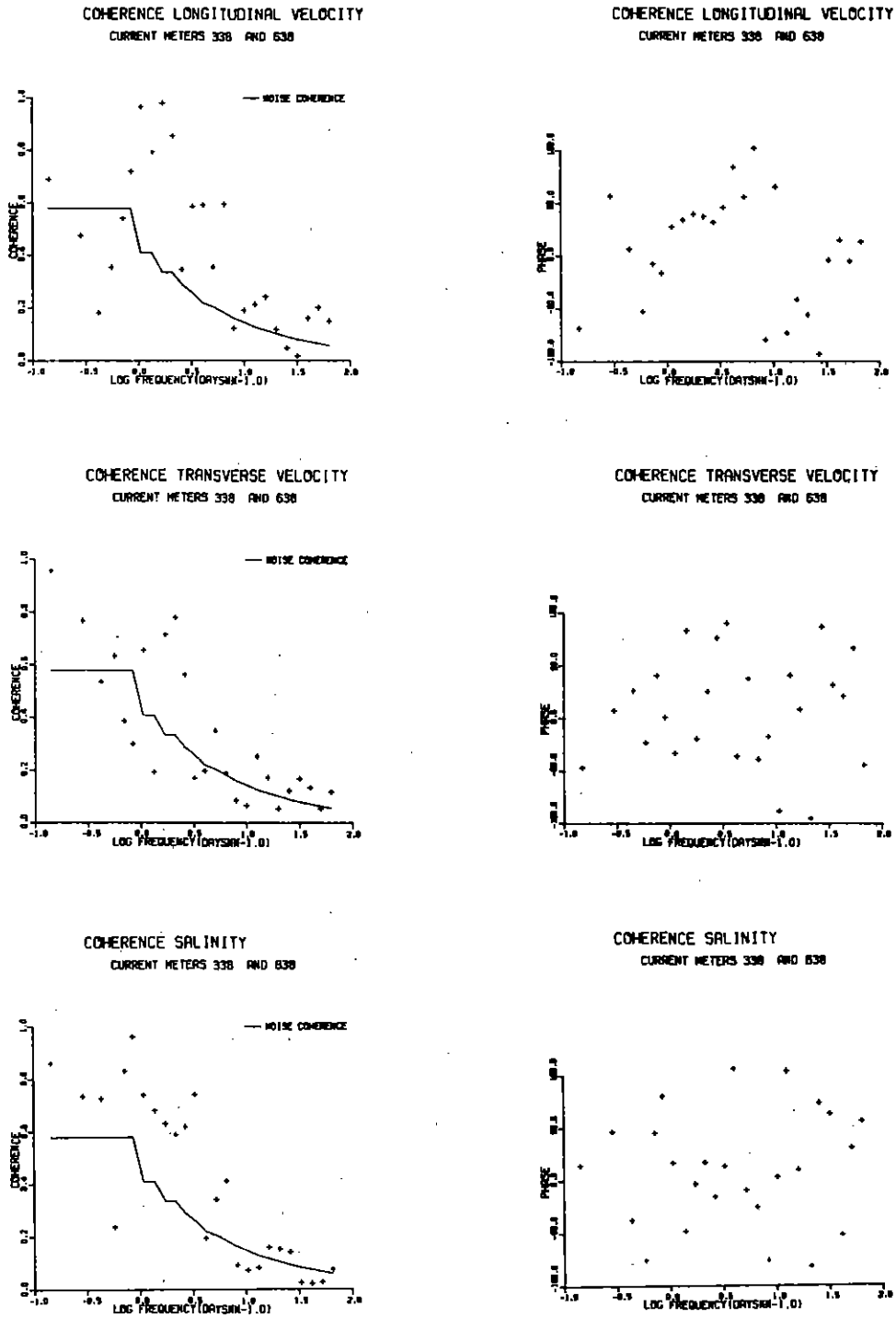

Figure 47. Coherences and phases between current meters #338 and #638.

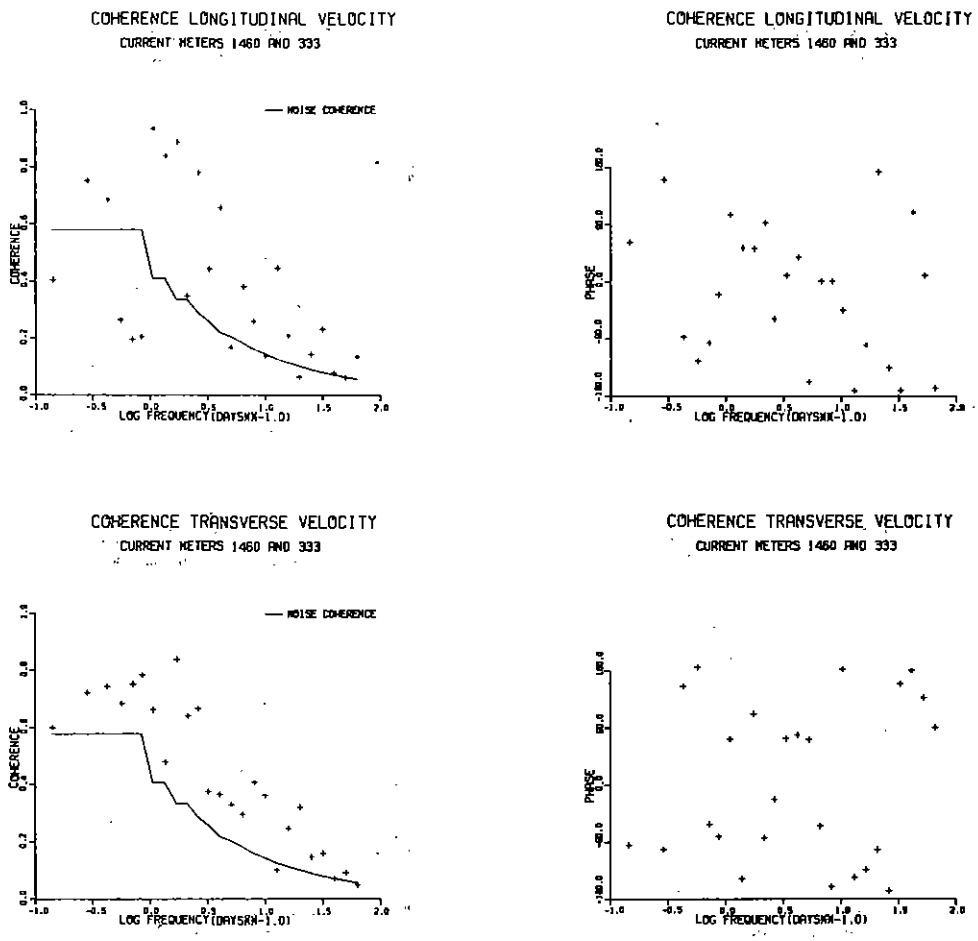

Figure 48. Coherences and phases between current meters #1460 and #333.

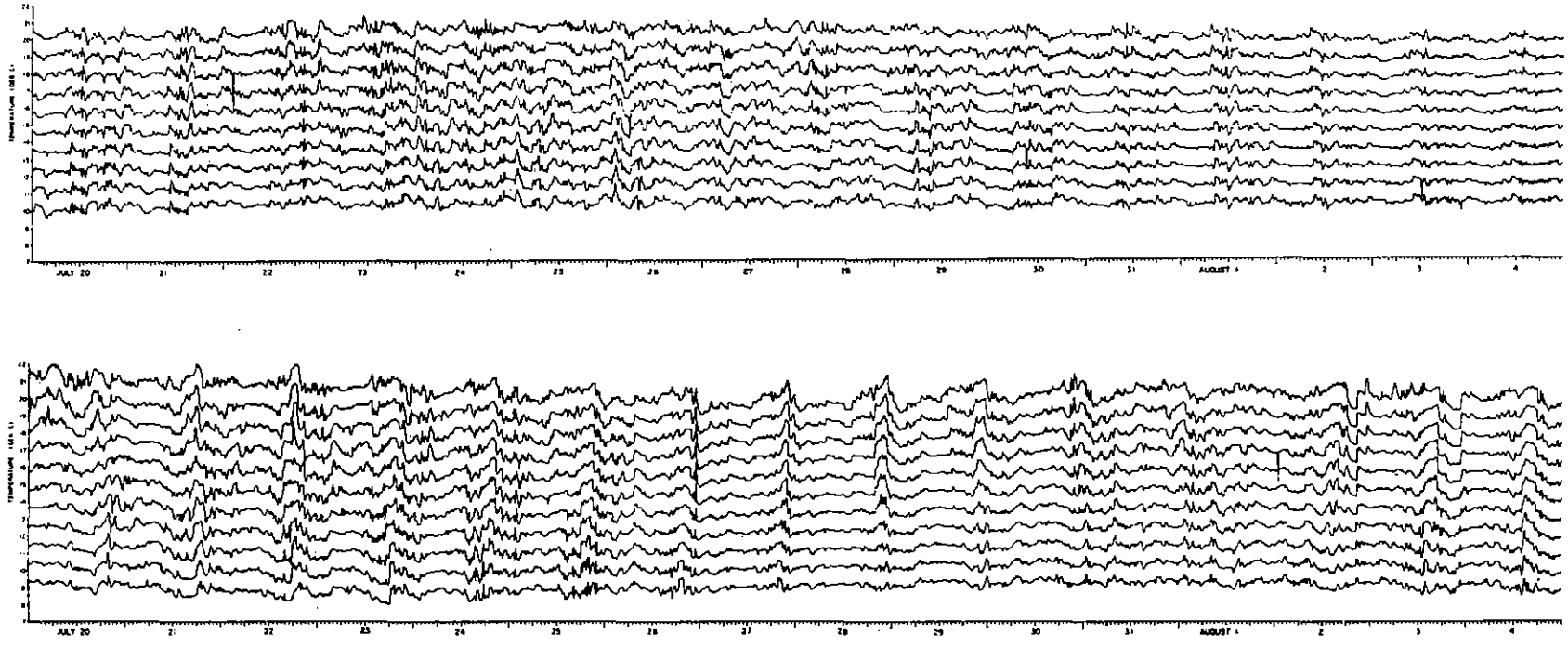

Figure 49. Thermistor chain time series, T63/17 (top) and T93/18 (bottom).

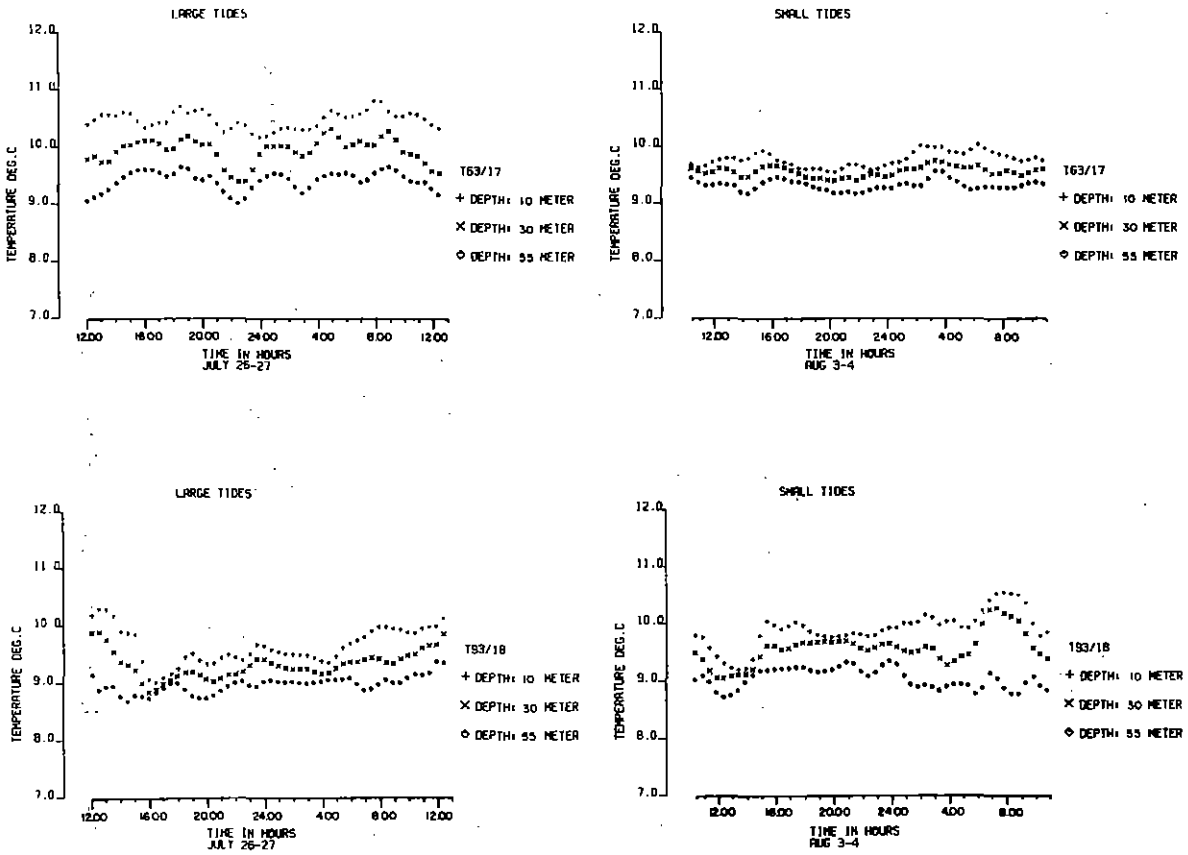

Figure 50. Two 25-hour sections of thermistor chain data, T63/17 and T93/18.

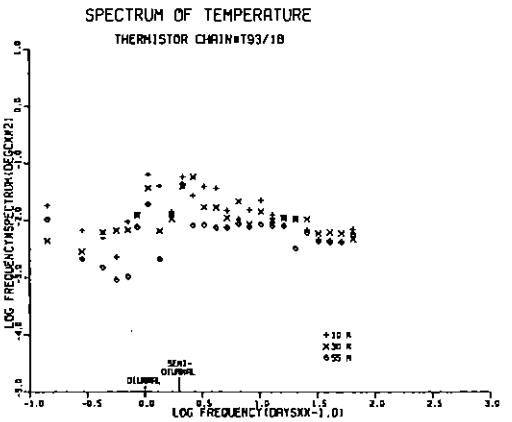

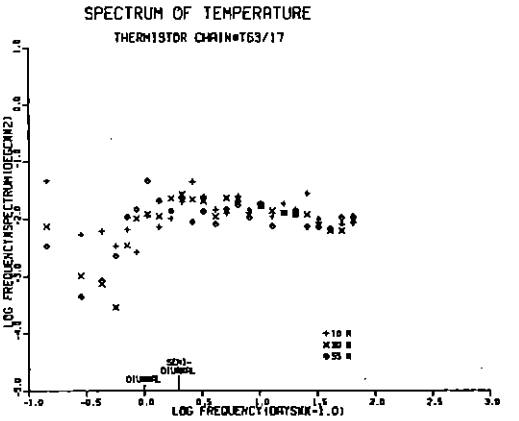

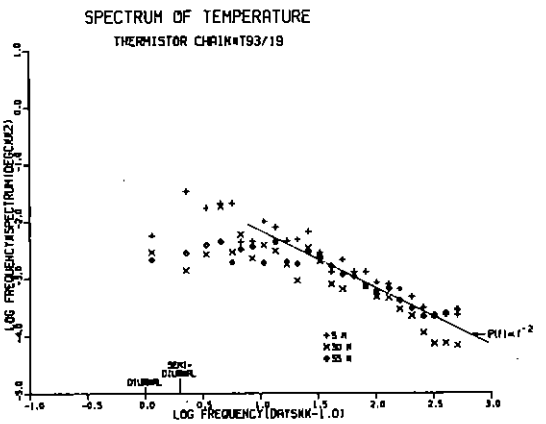

Figure 51. Power spectra for thermistor chains T17/17, T93/18 and T93/19.

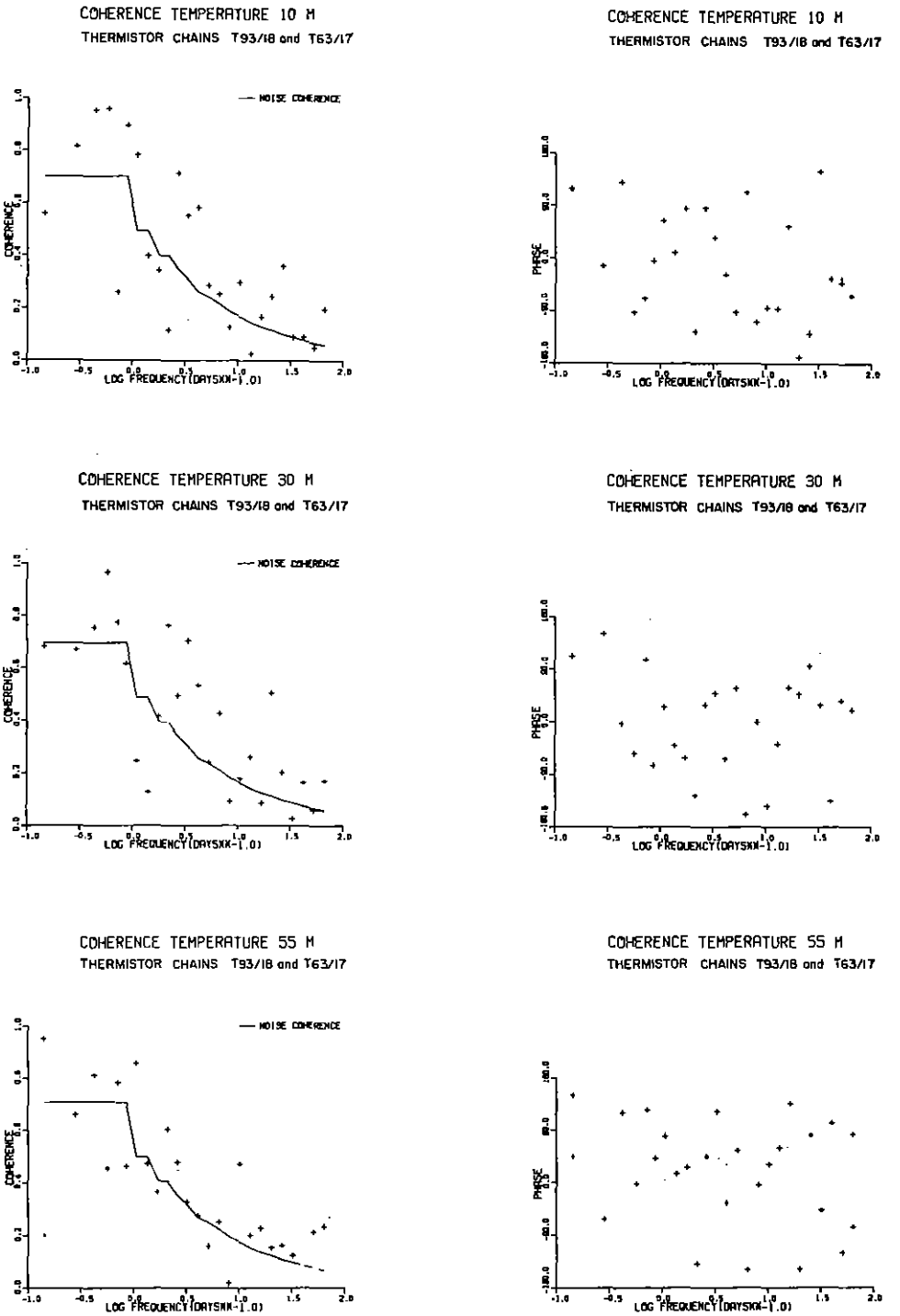

Figure 52. Coherences and phases between thermistor chains T67/17 and T93/18.

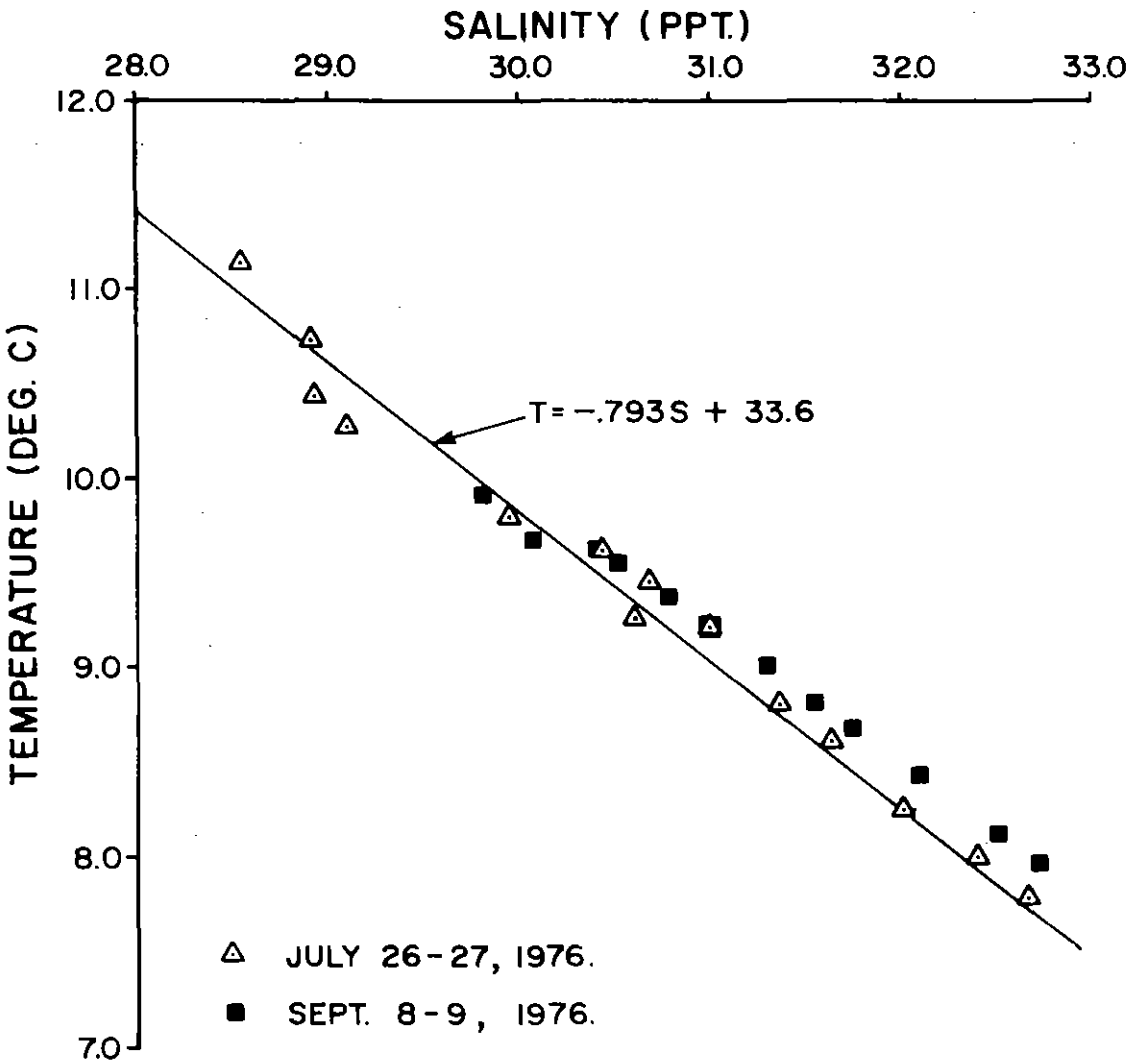

Figure 53. T,S diagram CTD Time Series #1 and #4.

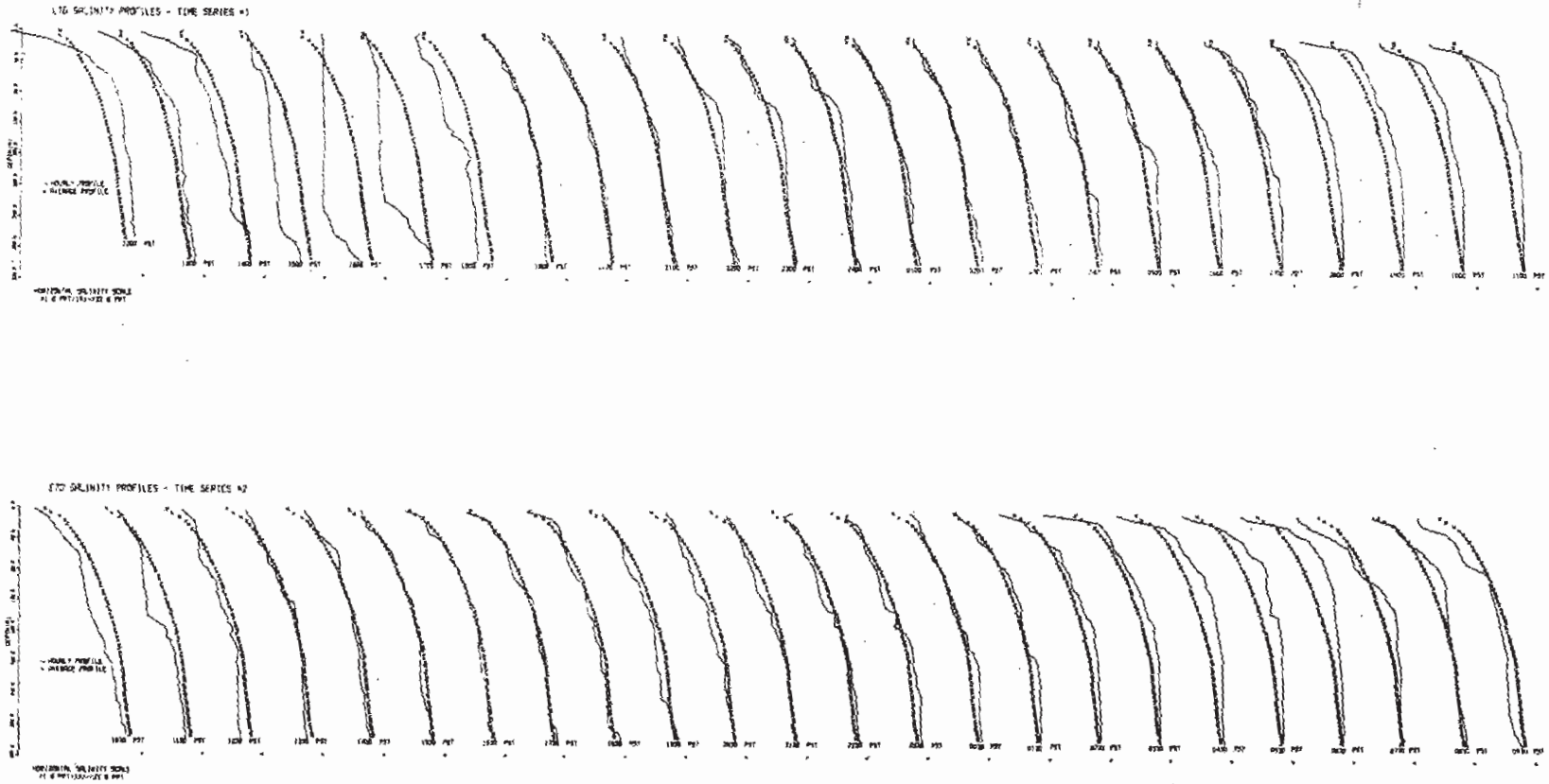

Figure 54. CTD Time Series #1 and #2.

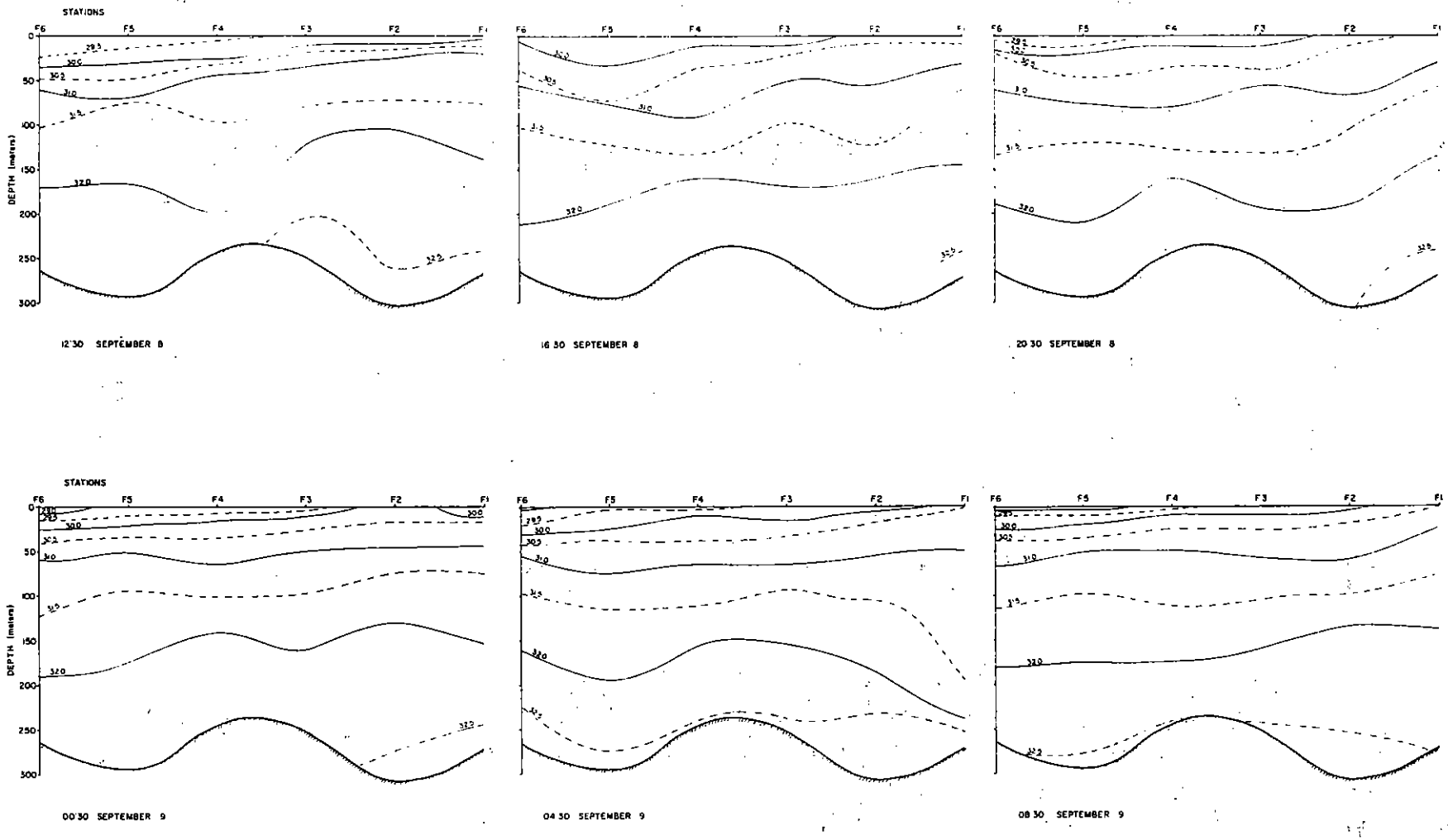

Figure 55. CTD Time Series #4.

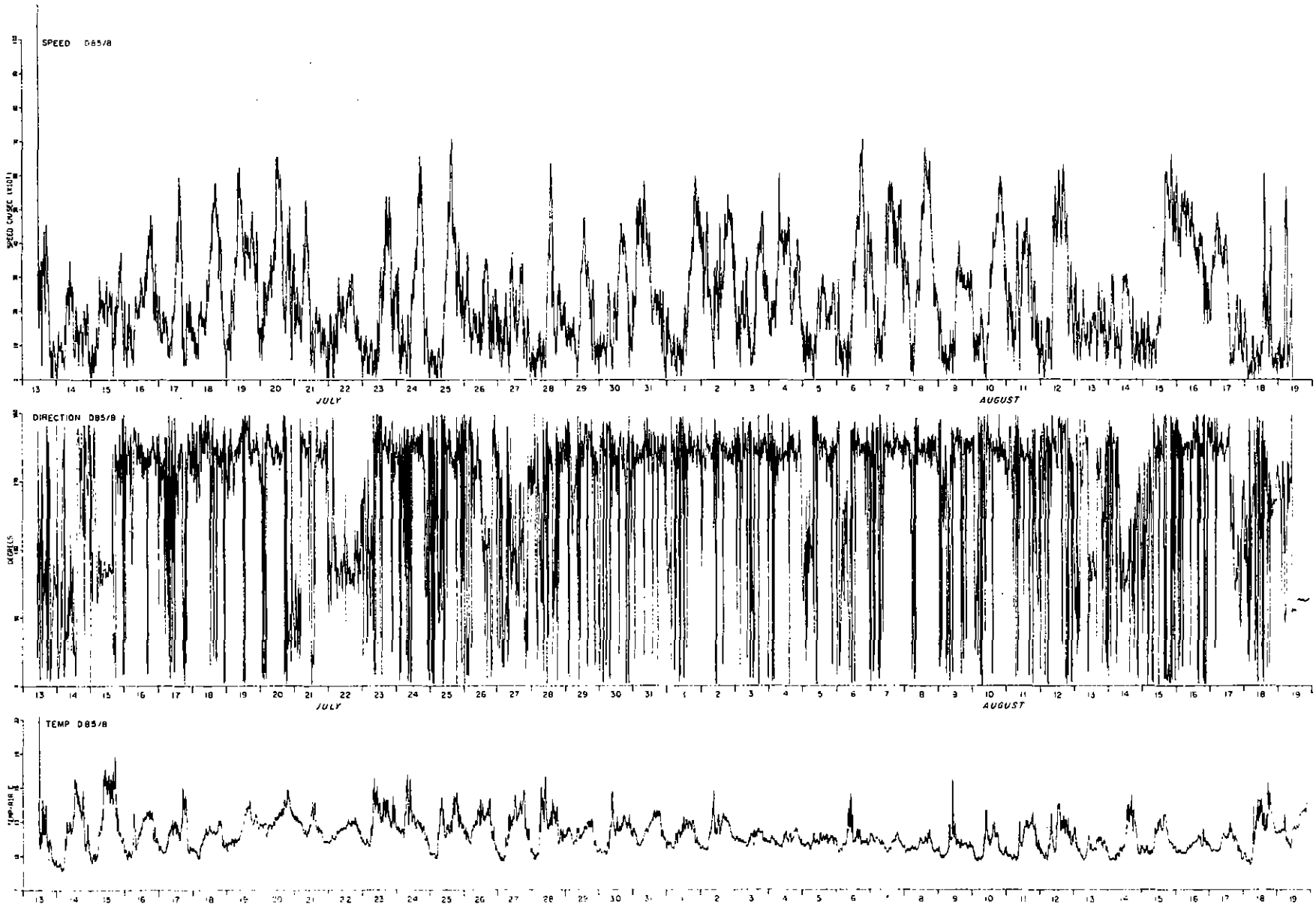

Figure 56. Wind speeds, wind directions and air temperature for anemometer #D85/8.